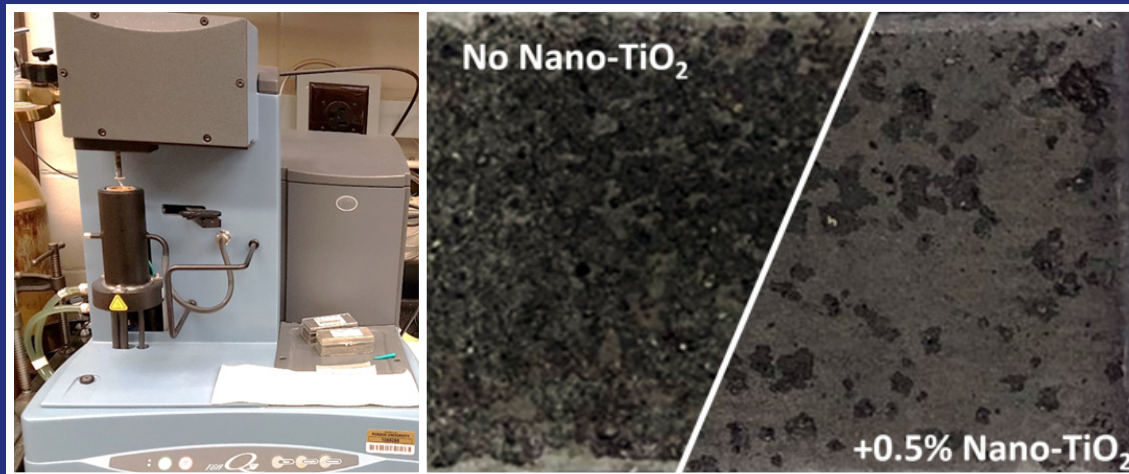


JOINT TRANSPORTATION RESEARCH PROGRAM

INDIANA DEPARTMENT OF TRANSPORTATION
AND PURDUE UNIVERSITY



Improving Scaling Resistance of Pavement Concrete Using Titanium Dioxide (TiO_2) and Nanosilica



Dan Huang, Mirian Velay-Lizancos, Jan Olek

RECOMMENDED CITATION

Huang, D., Velay-Lizancos, M., & Olek, J. (2022). *Improving scaling resistance of pavement concrete using titanium dioxide (TiO₂) and nanosilica* (Joint Transportation Research Program Publication No. FHWA/IN/JTRP-2022/32). West Lafayette, IN: Purdue University. <https://doi.org/10.5703/1288284317583>

AUTHORS

Dan Huang

Graduate Researcher
Lyles School of Civil Engineering
Purdue University

Mirian Velay-Lizancos, PhD

Assistant Professor of Civil Engineering
Lyles School of Civil Engineering
Purdue University

Jan Olek, PhD

James H. and Carol H. Cure Professor in Civil Engineering
Director of the North Central Superpave Center
Lyles School of Civil Engineering
Purdue University
(765) 494-5015
olek@purdue.edu
Corresponding Author

JOINT TRANSPORTATION RESEARCH PROGRAM

The Joint Transportation Research Program serves as a vehicle for INDOT collaboration with higher education institutions and industry in Indiana to facilitate innovation that results in continuous improvement in the planning, design, construction, operation, management and economic efficiency of the Indiana transportation infrastructure. https://engineering.purdue.edu/JTRP/index_html

Published reports of the Joint Transportation Research Program are available at <http://docs.lib.purdue.edu/jtrp/>.

NOTICE

The contents of this report reflect the views of the authors, who are responsible for the facts and the accuracy of the data presented herein. The contents do not necessarily reflect the official views and policies of the Indiana Department of Transportation or the Federal Highway Administration. The report does not constitute a standard, specification or regulation.

TECHNICAL REPORT DOCUMENTATION PAGE

1. Report No. FHWA/IN/JTRP-2022/32	2. Government Accession No.	3. Recipient's Catalog No.	
4. Title and Subtitle Improving Scaling Resistance of Pavement Concrete Using Titanium Dioxide (TiO ₂) and Nanosilica	5. Report Date June 2022		6. Performing Organization Code
	7. Author(s) Dan Huang, Mirian Velay-Lizancos, and Jan Olek		
9. Performing Organization Name and Address Joint Transportation Research Program Hall for Discovery and Learning Research (DLR), Suite 204 207 S. Martin Jischke Drive West Lafayette, IN 47907	8. Performing Organization Report No. FHWA/IN/JTRP-2022/32		10. Work Unit No.
	11. Contract or Grant No. SPR-4336		
12. Sponsoring Agency Name and Address Indiana Department of Transportation (SPR) State Office Building 100 North Senate Avenue Indianapolis, IN 46204	13. Type of Report and Period Covered Final Report		14. Sponsoring Agency Code
	15. Supplementary Notes Conducted in cooperation with the U.S. Department of Transportation, Federal Highway Administration.		
16. Abstract This project focused on the evaluation of the influence of nanoadditives on the hydration kinetics, mechanical properties, and durability of concretes with and without supplementary cementitious materials (SCMs). The types of nanomaterials used in the course of this study included nano-titanium dioxide (nano-TiO ₂) and two forms of nanosilica. A series of experimental tasks, including fabrication, curing, and conditioning of specimens, microstructure analysis, mechanical strength testing, and durability testing were conducted in the laboratory. Based on experimental results, it can be concluded that the addition of nanoparticles can accelerate the early-age hydration process of cementitious pastes, especially those containing fly ash and cured at low temperatures. Both the compressive and flexural strength of mortars and concretes were also enhanced by the addition of nanoparticles. In addition, incorporation of nanoparticles reduced the total amount and connectivity of pores present in concretes. That resulted in lowering the water permeability of concretes, regardless of the cementitious systems and curing temperatures used. The resistance of concretes to freeze-thaw cycles and scaling was also improved by the addition of nanoparticles, especially those containing fly ash. However, an excess of nanoparticles additions may reduce the scaling resistance of concretes.			
17. Key Words nanoparticles, scaling, freeze thaw durability	18. Distribution Statement No restrictions. This document is available through the National Technical Information Service, Springfield, VA 22161.		
19. Security Classif. (of this report) Unclassified	20. Security Classif. (of this page) Unclassified	21. No. of Pages 67 including appendices	22. Price

EXECUTIVE SUMMARY

Introduction

This report summarizes the findings from the study on the influence of nanoadditives on the properties of concretes with and without supplementary cementitious materials (SCMs) cured at ambient (23°C) and low (4°C) temperatures. The objective of the study was to determine how the processes that occur on the nanoscale will affect the engineering properties and durability of concrete. The nanomaterials used in the study included nanotitanium dioxide (nano-TiO₂) and two forms of colloidal nanosilica. A series of experiments, including fabrication, curing, and conditioning of specimens, microstructural analysis, mechanical strength testing, and durability testing were conducted in the laboratory. The effects of nanoparticles on the properties of concretes were evaluated for their influence on the following properties: (1) hydration kinetic of cementitious pastes, (2) mechanical properties of mortars and concretes, and (3) durability-related properties of concretes, including porosity, permeability, scaling, and freeze-thaw resistance. Selected fragments of the description of the experimental methods, quantitative results, and supporting discussion have been previously published in the *Proceedings of the 7th International Conference on the Durability of Concrete Structures* in 2022 (refer to Appendix A).

Findings

Effect of Nano-TiO₂ Addition in Cement Paste With and Without SCMs

Results suggest that nano-TiO₂ is beneficial in accelerating the hydration process of ordinary Portland cement, fly ash, and slag pastes based on isothermal calorimetry and Vicat setting time tests. Nonetheless, the effect of nano-TiO₂ in increasing the amount of hydration product is more significant in fly ash pastes, as indicated by thermogravimetric analysis. This indicates the enhancement strength of cement matrix produced by the addition of nano-TiO₂ is more relevant in fly ash cement pastes than in OPC and slag cement pastes.

Effect of Nano-TiO₂ Addition in Mortars With and Without SCMs

Results show that the addition of nano-TiO₂ can enhance the compressive and flexural strengths for both OPC and fly ash mortars. Such effect is more significant when cured at low temperature and when fly ash is used.

Impact of Nano-TiO₂ Addition in Mechanical Performance and Durability of Concretes With and Without SCMs

The 7-day and 28-day compressive strengths of concretes were proven to be improved by the addition of nano-TiO₂, for all studied concrete types (with or without SCMs) and curing temperatures. This effect is more significant in concretes containing slag and with higher w/c. Results from the fundamental resonant frequency test suggest that nano-TiO₂ addition improves the dynamic modulus of elasticity after 14 days of curing, especially at low curing temperature. Above findings indicate that the addition of nano-TiO₂ could reduce the porosity of the cementitious composites, especially when SCMs are used.

The study on the durability properties of concretes involves evaluating the pore systems and permeability and appraising the frost resistance of concretes modified by nano-TiO₂. It was found that nano-TiO₂ addition in concretes tends to reduce slump and increase the unit weight of fresh concretes. The resistivity and formation factor of fly ash concrete was improved by nano-TiO₂. Moreover, the total pore volume and water absorptions of all types of concretes were reduced by nano-TiO₂, and nano-TiO₂ seems to be more beneficial in improving the frost resistance of fly ash concretes compared to OPC and slag concretes. It seems that the addition of nano-TiO₂ to improve the scaling resistance of concrete is more effective when concretes are previously cured at low temperature.

Impact of Nanosilica Addition on Concrete's Performance

Like the addition of nano-TiO₂, the addition of nanosilica produced an improvement in the 28-day compressive and flexural strength of concretes, especially when cured at low temperature. The porosity can be reduced due to the addition of nanosilica in concretes. Furthermore, the overall scaling resistance of concretes fabricated for this study was good while the addition of nanosilica can still reduce the surface deterioration of concretes exposed to freeze-thaw cycles and deicers. The microstructural analysis suggests that the addition of nanoadditives reduces the cracks and porosity near the interfacial transition zone (ITZ), which can contribute to a higher strength of the bulk concrete. Further testing will be required to assess the effect on the air void system.

Overall Conclusions

Overall, applying nanoadditives in concrete is beneficial, but the degree of benefit depends on the cementitious system. Based on the results of this project, it seems that the addition of nano-TiO₂ is more effective in concrete containing fly ash. The improvement of nano-TiO₂ on the scaling and freeze-thaw resistance of fly ash concrete could be related to the densification of microstructure (e.g., strengthen of the paste matrix, less-cracked and less porous ITZ), less connected pore system, reduced porosity, finer and more well-distributed air void system. However, an excess of nanoadditives might affect the air void system negatively and produce negative effects on scaling resistance, as results showed. The optimum amount of nanoadditives would depend on the mixture proportioning of the concrete pavement.

Nanosilica addition has shown a great potential in terms of benefits for the performance of concrete pavements. However, further investigation will be required to determine the effect on the air void system. Results of both nano-TiO₂ addition and nanosilica addition effects on durability of concrete pavements were performed under lab conditions. Further investigation will be required to determine the effect of the use of nanoadditives in concrete pavement scaling resistance and freeze and thaw resistance when used in the field.

Implementation

Based on the findings established above, guidelines regarding the influence of nanoadditives on the properties of concrete are included in this report. The addition of nanoadditives (including nano-TiO₂ and nanosilica) have a potential in improving the scaling resistance of concrete pavement. The mechanisms of such improvements involve the accelerated hydration of cement pastes, reduced and modified pore system (hence the denser microstructure), enhanced mechanical properties, and lowered water

permeability of concretes based on experimental results. However, high percentages of nanoparticles showed a detrimental effect in terms of scaling resistance. Water to cement ratio and presence of different supplementary cementitious materials affect the final effect of the nanoadditives on concrete scaling resistance. Thus, to

determine the optimum amount of nanoadditives for a given mixture, further investigations should be performed. Recommendations for future work, including research suggestions for other types of durability testing, are also included in this report.

CONTENTS

1. INTRODUCTION	1
1.1 Background	1
1.2 Project Objectives	1
2. LITERATURE REVIEW	1
2.1 The Mechanisms of Freeze-Thaw and Scaling Damage in Concrete	1
2.2 The Freeze-Thaw Resistance of Concrete Containing Supplementary Cementitious Materials (SCMs)	2
2.3 The Effect of Nano-TiO ₂ on the Mechanical Properties and Durability of Cementitious Composites Containing SCMs	3
2.4 The Effects of Nano-Silica on the Performance of Cementitious Composites	3
3. MATERIALS	5
3.1 Aggregates	5
3.2 Cementitious Materials and Nanoparticles	5
3.3 Chemical Admixtures	6
4. IMPACT OF CURING TEMPERATURE ON THE EFFECT OF NANO-TiO ₂ ON THE HYDRATION PROCESS OF CEMENT PASTES CONTAINING SCMs	7
4.1 Preparation of Specimens and Testing Methods	7
4.2 Results and Discussions	9
5. THE EFFECT OF NANO-TiO ₂ ON MECHANICAL PROPERTIES OF MORTARS AND CONCRETES CONTAINING SCMs CURED AT DIFFERENT TEMPERATURES	16
5.1 Materials and Methods	16
5.2 Results and Discussions	18
6. THE EFFECT OF NANO-TiO ₂ AND CURING TEMPERATURES ON THE DURABILITY OF CONCRETES CONTAINING SCMs	24
6.1 Materials and Methods	24
6.2 Results and Discussions	27
7. THE EFFECT OF NANOSILICA AND CURING TEMPERATURES ON THE DURABILITY OF CONCRETE CONTAINING SCMs	37
7.1 Materials and Methods	37
7.2 Results and Discussions	37
8. THE INFLUENCE OF NANO-TiO ₂ AND NANOSILICA ON THE MICROSTRUCTURE OF CONCRETES CONTAINING SCMs	42
8.1 Sample Preparation and Methods	42
8.2 Results and Discussions	44
9. CONCLUSIONS	49
9.1 Findings	49
9.2 Recommendations and Future Work	51
REFERENCES	51
APPENDIX	
Appendix A. The Effects of Curing Temperature on the Hydration Kinetics of Plain and Fly Ash Pastes and Compressive Strength of Corresponding Mortars With and Without Nano-TiO ₂ Addition	55

LIST OF TABLES

Table 2.1 Typical physical characteristics of ordinary Portland cement and supplementary cementitious materials (SCMs)	3
Table 3.1 Properties of coarse and fine aggregate	5
Table 3.2 The chemical composition of Type I Portland cement, fly ash, and slag cement used in this study	6
Table 3.3 Physical properties of TiO ₂ nanoparticles	7
Table 4.1 Mixture proportions of nano-TiO ₂ modified cement pastes in this study (ratios are calculated based on weight basis)	8
Table 4.2 Physical and chemical changes in concrete as a function of temperature	9
Table 4.3 The time shift of the maximum value of the heat flow peak due to the addition of nano-TiO ₂ to OPC pastes (relative to the time for maximum value of the heat flow peak for pastes without nano-TiO ₂)	10
Table 4.4 The time shift of the maximum value of the heat flow peak due to the addition of nano-TiO ₂ to fly ash pastes (relative to the time for maximum value of the heat flow peak for pastes without nano-TiO ₂)	10
Table 4.5 The time shift of the maximum value of the heat flow peak due to the addition of nano-TiO ₂ to slag pastes (relative to the time for maximum value of the heat flow peak for pastes without nano-TiO ₂)	11
Table 4.6 Shortening of the setting time (based on the thermal indicator data from IC method) for OPC, fly ash, and IC pastes with 2% of nano-TiO ₂ cured at room and low temperatures	12
Table 4.7 Shortening of the Vicat setting time for OPC, fly ash, and slag pastes with 1% of nano-TiO ₂ addition tested at standard temperature (23°C)	13
Table 5.1 Mixture proportions of plain and nano-TiO ₂ mortars (all ratios calculated on weight basis)	17
Table 5.2 Mixture proportions of TiO ₂ nanoparticles modified concrete (all ratios calculated on weight basis)	17
Table 6.1 The rating for the surface scaling	27
Table 6.2 The total volume of pores (in %) and bulk densities of Class A concretes (with and without nano-TiO ₂) cured at different temperatures (28 days) with and without nano-TiO ₂	29
Table 6.3 The initial and secondary rates of water absorption and the values of correlation coefficients R ² for Class A concretes with and without nano-TiO ₂ and cured at different temperatures	30
Table 6.4 The visual appearance of Class A concretes (A-P, A-F, and A-S) with and without nano-TiO ₂ cured at different temperatures at the end of scaling test (after 50 freezing and thawing cycles)	32
Table 6.5 The visual appearance of Class C concretes (C-P and C-S) with and without nano-TiO ₂ cured at different temperatures at the end of scaling test (after 50 freezing and thawing cycles)	34
Table 7.1 The mix design for nanosilica-modified concretes	37
Table 7.2 Initial and secondary rates of water absorption results for concretes with and without nanosilica cured at different temperatures	41
Table 7.3 The visual appearance of concretes with and without nano-silica after 50 FT cycles of scaling test with and without nanosilica cured at different temperatures	42
Table 8.1 The mix design for concretes with the addition of (a) nanosilica and (b) nano-TiO ₂	43
Table 8.2 The characteristics of ITZ of fly ash concrete samples with and without nano-TiO ₂ (mag 100 ×)	45
Table 8.3 The characteristics of ITZ of slag concrete samples with and without nano-TiO ₂ (mag 100 ×)	46
Table 8.4 The characteristics of ITZ of OPC concrete samples with and without nanosilica (mag 100 ×)	46
Table 8.5 The characteristics of ITZ of fly ash concrete samples with and without nano-TiO ₂ (mag 200 ×)	47
Table 8.6 The characteristics of ITZ of slag concrete samples with and without nano-TiO ₂ (mag 200 ×)	48
Table 8.7 The characteristics of ITZ of OPC concrete samples with and without nanosilica (mag 200 ×)	48
Table 8.8 The air content, specific surface area (SSA), and spacing factor (SF) values for concretes with and without nano-TiO ₂	49
Table 8.9 Results of the air content, specific surface area (SSA), and spacing factor (SF) of concrete with and without nanosilica	49

LIST OF FIGURES

Figure 2.1 (a) Picture of a severely scaled sidewalk. (b) Sidewalk that was severely scaled, probably by internal frost damage, which led to a complete loss of mechanical integrity	2
Figure 2.2 SEM image of CH in T-engineered cementitious composites at curing age of 28 days: (a) without the addition of nano-TiO ₂ ; (b) with 0.78 vol.% of nano-TiO ₂ ; and (c) with 2.32 vol.% of nano-TiO ₂	4
Figure 2.3 Potential impacts of nano-silica in cementitious composites	4
Figure 3.1 The gradation curves of coarse and fine aggregates	5
Figure 3.2 The results of particle size analyzer (PSA) for cementitious materials (OPC, fly ash, and slag) used in this study	6
Figure 3.3 Transmission electron microscopy images of the particles of nano-TiO ₂	6
Figure 3.4 XRD patterns of nano-TiO ₂ used in this study	6
Figure 3.5 Schematic of the relative sizes of E5 nanosilica and cement grains	7
Figure 4.1 The normalized heat flow and normalized cumulative heat curves for OPC pastes cured at (a) room temperature (23°C), and (b) low temperature (4°C)	10
Figure 4.2 The normalized heat flow and normalized cumulative heat curves for fly ash pastes cured at (a) room temperature (23°C), and (b) low temperature (4°C)	10
Figure 4.3 The normalized heat flow and normalized cumulative heat curves for fly ash pastes cured at (a) room temperature (23°C), and (b) low temperature (4°C)	11
Figure 4.4 An example illustrating the way to obtain the thermal indicator of setting time using the heat flow curve from IC experiment	11
Figure 4.5 The variation in the final setting time (based on the thermal indicator data from the IC method) as a function of the nano-TiO ₂ addition for the OPC, fly ash, and slag pastes cured at (a) room temperature (23°C), and (b) low temperature (4°C)	12
Figure 4.6 The variation of Vicat setting time as a function of the nano-TiO ₂ addition for (a) OPC, (b) fly ash, and (c) slag pastes tested at standard temperature (23°C)	12
Figure 4.7 The TGA results of OPC paste with 0% and 2% of TiO ₂ nanoparticles cured for 3 days at low temperature	14
Figure 4.8 The amounts of hydration products in the OPC pastes with different levels of nano-TiO ₂ addition after 3, 7, and 28 days of curing at (a) room temperature (23°C), and (b) low temperature (4°C)	14
Figure 4.9 The amounts of hydration products in the fly ash pastes with different levels of nano-TiO ₂ addition after 3, 7, and 28 days of curing at (a) room temperature (23°C), and (b) low temperature (4°C)	15
Figure 4.10 The amounts of hydration products in the slag pastes with different levels of nano-TiO ₂ addition after 3, 7, and 28 days of curing at (a) room temperature (23°C), and (b) low temperature (4°C)	15
Figure 4.11 The values of Q_{labp} (quantitative increase in the amount of hydration products) for OPC, fly ash, and slag pastes cured for 3, 7, and 28 days cured at room and low temperatures. (a) OPC, room temp; (b) OPC, low temp; (c) fly ash, room temp; (d) fly ash, low temp; (e) slag, room temp; and (f) slag, low temp	16
Figure 5.1 Schematic of typical test apparatus for fundamental transverse frequency	19
Figure 5.2 The slump of fresh concretes (Class A and C) with and without nano-TiO ₂ . The highlighted region represents the target range of slumps for Class A and C concretes given in the INDOT's Standard Specifications, Section 700	19
Figure 5.3 The unit weights and air contents of fresh concretes with and without nano-TiO ₂ : (a) Class A concretes, and (b) Class C concretes	19
Figure 5.4 Values of the compressive strength of OPC and fly ash mortars at different ages for specimens cured at (a) room temperature (23°C), and (b) low temperature (4°C)	20
Figure 5.5 Values of the flexural strength of OPC and fly ash mortars at different ages for specimens cured at (a) room temperature (23°C), and (b) low temperature (4°C)	20
Figure 5.6 The values of the compressive strength of concretes (Class A) with different levels of nano-TiO ₂ addition cured at both room and low temperatures for (a) 7 days, and (b) 28 days	21
Figure 5.7 The values of the compressive strength of concretes (Class C) with different levels of nano-TiO ₂ addition cured at both room and low temperatures for (a) 7 days and (b) 28 days	21

Figure 5.8 The effects of addition of nano-TiO ₂ on the relative increase in compressive strength of Class A and C concretes cured at room (23°C) temperature for (a) 7 days and (b) 28 days	22
Figure 5.9 The effects of addition of nano-TiO ₂ on the relative increase in compressive strength of Class A and C concretes cured at low (4°C) temperature for (a) 7 days and (b) 28 days	22
Figure 5.10 The values of the flexural strength of concretes without (0%) and with 0.5% of nano-TiO ₂ cured at both room and low temperatures for (a) 7 days, and (b) 28 days	23
Figure 5.11 (a) The dynamic modulus of elasticity (DME) and (b) the relative increase in DME due to the addition of nano-TiO ₂ for Class A concretes cured for 14 days at standard (23°C) and low (4°C) temperatures	23
Figure 5.12 The effect of nano-TiO ₂ on the relationship between the static and dynamic moduli of elasticity of concretes cured at (a) room temperature (23°C), and (b) low temperature (4°C)	24
Figure 6.1 The setup of resistivity measurement	24
Figure 6.2 Schematic of the water absorption test	26
Figure 6.3 Schematic of the scaling test specimens	27
Figure 6.4 Illustration of the surface scaling rating scale for visual evaluation of scaling resistance	27
Figure 6.5 The 28 days resistivity of Class A concretes (with and without nano-TiO ₂) cured at (a) room temperature, and (b) low temperature	28
Figure 6.6 The 28-day formation factor of Class A concretes (with and without nano-TiO ₂) cured at (a) room temperature, and (b) low temperature	28
Figure 6.7 The reduction in porosity of Class A concretes due to the addition of nano-TiO ₂	29
Figure 6.8 The results of water absorption test for Class A concretes with and without nano-TiO ₂ after 28 days of curing at (a) room temperature, and (b) low temperature	30
Figure 6.9 The results of (a) initial absorption, and (b) secondary absorption for Class A concretes with and without nano-TiO ₂ cured at different temperatures	30
Figure 6.10 The evolution of the degree of saturation (DOS) of Class A concretes with and without nano-TiO ₂ after 28 days of curing at (a) room temperature, and (b) low temperature during the water absorption test	31
Figure 6.11 The cumulative mass loss due to scaling for Class A concretes with and without nano-TiO ₂ cured at different temperatures: (a) A-P-RT; (b) A-P-LT; (c) A-F-RT; (d) A-F-LT; (e) A-S-RT; and (f) A-S-LT	33
Figure 6.12 The cumulative mass loss due to scaling of Class C concretes with and without nano-TiO ₂ cured at different temperatures: (a) C-P-RT; (b) C-P-LT; (c) C-S-RT; and (d) C-S-LT	35
Figure 6.13 The relative dynamic modulus of elasticity (RDME) and actual dynamic modulus (DME) of A-P concretes with and without nano-TiO ₂ cured at (a) room temperature, and (b) low temperature and exposed to 300 FT cycles	35
Figure 6.14 The relative dynamic modulus of elasticity (RDME) and actual dynamic modulus (DME) of A-F concretes with and without nano-TiO ₂ cured at (a) room temperature, and (b) low temperature and exposed to ~ 800 FT cycles	36
Figure 6.15 The relative dynamic modulus of elasticity (RDME) and actual dynamic modulus (DME) of A-S concretes with and without nano-TiO ₂ cured at (a) room temperature and (b) low temperature and exposed to ~ 800 FT cycles	36
Figure 7.1 The fresh properties of concrete (slump, unit weight, and air content) with and without nanosilica	38
Figure 7.2 The 28-days compressive strength values of concretes with and without nanosilica cured at different temperatures	38
Figure 7.3 The flexural strength of concretes with and without nanosilica at different curing temperatures for (a) 7 days, and (b) 28 days	39
Figure 7.4 The 28 days values of (a) resistivity and (b) formation factor of concretes with and without nanosilica and cured at different temperatures	39
Figure 7.5 The total pore volume of concretes with and without nanosilica cured at different temperatures	40
Figure 7.6 The correlation between the total pore volume and the value of the formation factor for concretes with and without nanosilica cured at both room and low temperatures	40
Figure 7.7 The results of water absorption for concretes with and without nanosilica after 28-day curing at (a) room temperature, and (b) low temperature	40

Figure 7.8 The results of (a) initial absorption and (b) secondary absorption of concrete with and without nanosilica at different curing temperatures	41
Figure 7.9 The cumulative mass due to scaling of concretes with and without nanosilica cured at different temperatures	42
Figure 8.1 The RapidAir system for automatic analysis of the air void system in hardened concrete	43
Figure 8.2 The average particle size of unhydrated cement in concrete samples with and without nanoadditives	49

1. INTRODUCTION

1.1 Background

Porous materials (e.g., concrete) containing moisture are susceptible to damage under repeated cycles of freezing and thawing. Concrete infrastructure in cold climates is negatively impacted by such freeze-thaw cycling, which has been commonly reported (Harnik et al., 1980; Yuan et al., 2015). Frost damage in concrete can reduce its mechanical integrity and require expensive repairs.

Supplementary cementitious materials (SCMs) have proven to be good candidates of ordinary Portland cement (OPC) replacement. SCMs are used in many cases as they can be beneficial in many ways, including decreasing permeability, aiding in pumpability and finishability, mitigating alkali reactivity and improving the overall hardened properties of concrete through hydraulic or pozzolanic activity or both (Kosmatka & Wilson, 2016; Sukhvarsh & Nicholas, 2007; Thomas, 2007; Yu et al., 2018). Furthermore, the use of SCMs can lead to a more durable concrete in long term (Berry & Malhotra, 1980; Verian & Behnood, 2018; Xu & Shi, 2018).

However, concrete containing certain SCMs (i.e., fly ash and slag) shows a slower strength gain and a higher susceptibility to scaling damage (Jeong et al., 2018; Pigeon et al., 1996; Valenza & Scherer, 2007b). As a result, many state agencies tend to limit the degree of replacement of cement by SCMs and restrict their usage during the colder parts of the year.

Even though many cases of frost damage (especially surface scaling) in the field were related to poor mix design, bad finishing, inadequate curing, etc., there is still space for improvement of durability of concrete itself by incorporating additives. Usage of nanoparticles has received widespread attention from both industry and research communities due to their distinctive physical and chemical properties (very fine particle size, high specific surface area, etc.). It is reported that nanoparticles used in concrete can accelerate the hydration process (Ma et al., 2016; Ren et al., 2018). Studies on durability properties, including porosity and chloride penetration (Ying et al., 2017) suggest that the addition of nanoparticles can improve the overall durability of concrete. However, research on the effect of nanoparticles on the scaling resistance of concrete were not found.

With the emerging of nanotechnology in concrete, research-based guidance is needed to fabricate concrete with better performance. This guidance should address the extent of nanoadditive in the concretes, the potential of the modification of nanoadditives on the performance of concretes, and potential mechanisms of such modifications, etc. The focus of the study presented in this report is to utilize the in-depth understanding of mechanism of action of nanoadditives to develop a reliable and relatively inexpensive method of improving the scaling resistance (and other durability properties) of concretes.

1.2 Project Objectives

The main objectives of this project were to do the following.

- Conduct a literature review of the current state-of-knowledge regarding the effect of nanoparticles on the durability and performance of concretes.
- Determine the influence of nano-TiO₂ on the hydration kinetics of paste specimens containing SCMs at different curing temperatures.
- Understanding the effect of adding nano-TiO₂ on the mechanical properties of mortars and concretes when cured at different temperatures.
- Determine how nano-TiO₂ modifies the durability of concretes cured at different temperatures.
- Understanding the effect of nanosilica on the durability of concretes (at different curing temperatures).
- Develop recommendations and guidance for the utilization of nanoparticles to improve the scaling resistance of concrete.

2. LITERATURE REVIEW

2.1 The Mechanisms of Freeze-Thaw and Scaling Damage in Concrete

Water is the primary agent of both, creation and destruction of many natural materials and happens to be central to most durability problems in concretes (Mehta & Monteiro, 2006). There is a 9% volume expansion when water freezes into ice. Such a property can be a major cause of many types of physical processes of degradation in porous materials.

Frost damage is a very common type of durability issue in concrete structures exposed to combined wetting/drying and freezing/thawing cycles. The consequences of frost attack on concrete can include severe spalling and scaling of the top surface (resulting in exposure of aggregates), disintegration of the bulk volume into smaller pieces, internal cracking parallel to the proposed surface, formation of gaps around aggregate, and so on.

Frost damage can be divided into two different categories: surface damage and internal damage. Figure 2.1 shows some typical examples of scaling damage of concrete.

Powers (1945) firstly proposed the hydraulic pressure is the source of stress that causes the internal frost damage in 1945. He proposed that when water freezes, it expands and generates pressure on the pore wall. Based on this theory, Powers also suggested that introducing air voids into the concrete microstructure can offer a potential way to improve the frost resistance of concrete as the extra air voids can provide more space for the expansion. However, other researchers found this mechanism by itself is not sufficient to explain some of the other sources of stress were found. A specific mechanism should be determined by different situations. Later, Powers (1975) added another theory which considered osmotic pressure to be the primary cause of excessive internal stress as he realized that the

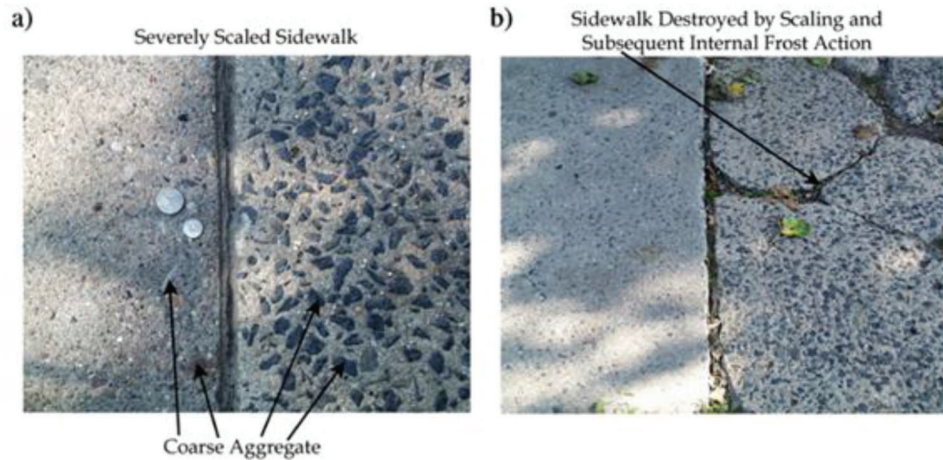


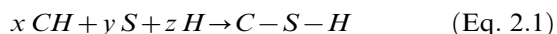
Figure 2.1 (a) Picture of a severely scaled sidewalk. (b) Sidewalk that was severely scaled, probably by internal frost damage, which led to a complete loss of mechanical integrity (Valenza & Scherer, 2007b).

temperature at which water will freeze in concrete is a function of the alkali concentration as well as the size of the pores present in the microstructure.

2.2 The Freeze-Thaw Resistance of Concrete Containing Supplementary Cementitious Materials (SCMs)

Fly ash and blast furnace slag, commonly referred to as supplementary cementitious materials (SCMs), are incorporated in concrete by replacing, typically on the weight basis, of ordinary Portland cement (15% to 25% for Class F fly ash, 15% to 40% for Class C fly ash, and 30%–50% for slag cement). As shown in Table 2.1, the sizes of SCMs can be finer than cement OPC particles, therefore, they can increase the density of concrete by filling voids between adjacent cement grains and between cement grains and aggregate particles.

In the presence of calcium hydroxide (CH), the amorphous silica (S) in fly ash (and other materials like silica fume, metakaolin, natural pozzolans, etc.) will undergo the pozzolanic reaction to form C-S-H gel (Equation 2.1):



However, a high pH is needed to start the pozzolanic reaction in cementitious system (Valenza & Scherer, 2007a), which is about 13. Normally, the pozzolanic reaction will not happen until the concrete has cured for about 3 days, when enough alkalis have been released to raise pH to about 13 and enough CH forms for the reaction.

On the other hand, slag is a latent hydraulic cement that hydrates after it is activated at high pH. In general, the hydration products are the same as those resulting from hydration of the ordinary Portland (OPC), except for a lower content of CH (Valenza & Scherer, 2007a).

In general, the particle size of fly ash is only slightly smaller than cement grains, and it takes a very long time for the amorphous silica in fly ash to be activated. Therefore, concrete containing fly ash can have a lower strength at early ages compared to OPC concrete. However, in long term (1 to 2 months), the pozzolanic reaction of fly ash can produce a very dense microstructure. Therefore, the strength of fly ash concrete will eventually be comparable or even higher than that of the OPC concrete. Similarly, concrete containing slag also shows lower early strength, though the time needed for the strength to increase above that realized with OPC concrete is much shorter (7 to 28 days) compared to the time needed for fly ash containing systems. The reason is the particle size of slag is typically smaller than that of the OPC grains.

As water demand can be reduced by incorporating some SCMs (e.g., fly ash) in concrete, especially at high substitution, durability of concrete might be improved partly because the lower w/c. However, the addition of SCMs can cause extended period of bleeding compared to OPC-only concrete, which can compromise the strength of the surface (Valenza & Scherer, 2007a). Therefore, a higher susceptibility to salt scaling might be found in concrete containing SCMs.

Salt scaling experiments on concrete containing fly ash indicate that fly ash addition reduces the resistance to salt scaling (Bilodeau et al., 1991; Gebler & Klieger, 1986; Johnston, 1987). This can be partly explained by the fact that short moist curing periods (28 days) result in lower strength. Unlike fly ash, there are very few studies on the salt scaling resistance of slag concrete. One study (Bouzoubaâ et al., 2008) indicated that the incorporation of slag can reduce the scaling resistance of concrete even when the concrete was cured for 28 days. The authors of the study indicated that the observed reduction in scaling resistance is likely due to the formation of a weak surface (with unsatisfactory quality of their air-void parameters).

TABLE 2.1

Typical physical characteristics of ordinary Portland cement and supplementary cementitious materials (SCMs) (Valenza & Scherer, 2007a)

Material	Specific Surface Area, m ² /kg	Particle Size, μm	Silica, %
Ordinary Portland cement	150–250	3–100	–
Fly ash	250–600	1–100	45–50
Slag	350–500	–	20–30

2.3 The Effect of Nano-TiO₂ on the Mechanical Properties and Durability of Cementitious Composites Containing SCMs

The nanoscale material is defined as the one that has at least one dimension that is considered to be in the nanoscale range (1 to 100 nm). As one of the most popular zero-dimensional nano materials, nano titanium dioxide (nano-TiO₂) has attracted a lot of attention in both, academia, and industry. In concrete industry, many studies indicated that TiO₂ nanoparticles can modify material microstructure, thus providing a new approach to develop high performance, durable, multifunctional, and environmentally friendly cementitious composites (Li, Ding, et al., 2018).

2.3.1 Hydration Process and Microstructure

Nano-TiO₂, as a type of zero-dimensional nanomaterial, has the “small size effect” and the “filling effect” which enables it to modify the pore structure of cementitious material (Li, Ding, et al., 2018). Porosity of nano-TiO₂-engineered cementitious composites containing fly ash is reported (by Li, Wang, et al., 2018) to decrease compared to the reference samples (without the addition of nano-TiO₂).

According to (Li et al., 2017), due the nucleation effect of nano-TiO₂, the hydration process of the cementitious composites containing fly ash is accelerated at early ages by an addition of 0.25 wt. % of nano-TiO₂. It is also reported that nano-TiO₂ can limit the growth space of CH, and therefore decrease the size of CH (Li, Wang, et al., 2018). The SEM results confirmed that the nucleation effect of nano-TiO₂ can restrict the size of CH in pastes containing fly ash, as shown in Figure 2.2 (Li et al., 2017).

Chen et al. (2012) also proposed that the addition of nano-TiO₂ will significantly accelerate the hydration rate and promote the degree of hydration of the cementitious materials at early ages. Nazari and Riahi (2011) were using ground granulated blast furnace slag as partial replacement of OPC for concrete mixtures and found out adding nano-TiO₂ into the concrete can promote the physical and mechanical properties of concrete. They proposed that the nano-TiO₂, when used as a partial (up to 3 wt.%) replacement for cement can accelerate C-S-H gel formation as a result of increased production of crystalline calcium hydroxide at early age of hydration, which can also be the reason for the observed increase in compressive strength.

2.3.2 Mechanical Properties

The mechanical properties of cementitious composites are strongly related to the type, amount, and forms of the hydration products within the matrix of the composites. Most researchers report that the compressive strength of cementitious materials can be enhanced by the incorporation of nano-TiO₂. Jalal et al. (2013) also found that the addition of nano-TiO₂ can improve the compressive strength compared to the normal concrete containing fly ash. However, such improvement has a limitation in terms of the content of nano-TiO₂ addition. Jalal et al. (2013) mentioned that using nano-TiO₂ as a partial replacement of cement at levels higher than 4 wt.% caused reduction in flexural and split tensile strength values due to the decreased crystallinity of CH (Jalal et al., 2013).

2.3.3 Durability

The durability of cementitious materials can be largely influenced by freeze-thawing cycles in places which has cold winter. Taking advantage of admixtures to improve the freeze-thaw resistance of cementitious materials can be of great benefit to the durability of construction applications. Applying nano-TiO₂ in cementitious materials has been proven to be helpful to improve durability by decreasing the strength loss after freeze-thawing cycles of cementitious material by some research (Li et al., 2017; Salemi & Behfarnia, 2013). According to Salemi et al. (2014), the strength loss of cementitious composites containing 2 wt.% nano-TiO₂ particles is lower than that of control cementitious composites after 300 freeze-thaw cycles. The reason can be concluded as follow: nano-TiO₂ works as nuclei and accelerate the cement hydration to obtain more C-S-H, which contributes to higher strength; the pressure generated by the volume change of water in the pores decreases due to the decreased porosity. As a result, the freeze-thawing resistance can be improved by adding nano-TiO₂ in cementitious materials (Li, Ding, et al., 2018). Mohseni et al. (2015) found out that nano-TiO₂ has the tendency to decrease the chloride permeability.

2.4 The Effects of Nano-Silica on the Performance of Cementitious Composites

Nano-scaled silica (nano-silica) can also work as nano-admixture in concrete. As Singh et al. (2013)

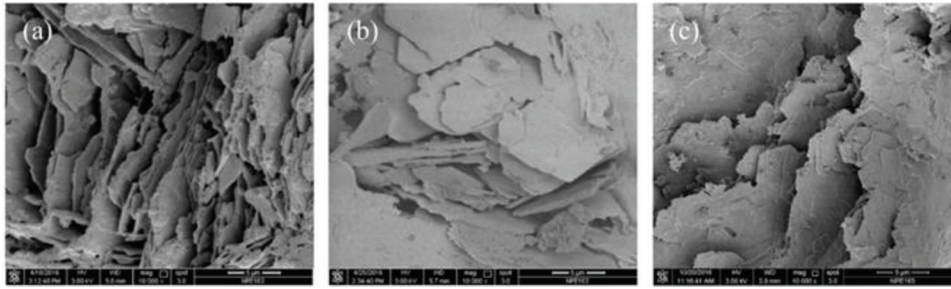
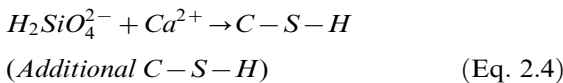
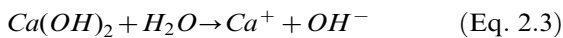
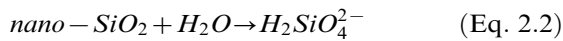


Figure 2.2 SEM image of CH in T-engineered cementitious composites at curing age of 28 days: (a) without the addition of nano-TiO₂; (b) with 0.78 vol.% of nano-TiO₂; and (c) with 2.32 vol.% of nano-TiO₂ (Li et al., 2017).

point put, applying nano-silica in cementitious materials can be beneficial for strength and durability enhancements, which are the results of pore structure refining and hydration accelerating effects of the nano-silica. The potential impacts of adding nano-silica in cementitious composites are presented in Figure 2.3. Based on literature review, the mechanisms of such impacts of nano-silica on cementitious materials are concluded as follows: (1) pore-filling effect: the addition of nano-silica can enhance the particle packing density of cementitious system, which can lead to a lower water demand of the mixture and a higher strength (due to the reduced capillary porosity) (Singh et al., 2013); and (2) pozzolanic reactivity—nano-silica has a much higher pozzolanic reactivity compared to silica fume (Hou et al., 2013; Madani et al., 2012) due to its higher specific surface area. The pozzolanic reaction of nano-silica are listed below (Singh et al., 2013):



2.4.1 Hydration and Microstructure

Pastes with the addition of nano-silica showed reduced setting time, shortened duration of dormant and induction period of hydration, shortening of time to reach peak heat of hydration and increased production of calcium hydroxide at early ages (Madani et al., 2012; Senff et al., 2009). As aforementioned, nano-silica has a much higher pozzolanic reaction rate than silica-fume, which is related to the higher specific surface area. This can contribute to the acceleration of hydration process in pastes with the addition of nano-silica.

The microstructure of the cementitious materials with nano-silica is found to be denser and more compact with lesser amount of calcium hydroxide crystals (Jo et al., 2007b). According to (Said et al., 2012), significant densification was observed in the matrix at

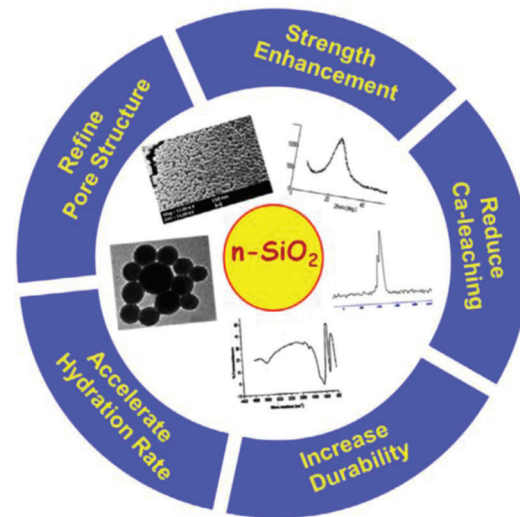


Figure 2.3 Potential impacts of nano-silica in cementitious composites (Singh et al., 2013).

the interfacial transition zone (ITZ) for specimens with nano-silica.

2.4.2 Mechanical Properties

Experimental results show that the compressive strengths of mortars with nano-silica were all higher than those of mortars containing silica fume at 7 and 28 days (both types of mortars have a higher compressive strength than reference mortars) (Jo et al., 2007a). This can be related to the fact that C-S-H formation is quicker by nano-sized silica compared to silica fume. Nanoindentation test was performed to study the mechanical properties of nano-silica modified cement pastes (Mondal et al., 2010), and it was found that the modulus of elasticity and hardness were improved compared to the reference pastes.

Compressive strength of concrete with the addition of nano-silica is higher than reference concrete to a significant level (Riahi & Nazari, 2011; Said et al., 2012). Ji (2005) pointed out that applying a small amount of nano-silica in concrete containing Class F fly ash can be beneficial as the inherently slower rate of strength development can be controlled by the

increased strength due to the addition of nano-silica. Riahi and Nazari (2011) reported the addition of nano-silica in concrete can improve the abrasive resistance and compressive strength of concretes.

2.4.3 Durability

Calcium hydroxide is very susceptible to leaching in cementitious materials, and the addition of nano-silica can reduce this issue, which is related to its ability to modify the porosity of cement pastes and increase the average chain length of silicate chains (Gaitero et al., 2008; Singh et al., 2012). The increased silicate chain length is also related to the improved resistance to chemical attacks and calcium stabilization.

Many studies have been carried out to investigate the effect of nano-silica on the durability of concrete (Said et al., 2012; Zhang & Li, 2011). Nano-silica can reduce the water absorption, capillary absorption, rate of water absorption, and water permeability compared to reference concretes. Zhang and Li (2011) reported the refined pore structure, considerably reduced permeability, and reduced chloride ion penetration in their study. Said et al. (2012) presented that the total porosity and threshold pore diameter were considerably lowered, confirmed by the mercury intrusion porosimetry (MIP) test.

3. MATERIALS

3.1 Aggregates

Crushed limestone, meeting the requirements of Section 904.03 of the Indiana Department of Transportation (INDOT) Standard Specification for No. 8 Stone (INDOT, 2020b) was used as coarse aggregate. The maximum size of the coarse aggregate was 1.0 in. (25 mm). The coarse aggregate was obtained from the US Aggregates plant in Delphi, IN. The fine aggregate used was a natural siliceous sand meeting the requirements of Section 904.02 of INDOT's Standard Specification for No. 23 Aggregate (INDOT, 2020b). The sand was obtained from the US Aggregates Swisher Plant in Battleground, IN. The physical properties of aggregates are shown in Table 3.1. The gradation of both coarse and fine aggregates is illustrated in Figure 3.1.

3.2 Cementitious Materials and Nanoparticles

The ASTM C150M-20 Type I Portland cement (OPC) was used in this study. The ASTM C618-19

Class C fly ash (FA) and Grade 100 slag cement were used in this study as the supplementary cementitious materials. The chemical compositions of cementitious materials are provided in Table 3.2. Figure 3.2 presents the particle size distribution of OPC, fly ash, and slag cement used in this study, obtained using particle size analyzer. The reported results represent the average from three replicate samples for each type of material. The analysis was performed using liquid (isopropanol) dispersion method. Fraunhofer model was used to drive the data analysis of particle size distribution. The results show that slag cement particles have a finer size than that of the OPC and fly ash.

Nano-TiO₂ particles were used in this study. Figure 3.3 shows the image of the cluster of the particles of the nano-TiO₂ provided by US Research Nanomaterials, Inc. The XRD analysis of the nano-TiO₂ particles has shown that the only phase present in the material was anatase (see Figure 3.4). Table 3.3 provides the physical properties of the nano-TiO₂ particles.

Nanosilica was used in this study as a second type of nano-additives. There are two different types of nanosilica: E5-LFA (short for E5-liquid fly ash) and E5-IC (E5-internal curing), and both are proprietary products. According to the manufacturer, E5-LFA can achieve the same pozzolanic reactivity as traditional SCMs, promotes secondary C-S-H development, and create better interfacial bonds. Furthermore, E5-IC can control the water of transport and the water of convenience to cure, eliminate wet curing and topical curing compounds, increase finishability and workability, and reduce drying shrinkage and curling. Figure 3.5 presents the schematic of the relative size of E5 nanosilica and cement grains.

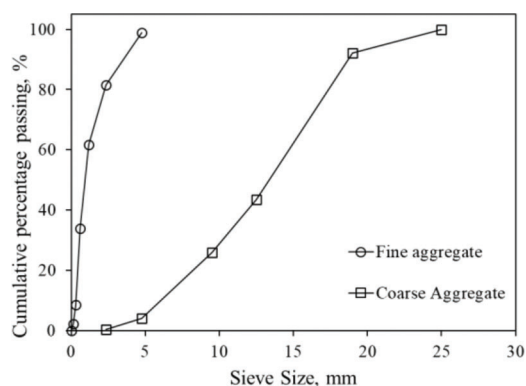


Figure 3.1 The gradation curves of coarse and fine aggregates.

TABLE 3.1
Properties of coarse and fine aggregate

Aggregates	Specific Gravity (SSD)	Absorption, %	Specification
Coarse aggregate	2.61	2.28	INDOT Section 904.03
Fine aggregate	2.74	1.97	INDOT Section 904.02

TABLE 3.2
The chemical composition of Type I Portland cement, fly ash, and slag cement used in this study

Oxide/Phase, wt. %	Type I OPC	Class C Fly Ash	Grade 100 Slag
Silicon dioxide/SiO ₂	19.55	41.62	34.57
Aluminum oxide/Al ₂ O ₃	5.22	18.07	9.65
Iron oxide/Fe ₂ O ₃	2.74	6.06	0.73
Calcium oxide/CaO	62.91	21.81	40.69
Magnesium oxide/MagO	2.94	5.25	10.76
Sulfur oxide/SO ₃	3.22	1.08	1.75
Sodium oxide/Na ₂ O	0.69	1.58	0.34

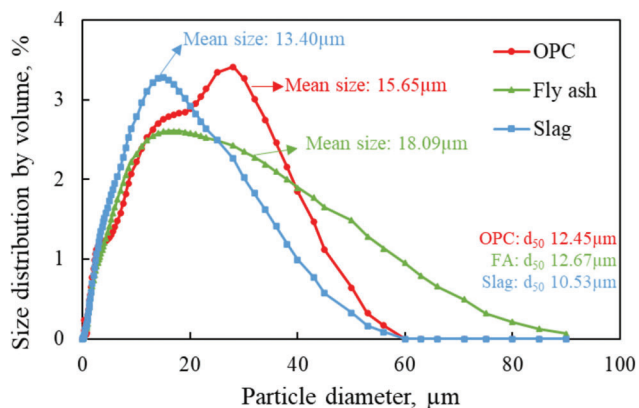


Figure 3.2 The results of particle size analyzer (PSA) for cementitious materials (OPC, fly ash, and slag) used in this study.

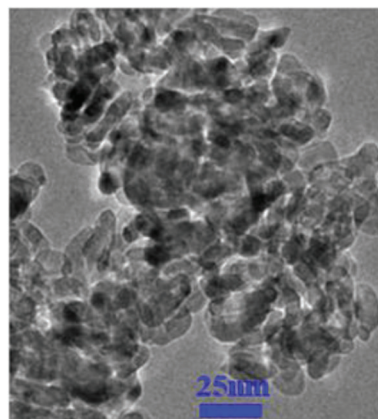


Figure 3.3 Transmission electron microscopy images of the particles of nano-TiO₂ (US Research Nanomaterials, n.d.).

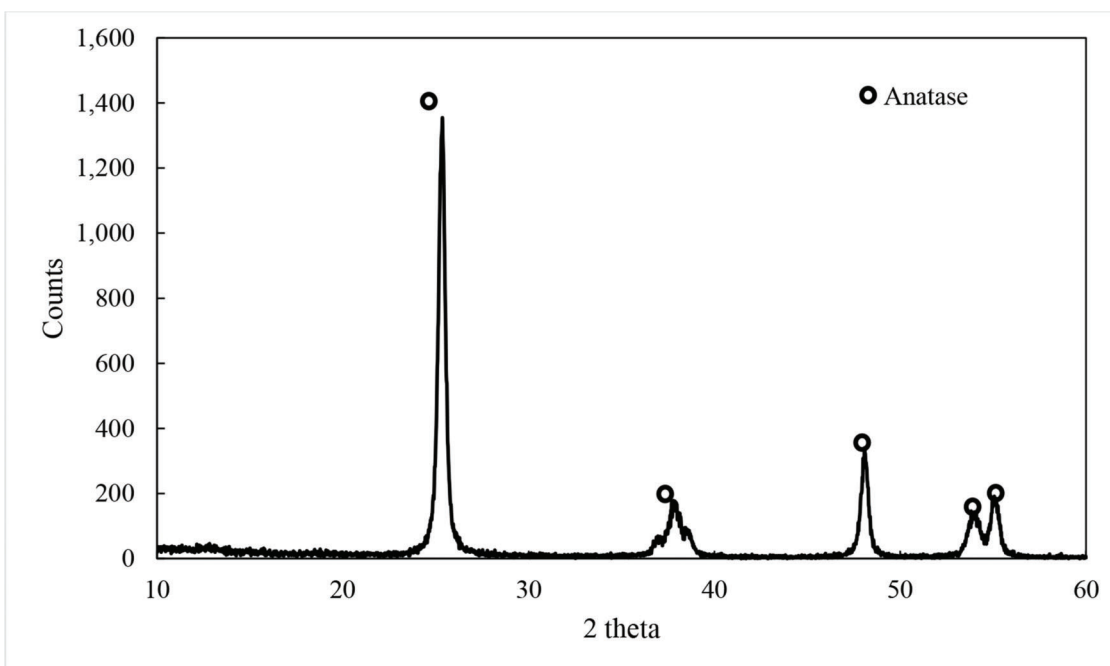


Figure 3.4 XRD patterns of nano-TiO₂ used in this study.

3.3 Chemical Admixtures

Air entrainer (satisfying ASTM C260-16) was used when air-entrainment was required. The ASTM C494-19

high-range water-reducing admixture (HRWR) was used during mixing to ensure adequate level of workability and aid with the dispersion of nano-TiO₂

TABLE 3.3
Physical properties of TiO₂ nanoparticles (US Research Nanomaterials, n.d.)

Purity	APS ^a	SSA ^b	Density
99.9%	18 nm	200–240 m ² /g	0.24 g/cm ³

^aAPS: average particle size.

^bSSA: specific surface area.

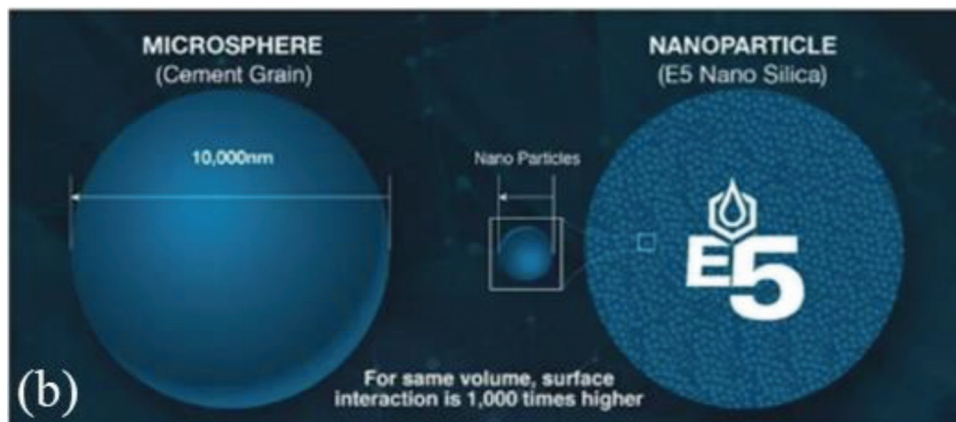
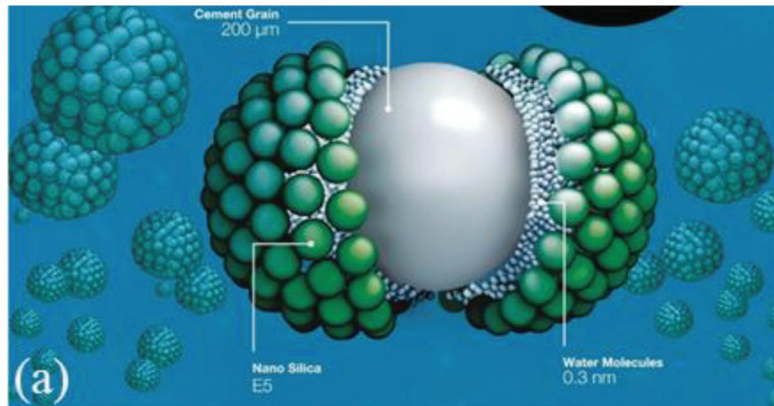


Figure 3.5 Schematic of the relative sizes of E5 nanosilica and cement grains (ENR, 2021).

(Li, Ding, et al., 2018). A constant amount of HRWR (0.25 wt.% of the total weight of the cementitious materials) was used in all mixtures.

4. IMPACT OF CURING TEMPERATURE ON THE EFFECT OF NANO-TiO₂ ON THE HYDRATION PROCESS OF CEMENT PASTES CONTAINING SCMs

4.1 Preparation of Specimens and Testing Methods

4.1.1 Preparation of Specimens

Mixture proportions of pastes used in this study are shown in Table 4.1. As can be seen, pastes were prepared using three different types of binders: cement only (OPC), OPC + 24% (by total weight of cementitious

materials) of fly ash (FA) and OPC +30% (by weight of total cementitious materials) of slag cement (S). Different levels (0%, 0.5%, 1%, and 2%) of nano-TiO₂ were added as the weight percentages (wt.%) of the total cementitious materials (i.e., the total weight of OPC, OPC+FA, or OPC+slag).

The component materials were all conditioned at room temperature and weighted before mixing. Paste samples were prepared according to the requirements of ASTM C305-20. All batch water and HRWR were pre-mixed (by hand) in a small container first, and then the nano-TiO₂ was added into the same container and mixed for a few minutes by hand. The resulting liquid-solid mixture (slurry) was then transferred to the mixing bowl of the mechanical mixer. The dry cementitious materials were added next, and all components were then mechanically mixed following the procedure given

TABLE 4.1
Mixture proportions of nano-TiO₂ modified cement pastes in this study (ratios are calculated based on weight basis)

Sample Type	Sample	FA (or slag)/Cem ^a	Water/(SCMs+OPC)	Nano-TiO ₂ (wt.%)
Paste	OPC-0T	–	0.45	0
	OPC-0.5T	–		0.5
	OPC-1T	–		1.0
	OPC-2T	–		2.0
	FA-0T	0.24	0.45	0
	FA-0.5T			0.5
	FA-1T			1.0
	FA-2T			2.0
	S-0T	0.30	0.45	0
	S-0.5T			0.5
	S-1T			1.0
	S-2T			2.0

^aNote: Cem = total wt. of cementitious materials.

in ASTM C305-20. Once mixed, the fresh pastes were used to cast specimens designed for the corresponding tests. Once cast, the specimens were stored in the molds for 24 hours (at 23°C). After that, pastes specimens were demolded and cured at two different temperatures (room or standard = 23°C and low = 4°C) in lime-saturated water until the time of testing.

4.1.2 Testing Methods

4.1.2.1 Isothermal calorimetry (IC). In this study, the isothermal calorimetry (IC) test was used to study the kinetics of hydration of pastes with and without the addition of nano-TiO₂. The IC tests were performed using the Tam Air isothermal calorimeter from TA Instruments following the procedure outlined in ASTM C1702-17. The tests were performed at both room (23°C) and low (4°C) temperatures and the instrument recorded the total heat evolved, and the rate of heat evolution (thermal power).

To prepare pastes for IC test, the mixing water, and the cementitious materials, as well as the glass mixing rod and the glass mixing vessel, were all conditioned at the corresponding temperatures (23°C or 4°C) for at least 24 hours before mixing. At the end of the conditioning period, the water was added to the cementitious material contained in the glass vessel and mixed using the glass rod. The resulting paste (around 10 grams) was then transferred to the ampules used for the IC test. The entire process (from the moment of combining cementitious materials with water to placing the ampules in the calorimeter) took less than 5 minutes. The data collected during the initial 45 minutes after mixing of water with cementitious materials were excluded from the analysis as the samples were in the process of thermal equilibration. The measurements were performed over a period of up to 50 hours from the time of the addition of water.

4.1.2.2 Thermal indicator of setting time. According to ASTM C1679-17, the IC test results can be used to determine so called “thermal indicator of setting time” of cementitious mixtures, which is defined as “the hydration time to reach a thermal power of 50% of the maximum value of the main hydration peak.” This data was used as a supplementary information to aid in evaluating the effects of nano-TiO₂ on the hydration process of cement pastes characterized in this study.

4.1.2.3 Vicat setting time. Setting time was measured according to ASTM C191-19 Method A using Vicat needle. The determination of the Vicat setting time was performed on pastes with normal consistency as defined in the ASTM C187-16. This procedure enabled a direct comparison between samples with different levels of nano-TiO₂ addition. The Vicat penetration depth was measured every 15 minutes until final setting.

4.1.2.4 Thermogravimetric analysis (TGA). Since the TGA is age-sensitive (i.e., the test reveals the extent of hydration at a given age) if data is required at a particular age the condition of the specimen at that particular age needs to be preserved by stopping the hydration process (Scrivener et al., 2016). To prepare the TGA specimens freshly mixed pastes were cast in cylindrical plastic containers (diameter of 25 mm and the height of 12 mm) and cured at different temperatures (23°C and 4°C) in the environmental chambers. At desired testing age (i.e., after 3, 7, or 28 days of curing) hardened pastes were removed from the plastic containers and small pieces of the material were broken-off from the body of the cylinder. These broken-off pieces were then immersed for 10–15 minutes in an isopropanol in order to replace the pore water and thus stop the hydration process (Scrivener, 2016). Subsequently, the isopropanol was washed-off from the samples by soaking them in the diethyl ether for 30 sec. Samples were then dried in an aerated oven at a

temperature of 40°C for no more than 10 minutes and ground to pass the #200 (75 μm) sieve. The weight percentage of hydration products was determined using the TA Instruments 2050 thermogravimetric analyzer. During the test, the powder samples were heated up from room temperature (around 20°C) to 900°C at a constant rate of 10°C/minutes. The sizes of the test samples were around 20 mg. A 99.9% pure N₂ gas was used as a purge gas to provide an inert environment when operating the TGA instrument. The curves of weight loss of samples versus temperature were captured and analyzed to calculate the weight loss due to the decomposition of hydration product (C-S-H, ettringite, etc.). The quantification of calcium hydroxide can be achieved by applying the modified interpretation developed by Kim and Olek (2012).

Table 4.2 presents the information of the physical and chemical processes (and the corresponding temperature ranges) taking place in a typical cementitious system during the TGA testing (Hager, 2013). These processes are mainly associated with decomposition of C-S-H, ettringite, and calcium hydroxide (CH) phases, which are the most abundant hydration products in cementitious systems based on the OPC (Scrivener et al., 2019). Typically, most of the hydration products lose water from the beginning of the TGA test (at about 20°C) up to the end of decomposition of CH phase (at around 450°C).

4.2 Results and Discussions

4.2.1 Rate and Total Heat of Hydration

The rate and total heat of hydration of cementitious materials were evaluated by IC. As shown in Figure 4.1 a and b, the addition of nano-TiO₂ to both the room temperature cured and the low temperature cured OPC pastes increases the values of the heat flow, as indicated by the higher maximum heights of the peaks for specimens with nano-TiO₂ (dotted lines) compared to the heights of the peaks for pastes without nano-TiO₂ (solid lines). In addition, the main hydration peaks for pastes with nano-TiO₂ appeared earlier when compared to the main hydration peaks for pastes without nano-

TiO₂ (as indicated by the black arrows shown in Figure 4.1). Since the heat flow (thermal power) curves reflect the rate (kinetics) of hydration, the increase in the maximum values of these peaks, and shortening of time needed to reach their maximum values, indicate that hydration process of specimens with nano-TiO₂ was faster compared to hydration process of specimens without the nano-TiO₂. Similarly, the total heat of hydration values (as indicated by the cumulative heat curves) was higher for the pastes with nano-TiO₂ when compared to pastes without nanoparticles. That indicates that the extent of cement hydration reactions in pastes with nano-TiO₂ was greater than that observed in pastes without nano-TiO₂.

As shown in Figure 4.1b, when cured at low temperature, the hydration reactions of OPC pastes slowed down significantly, as both the maximum values of the heat flow peaks and maximum values of the cumulative heat curves were much lower than the corresponding results shown in Figure 4.1a. That 50-hour reaction period was just long enough to capture the majority of the heat flow peaks for OPC pastes. The addition of nano-TiO₂ seems to be more effective in accelerating the hydration process when curing temperature was low. This is clearly illustrated by larger values of the time shift of the maximum value of the main hydration peaks due to the addition of nano-TiO₂ in low temperature cured pastes compared to the time shift values observed in pastes cured at room temperature (see Table 4.3). It should also be noted that, regardless of the curing temperature, the increase in the nano-TiO₂ addition increases the time shift values.

Figure 4.2 a and b present the normalized heat flow and the normalized cumulative heat curves for fly ash pastes cured at room and low temperatures, respectively. The trends on the acceleration of hydration observed in fly ash pastes with respect to the effects of nano-TiO₂ were very similar to those observed in the OPC pastes (Figure 4.2).

As presented in Table 4.4, the acceleration of hydration process (as indicated by the shift in the position of the maximum value of the main hydration peak) for low temperature cured fly ash pastes containing nano-TiO₂ was considerably greater than that observed for the same type of pastes but cured at room temperature. Specifically, for each curing temperature and for each percentage of nano-TiO₂, the time shift for the location of the main hydration peak was greater in samples containing fly ash than in OPC samples (compare values in Table 4.3 vs. values in Table 4.4). These results suggest a greater effect of nano-TiO₂ on hydration process of fly ash pastes when compared to OPC pastes.

Lastly, the normalized heat flow and the normalized cumulative heat curves for slag pastes cured at room and low temperatures are presented in Figure 4.3 a and b. Although the same effect of addition of nano-TiO₂ on the acceleration of hydration in slag paste was also observed in this case, that effect was not very significant compared to that observed in the case of

TABLE 4.2
Physical and chemical changes in concrete as a function of temperature (adopted from Hager, 2013)

Temperature (°C)	Physical/Chemical Effect
20–200	Loss of capillary water
70–80	Dissociation of ettringite
120–160	Dehydration of gypsum to hemihydrate and anhydrite
200–350	Loss of bound water from cement paste (C-S-H)
400–450	Calcium hydroxide (CH) loses water
575	Quartz changes from α to β form (volume increase)
600–850	Decomposition of carbonates

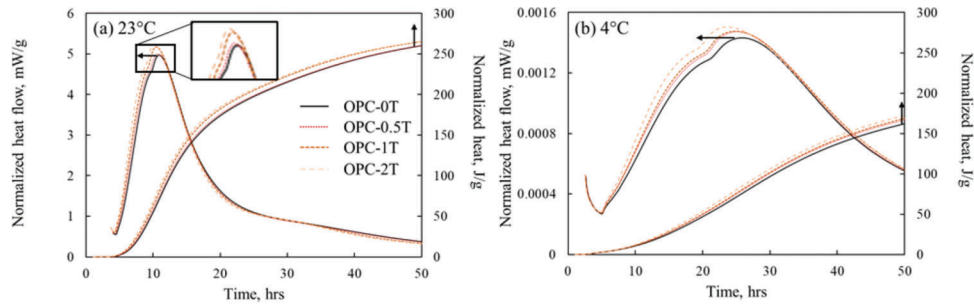


Figure 4.1 The normalized heat flow and normalized cumulative heat curves for OPC pastes cured at (a) room temperature (23°C), and (b) low temperature (4°C).

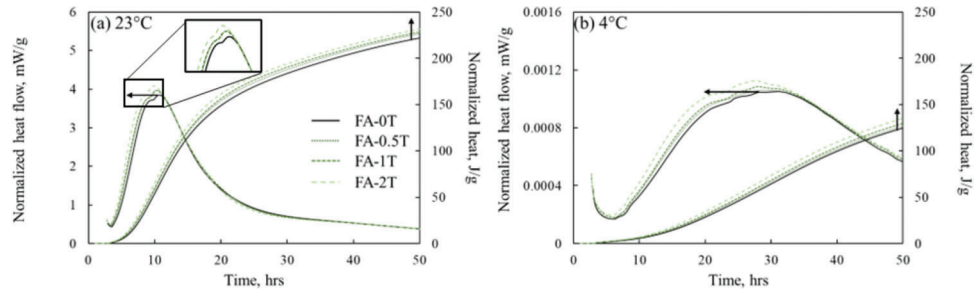


Figure 4.2 The normalized heat flow and normalized cumulative heat curves for fly ash pastes cured at (a) room temperature (23°C), and (b) low temperature (4°C).

TABLE 4.3

The time shift of the maximum value of the heat flow peak due to the addition of nano-TiO₂ to OPC pastes (relative to the time for maximum value of the heat flow peak for pastes without nano-TiO₂)

Curing Temperature	Mixture	Time Shift of the Max Temperature Peak, Min ^a
23°C	OPC-0.5T	-14
	OPC-1T	-26
	OPC-2T	-43
4°C	OPC-0.5T	-43
	OPC-1T	-59
	OPC-2T	-129

^aWith respect to the location of the maximum temperature peak of mixtures without nano-TiO₂ addition.

TABLE 4.4

The time shift of the maximum value of the heat flow peak due to the addition of nano-TiO₂ to fly ash pastes (relative to the time for maximum value of the heat flow peak for pastes without nano-TiO₂)

Curing Temperature	Mixture	Time Shift of the Max Temperature Peak, Min ^a
23°C	FA-0.5T	-20
	FA-1T	-26
	FA-2T	-50
4°C	FA-0.5T	-143
	FA-1T	-178
	FA-2T	-207

^aWith respect to the location of the maximum temperature peak of mixtures without nano-TiO₂ addition.

OPC (Figure 4.3) and, in particular, in the case fly ash pastes (Figure 4.2).

Table 4.5 summarizes the changes in the position of the maximum of the main hydration peak resulting

from the addition of nano-TiO₂ to slag pastes. Although the addition of nano-TiO₂ accelerated the hydration of slag pastes at both of the studied curing temperatures, in some cases (e.g., S-0.5T paste) this

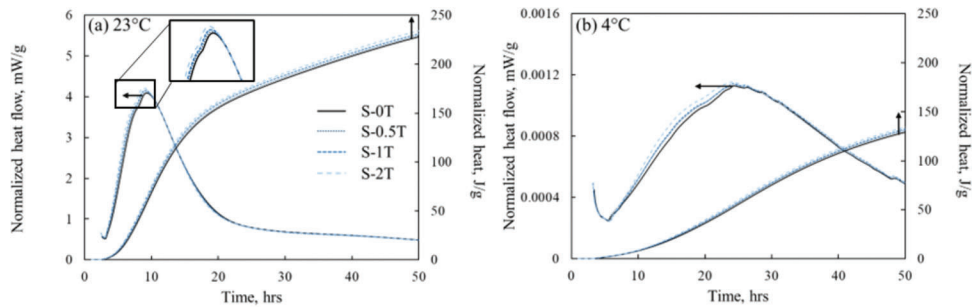


Figure 4.3 The normalized heat flow and normalized cumulative heat curves for fly ash pastes cured at (a) room temperature (23°C), and (b) low temperature (4°C).

TABLE 4.5

The time shift of the maximum value of the heat flow peak due to the addition of nano-TiO₂ to slag pastes (relative to the time for maximum value of the heat flow peak for pastes without nano-TiO₂)

Curing Temperature	Mixture	Time Shift of the Max Temperature Peak, Min. ^a
23°C	S-0.5T	-8
	S-1T	-14
	S-2T	-26
4°C	S-0.5T	-0.7
	S-1T	-13
	S-2T	-19

^aWith respect to the location of the maximum temperature peak of mixtures without nano-TiO₂ addition.

acceleration was negligibly small. Furthermore, in this case, the accelerating effect of nano-TiO₂ was much less prominent compared to that observed in the OPC and fly ash pastes. Besides, in pastes with slag, the acceleration of hydration due to the use of nano-TiO₂ was greater for samples cured at 23°C than in samples that were cured at lower temperature, while for plain cement paste and cement paste with fly ash, the greater effect of nano-TiO₂ was observed at lower curing temperature.

In summary, the test results obtained from the IC experiments indicates that nano-TiO₂ is more effective in accelerating the hydration in cases when fly ash is used as a replacement for part of the cement and when curing temperature is low (except for cement pastes with slag).

4.2.2 Thermal Indicator of Setting Time of Pastes

As mentioned previously (Section 4.1.2.2) the IC data can be used to obtain a thermal indicator of the setting time of the hydrating system. For a given mixture, the thermal indicator of the setting time is a relative value, which can be correlated with a physical setting time determined using such methods as ASTM C191-19 (Vicat needle). Figure 4.4 shows an example regarding how to obtain the thermal indicator of the setting time from the IC data.

Figure 4.5 shows the variation in the setting time (based on the thermal indicator data from the IC method) for the OPC, fly ash, and slag mixtures as a function of the level of nano-TiO₂ addition and the curing temperatures. As can be seen, the addition of

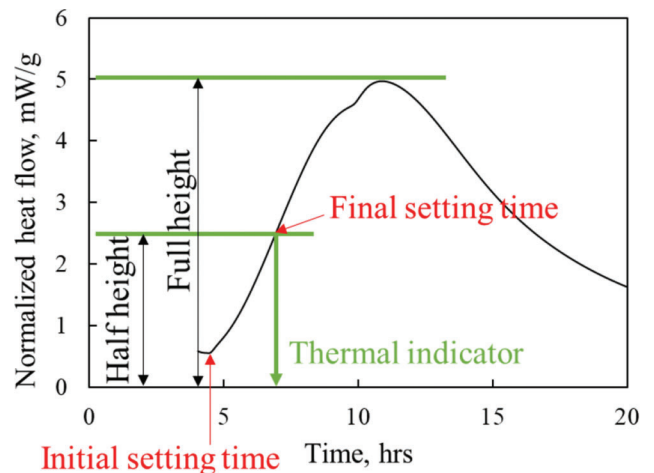


Figure 4.4 An example illustrating the way to obtain the thermal indicator of setting time using the heat flow curve from IC experiment.

nano-TiO₂ shortens the setting time for OPC, fly ash, and slag mixtures, regardless of the curing temperatures. Furthermore, the increase in the percentage of the added nanoTiO₂ resulted in the shortening of the thermal indicator of the final setting time.

For slag pastes cured at room temperature the values of the IC-based setting time were always lower than those of the OPC pastes. However, when the same types of pastes were cured at low temperature, their setting times very comparable, further underscoring the fact that addition of nano-TiO₂ was more effective in the

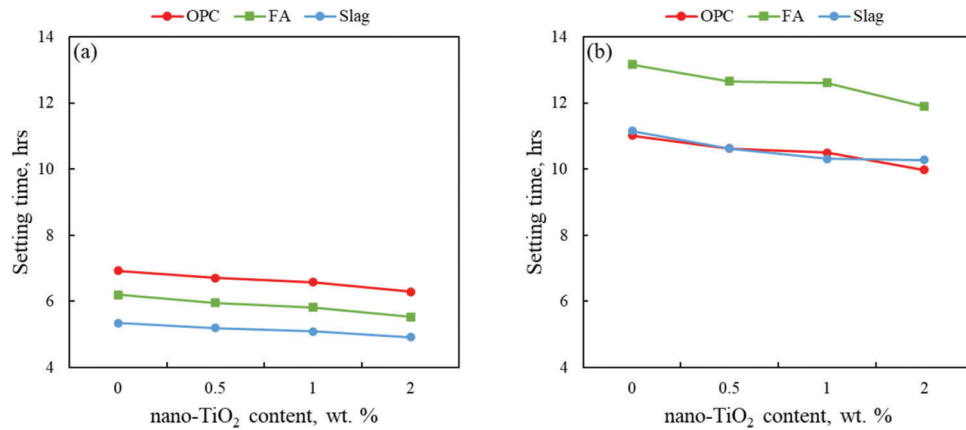


Figure 4.5 The variation in the final setting time (based on the thermal indicator data from the IC method) as a function of the nano-TiO₂ addition for the OPC, fly ash, and slag pastes cured at (a) room temperature (23°C), and (b) low temperature (4°C).

TABLE 4.6
Shortening of the setting time (based on the thermal indicator data from IC method) for OPC, fly ash, and IC pastes with 2% of nano-TiO₂ cured at room and low temperatures

Curing Temperature	Mixture	Shortening of Setting Time, min ^a
23°C	OPC	38
	FA	41
	Slag	25
4°C	OPC	63
	FA	76
	Slag	53

^aCalculated with respect to setting time of specimens without nano-TiO₂ addition.

case of OPC than in the case of slag mixtures. Table 4.6 shows the summary of the actual values of the reduction of setting times for OPC, fly ash, and slag pastes containing 2% of nano-TiO₂ addition and cured at room and low temperatures.

When comparing the values of the shortening of the setting time, it can be observed that nano-TiO₂ seems to be more effective in accelerating the setting when the curing temperature is low compared to room temperature for OPC, fly ash, and slag mixtures.

4.2.3 Setting Time

Figure 4.6 shows the variation of the Vicat setting time as a function of the percentage of the nano-TiO₂ addition for the OPC, fly ash, and slag pastes tested at standard temperature (23°C). The effects of nano-TiO₂ on the setting time of OPC, fly ash, and slag pastes are similar, in a sense that both the initial and the final setting times of all three types of pastes were reduced due to the addition of nano-TiO₂. Moreover, as shown in Table 4.7, the addition of 1% of nano-TiO₂ seems to reduce the setting time of slag pastes to a larger extent compared to OPC and fly ash pastes.

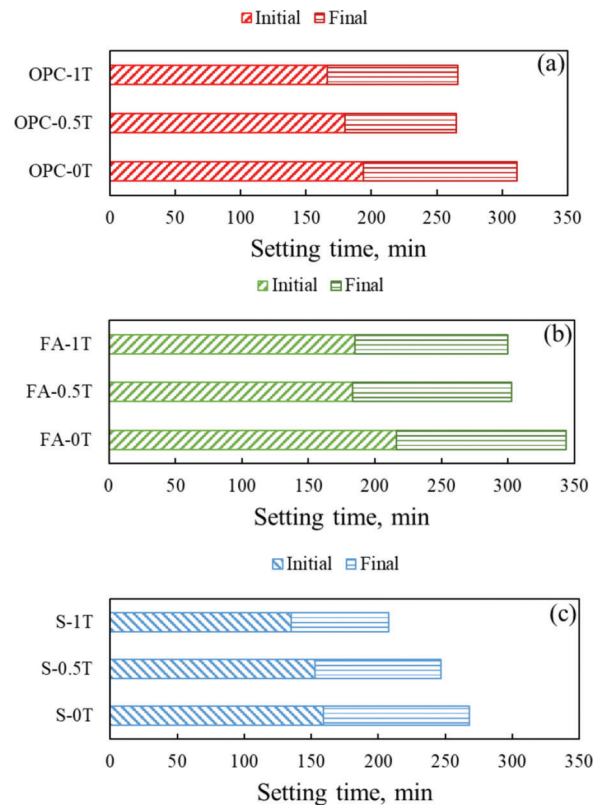


Figure 4.6 The variation of Vicat setting time as a function of the nano-TiO₂ addition for (a) OPC, (b) fly ash, and (c) slag pastes tested at standard temperature (23°C).

4.2.4 Amount of Hydration Product

The changes in the content of calcium hydroxide (CH) in the hydrating cementitious system can be used to evaluate the kinetic of hydration as CH is a byproduct of the primary hydration reaction. This approach works in cases when there is only the ordinary Portland cement (OPC) presents as cementitious binder in the hydrating system is. Nevertheless, the CH

TABLE 4.7
Shortening of the Vicat setting time for OPC, fly ash, and slag pastes with 1% of nano-TiO₂ addition tested at standard temperature (23°C)

Samples	A-P	A-F	A-S
Reduction in setting time, 1% of nano-TiO ₂ ^a	45 min	44 min	60 min

^aCalculated with respect to the setting time of specimens without nano-TiO₂ addition.

content might not be a good indicator of the degree of hydration in samples with the blended binders (e.g., in the system containing both, the cement and the fly ash, and the cement and the slag cement), as the changes in the CH content will reflect the combined effects of cement hydration (addition of CH) and pozzolanic reaction (consumption of CH). Therefore, rather than focusing exclusively on the changes in the CH content (the degree of weight loss in the temperature ranges from 400°C to 450°C in TGA test) as an indicator of the hydration process, a broader temperature range should be considered when evaluating the amount of hydration products when SCMs is present as part of the cementitious binder.

The temperature range selected for this study when evaluating the influence of nano-TiO₂ on the hydration process of OPC, fly ash, and slag pastes was from 20°C to about 450°C (the temperature where the CH decomposition ends). As mentioned earlier (Section 4.1.2.4), the free water initially present in the specimens was removed by the solvent exchange procedure, any weight changes taking place in this broader temperature range should only capture the removal of the chemically/structurally bound water in the phases of interest, i.e., C-S-H, ettringite, monosulfate, CH, and other hydration products. Changes in the amounts of these phases can be used as indicators of the kinetics of hydration as higher weight losses in the TGA results will indicate higher amount of hydration products, and thus an accelerated rate of the hydration process.

4.2.4.1 The influence of nano-TiO₂ on the amount of hydration products. For instance, Figure 4.7 shows the TGA curves for OPC pastes with and without nano-TiO₂ cured for 3 days at low temperature. The TGA results from the reference sample OPC-0T (0 wt.% of nano-TiO₂ addition) were presented by the solid green line, whereas the dashed green line represents paste containing 2% of nano-TiO₂ (OPC-2T). The amount of hydration products (assumed to be directly proportional to the weight loss in the temperature range from 20°C to about 450°C) increases because of the addition of nano-TiO₂. This indicates that for this particular case (3-day old OPC pastes cured at low temperature), the addition of nano-TiO₂ accelerates the hydration process. As mentioned in the literature review part, such acceleration of hydration can be explained by the fact that nano-TiO₂ particles serve as the nucleation sites for the formation of the hydration products.

Figure 4.8 a and b present the overall trends in the amounts of the hydration product obtained from TGA results for the *OPC pastes* with varying amounts of added nano-TiO₂ and cured for 3, 7, and 28 days at room and low temperatures, respectively. When cured at room temperature, the addition of nano-TiO₂ accelerated the hydration process, if at early ages (3 and 7 days, green and blue lines, respectively), but not at later age (28 days-yellow line).

A plateau can also be observed that the lines representing 3-day and 7-day results past the 1.0 wt.% of nano-TiO₂ addition. This similar observation is also reported by other researchers (Jalal et al., 2013; Nazari & Riahi, 2010; Zhang & Li, 2011), which argue that the space available for the growth of various hydration products within the cementitious system is limited when a higher dosage of nano-TiO₂ is added. To a certain degree, this hypothesis is corroborated by the results from specimens cured for 28 days, which show the decreasing trend in the amount of hydration products with the increase in the addition level of the nano-TiO₂ past 0.5% (as shown by the solid yellow line). At the end of 28-days, it is likely that most of the cement phases have already reacted and the addition of higher amounts of nano-TiO₂ is not promoting more hydration due to the lack of space.

When OPC paste samples was cured at low temperature, see Figure 4.8b, nano-TiO₂ also seems to have accelerated the hydration process. Compared to specimens cured at room temperature, the acceleration of hydration process due to the addition of nano-TiO₂ happened at both, later ages and at higher contents of nano-TiO₂. As evident from the trends shown by the green and blue lines in Figure 4.8b, 2.0 wt.% addition of nano-TiO₂ still accelerates the hydration process of OPC pastes cured at low temperature for 3 days and the addition of up to 1% of nano-TiO₂ accelerates the hydration process for both 7 days and 28 days. Therefore, it appears that since the low temperature significantly slows down the hydration process, the addition of nano-TiO₂ is more effective at low temperature when compared to its effects at room temperature.

Figure 4.9 a and b present the amounts of hydration product obtained from the TGA results for *fly ash pastes* with different levels of nano-TiO₂ addition after 3, 7, and 28 days of curing at room temperature and low temperature. The trends shown in Figure 4.9a are similar to those shown in Figure 4.8a. Nevertheless, as indicated by the slopes of the green and blue lines, a more significant acceleration of hydration was observed in fly ash pastes compared to OPC pastes, especially at early ages. This might be related to the addition of nano-TiO₂ that was reported to reduce the size of CH crystals (Li, Ding, et al., 2018). The smaller crystals of CH may be accelerating the rate of the pozzolanic reaction, thus producing higher amount of C-S-H (and other hydrates) which will lead to higher weight losses in the temperature range of interest (20°C to about 450°C) in the fly ash pastes.

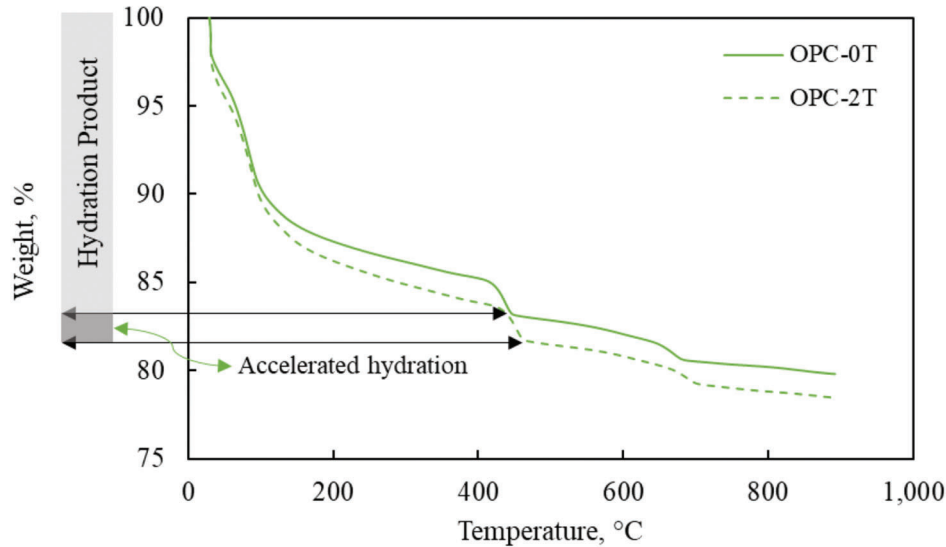


Figure 4.7 The TGA results of OPC paste with 0% and 2% of TiO_2 nanoparticles cured for 3 days at low temperature.

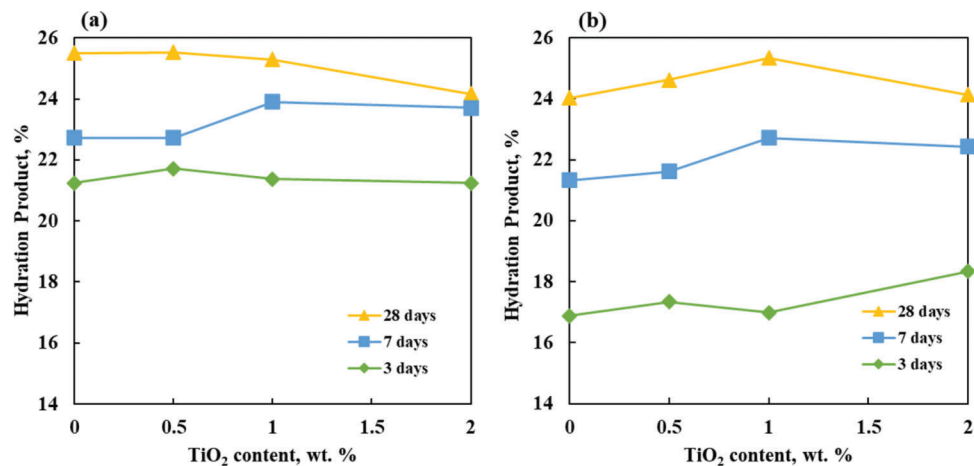


Figure 4.8 The amounts of hydration products in the OPC pastes with different levels of nano- TiO_2 addition after 3, 7, and 28 days of curing at (a) room temperature (23°C), and (b) low temperature (4°C).

Figure 4.9b presents that the addition of nano- TiO_2 also accelerates the hydration process of fly ash pastes cured at low temperature. The amounts of hydration products formed at the 7 days and 28 days were very comparable, when comparing the data from these two ages for 1% addition of nano- TiO_2 (shown in Figure 4.9b). However, such an effect was not observed in OPC pastes cured at low temperature (Figure 4.8b). This is a confirm that when cured at low temperature, the nano- TiO_2 is more effective in fly ash pastes than in OPC pastes.

Figure 4.10 a and b show the amounts of hydration products in the *slag pastes* with different levels of nano- TiO_2 addition after 3, 7, and 28 days of curing at: (a) room temperature, and (b) low temperature. Similarly, the trends in Figure 4.10a are comparable to those shown in Figure 4.8a and Figure 4.9a. However, the effect of nano- TiO_2 on the acceleration of hydration at

early ages in slag pastes is not as significant as in fly ash pastes. This might be related to the fact that the pozzolanic reaction in fly ash pastes was also accelerated, and thus produced pozzolanic C-S-H, while no such mechanism exists in slag pastes.

However, when cured at low temperature (as shown in Figure 4.10b), the acceleration of hydration due to nano- TiO_2 seems to be less significant compared to the same pastes but cured at room temperature (Figure 4.10a). There is even a significant reduction in the amount of hydration product at 28 days when cured at low temperature for slag pastes (yellow line in Figure 4.10b). As slag particles are finer than the articles of OPC and fly ash, the addition of nano- TiO_2 might limit the growth space for hydration product. Therefore, the addition of nano- TiO_2 is not as effective in the case of slag system as in the case of the OPC and fly ash systems.

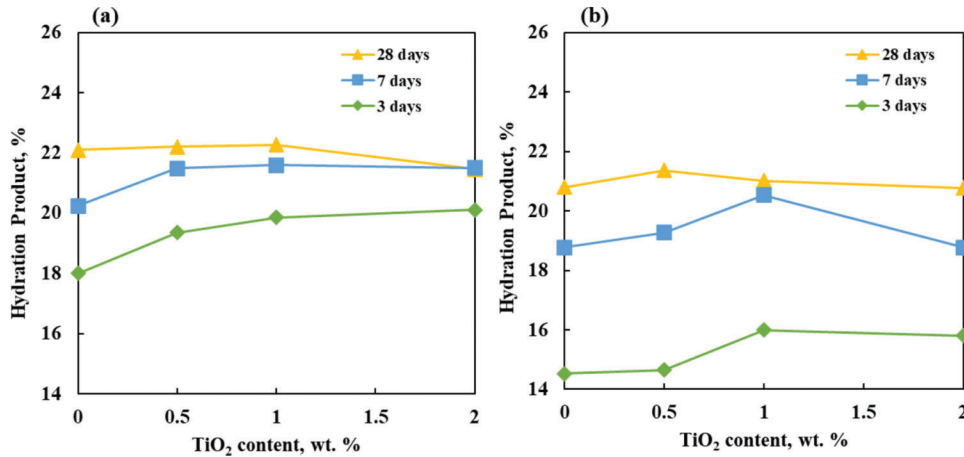


Figure 4.9 The amounts of hydration products in the fly ash pastes with different levels of nano-TiO₂ addition after 3, 7, and 28 days of curing at (a) room temperature (23°C), and (b) low temperature (4°C).

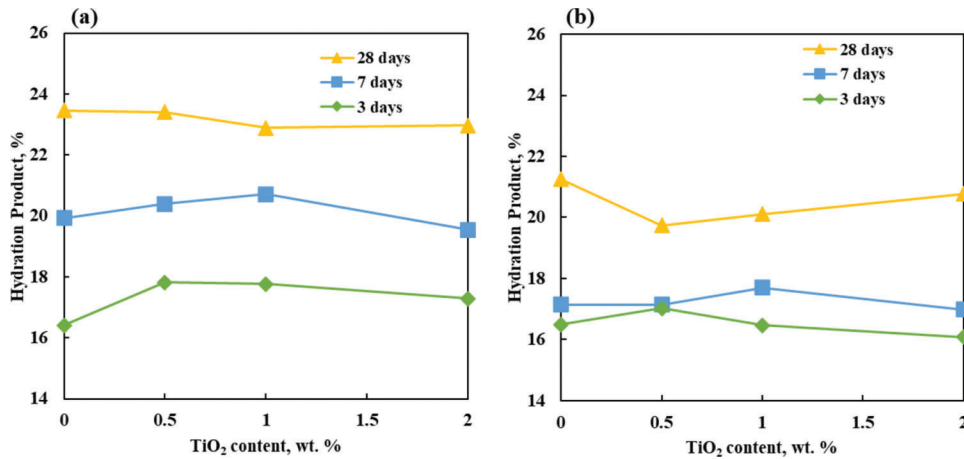


Figure 4.10 The amounts of hydration products in the slag pastes with different levels of nano-TiO₂ addition after 3, 7, and 28 days of curing at (a) room temperature (23°C), and (b) low temperature (4°C).

In conclusion, data presented indicate that the addition of nano-TiO₂ is more effective in accelerating the hydration process of OPC pastes cured at low temperature compared to those cured at room temperature. From the comparison of Figure 4.8 and Figure 4.9, it seems that a higher content of nano-TiO₂ is more beneficial at earlier ages (3 and 7 days), irrespective of binder composition and curing temperature. These observations agree with the results from the IC and setting time tests presented in previous sections, which indicated formation of higher amounts of the hydration products in the same type of cementitious systems. These findings are also in agreement with those reported by other researchers (Moro et al., 2020). The effect of nano-TiO₂ on the hydration process is least significant in slag pastes than in the OPC and fly ash pastes.

4.2.4.2 Influence of nanoadditives on the QI_{ahp} of pastes. To appraise the relative increase in the amount of hydration products formed in fly ash pastes (with respect to the reference sample without the addition of

nano-TiO₂), the parameter QI_{ahp} (a quantitative increase in the amount of hydration product) was introduced. The value of the QI_{ahp} was calculated using Equation 4.1.

$$QI_{ahp} = \frac{W_x - W_0}{W_0} \quad (\text{Eq. 4.1})$$

Where: W_x = weight loss in specimens with “x” % nano-TiO₂ and W_0 = weight loss in specimens with 0% nano-TiO₂.

The values of the QI_{ahp} for pastes cured for 3, 7, and 28 days at both the standard and low temperatures, are shown in Figure 4.11. The values of QI_{ahp} for different ages follow the sequence: 3 days > 7 days > 28 days, for OPC, fly ash, and slag pastes. That sequence confirms the previously discussed trends in TGA results (see Section 4.2.4.1), which indicates that nano-TiO₂ is more effective in accelerating the hydration process at earlier ages, regardless of the curing temperature.

The values of QI_{ahp} for OPC pastes at 3, 7, and 28 days cured at room temperature are shown in Figure 4.11a. It seems that the addition of nano-TiO₂ is only

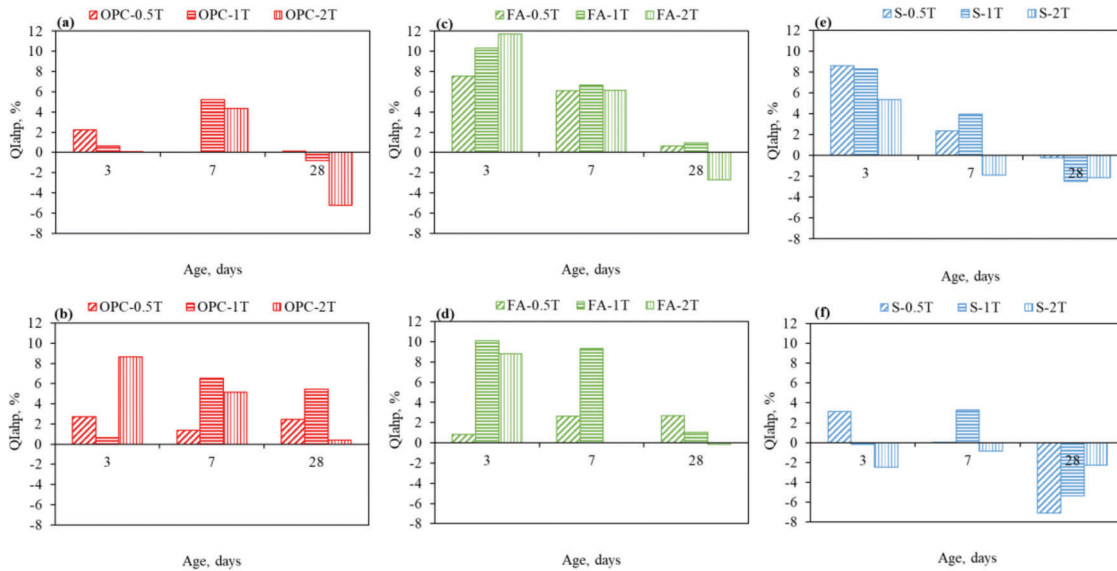


Figure 4.11 The values of Q_{Iahp} (quantitative increase in the amount of hydration products) for OPC, fly ash, and slag pastes cured for 3, 7, and 28 days cured at room and low temperatures. (a) OPC, room temperature; (b) OPC, low temperature; (c) fly ash, room temperature; (d) fly ash, low temperature; (e) slag, room temperature; and (f) slag, low temperature.

beneficial at early age for OPC pastes. As shown in Figure 4.11c, the amount of hydration product increases with the increase in the amount of nano-TiO₂ addition (up to 2.0 wt.%) at early ages (3 and 7 days) for fly ash pastes. However, the addition of 2.0 wt.% of nano-TiO₂ negatively affects the amount of hydration products at 28 days. Similar effect of nano-TiO₂ is also observed in slag pastes, as shown in Figure 4.11e.

Several previously published works also reported on diminishing effectiveness of increased dosages of nano-TiO₂ with respect to improving the properties of cementitious materials (Jalal et al., 2013; Nazari & Riahi, 2010; Zhang & Li, 2011). Some of the reasons for this behavior might be related to the difficulty in achieving a good dispersion of higher amounts of nano-TiO₂ within the cementitious system. More importantly, some researchers (such as Jalal et al., 2013), argue that higher content of nanoparticles can effectively reduce the distance between the particles in the cementitious system and thus limit the space available for growth of the hydration products. Moreover, as mentioned previously (Section 4.2.4.2) for specimens which are cured at room temperature, by the age of 28 days most of the hydrating phases have likely already reacted, thus limiting the effectiveness of nano-TiO₂ addition.

For OPC and fly ash pastes cured at low temperature (Figure 4.11 b and d), the addition of nano-TiO₂ seems to be more beneficial in accelerating the hydration at 28 days compared to pastes cured at room temperature (Figure 4.11 a and c). However, such a trend was not observed in slag pastes (compare Figure 4.11 e and f).

5. THE EFFECT OF NANO-TiO₂ ON MECHANICAL PROPERTIES OF MORTARS AND CONCRETES CONTAINING SCMs CURED AT DIFFERENT TEMPERATURES

5.1 Materials and Methods

5.1.1 Materials

All details regarding materials to prepare specimens described in this chapter were presented in Chapter 3.

5.1.2 Preparation of Specimens

All OPC, fly ash, and slag cementitious mixtures (mortars and concretes) with and without nano-TiO₂ used in the study were prepared using either standard laboratory mortar mixer or pan concrete mixer. Various levels of nano-TiO₂ were added as the weight percentages of the total cementitious materials (i.e., the total weight of OPC, OPC+FA, or OPC+slag). The mixture proportions of mortars and concretes used in this study are shown in Table 5.1 and Table 5.2, respectively.

Mortar specimens were prepared according to the requirements of ASTM C305-20. Water and high range water reducer (HRWR) were pre-mixed in a mixing bowl first, and then nano-TiO₂ was added into the same mixing bowl. The resulting mixture was transferred into the mixing bowl of the mechanical mixer. Fine aggregate was added in the following step. Finally, OPC or OPC+FA or OPC+slag was added. After completion of the mixing process mortars were placed either in 160 × 40 × 40 mm prismatic steel molds (to prepare beams for flexural strength testing) or a 50 × 50 × 50 mm

TABLE 5.1
Mixture proportions of plain and nano-TiO₂ mortars (all ratios calculated on weight basis)

Sample Type	Sample	FA/OPC	Sand/(FA+OPC)	Water/(FA+OPC)	Nano-TiO ₂ (wt.%)
Mortar	P-0	0	3.55	0.45	0
	P-0.5	0	3.55	0.45	0.5
Mortar	F-0	0.313	2.48	0.45	0
	F-0.5	0.313	2.48	0.45	0.5

TABLE 5.2
Mixture proportions of TiO₂ nanoparticles modified concrete (all ratios calculated on weight basis)

Material	Mix Designs				
	C-P	C-S	A-P	A-F	A-S
Cement (lbs/cu yd)	658	460	564	451	395
Fly ash (lbs/cu yd)	/	/	/	141	/
Slag (lbs/cu yd)	/	198	/	/	169
Water/cement ratio	0.42	0.42	0.44	0.44	0.44
Cement/fly ash ratio	/	/	/	3.2	/
Cement/slag ratio	/	2.3	/	/	2.3
Total cementitious material (lbs/cu yd)	658	658	564	592	564
Fine aggregate (lbs/cu yd)	1,255	1,240	1,350	1,315	1,350
Coarse aggregate (lbs/cu yd)	1,650	1,650	1,700	1,670	1,700
Air entrainer (fl oz/cwt)	1.5	1.5	1.5	1.5	1.5
HRWR (fl oz/cwt)	3.6	3.6	5.3	5.3	5.3

steel cubical molds (to prepare specimens for compressive strength testing). The molds were tamped by hand to ensure homogenous compaction. Then the molds were stored in the lab for 24 hours (at 23°C and 50% RH). After that, mortars were demolded and cured at two different temperatures (room 23°C and low 4°C) until tested (at the age of 3, 7, and 28 days).

All materials used for preparation of the concrete mixtures were conditioned at room temperature and weighted before mixing. The batch weights of the aggregates and water were adjusted as needed to account for the moisture content and absorption of both coarse aggregate and fine aggregate. The process involved placing the approximate amounts of aggregates needed for the mixture in sealed containers a day before the batching. Representative samples of the same aggregates were then oven dried for 24 hours to determine their actual moisture contents.

At the day of mixing, fine and coarse aggregate were put into the mixer along with part of a batch water. These components were then mixed for a short time after which all cementitious materials and another part of the batch water were added to the mixer. For mixtures containing the nano-TiO₂, this material was added to the remaining part of the batch water and mixed by hand to form a uniform suspension. The suspension of nanoparticles in water was then added into the mixer for the final mixing step. Once the mixing process was completed, the fresh concrete was tested for slump and air content. Afterwards the fresh concrete was cast into molds (4-in. by 8-in. cylinder molds and 3-in. by 4-in. by 16-in. steel molds) to prepare various specimens needed for future

tests. Upon completion of the casting process the molds were stored in the lab for 24 hours (at 23°C and 50% RH). After that, concrete samples were demolded and cured in lime saturated water at two different temperatures (room: 23°C and low: 4°C) until tested.

5.1.3 Testing Methods

5.1.3.1 Fresh properties of concrete: slump, density, and air content. After mixing, the fresh concrete was tested for slump, density (unit weight), and air content according to ASTM C143-20 and ASTM C138-17, respectively. The cylindrical metal container with the internal volume of 0.25 ft³ and the empty mass of M_m was used for determination of the unit weight and air content of the fresh concrete. The test involved filling the container with the concrete mixture and using a flat strike-off plate to finish the top surface so that the container was level full. Excess concrete was then cleaned from the exterior of the container and the mass of the container and concrete was measured (M_c). The density (unit weight) (D) of concrete was calculated following the Equation 5.1.

$$D = \frac{M_c - M_m}{M_m} \quad (\text{Eq. 5.1})$$

The theoretical density of concrete (T) can be calculated as follows:

$$T = \frac{M}{V} \quad (\text{Eq. 5.2})$$

Where M is the total mass of all materials batched; and V is the total absolute volume of the component ingredients in the batch.

Finally, the air content (A) can be calculated as:

$$A = \frac{T - D}{T} \times 100 \quad (\text{Eq. 5.3})$$

5.1.3.2 Compressive and flexural strength of mortars.

The flexural strength testing of mortar specimens was performed according to the ASTM C348-18 whereas the compressive strength testing was performed according to the ASTM C109M-16.

5.1.3.3 Compressive and flexural strength of concretes.

The compressive and flexural strength of concretes were tested following ASTM C39-20 and ASTM C78-18, respectively.

For studying the effect of nano-TiO₂ on the strength of concretes, five types of concrete specimens (with mix proportions listed in Table 5.2) were prepared and cured at either standard (23°C) or low (4°C) temperatures. In total, two classes of concrete were fabricated according to INDOT specification (INDOT, 2020). Class A and Class C concrete were selected as they have a lot of applications as structural concretes. In Indiana, concrete in superstructure, integral bents, and railings should be Class C concrete. Concrete in bent caps, pier caps, abutment caps, pier stems, abutment walls, columns, crash walls, collision wall, and wind walls shall be Class A concrete (INDOT, 2020a). The naming system for the mixtures was as follows: the first letter indicates the class of concrete (Class A or Class C), and the second letter is to indicate the composition of its cementitious system (P for plain, F for fly ash, and S for slag). The number following the second letter indicates the percentages of nano-TiO₂ in the mixtures (0, 0.5, and 1). These numbers are accompanied by a letter "T" to emphasize that they pertain to the level of TiO₂ in the mix. As an example, Class C concrete with slag and 0.5% of nano-TiO₂ will be labeled as C-S-0.5T.

5.1.3.4 Static and dynamic moduli of elasticity of concretes. The values of static modulus of elasticity at 28 days were calculated based on the corresponding compressive strength of concretes, using Equation 5.4 from the ACI 318 (ASTM, 2019).

$$E = 33 \times w^{1.5} \times \sqrt{f_c'} \quad (\text{Eq. 5.4})$$

Where, E is the static modulus of elasticity (in psi), w is the unit weight of concrete, in lb/ft³, and f_c' is the specified compressive strength of concrete at 28 days (in psi).

The dynamic modulus of elasticity was determined on the same prismatic (3 in. × 4 in. × 16 in.) specimens as those used for freeze-thaw (FT) test (see Section 6.1.4). The values of the dynamic modulus of elasticity were determined just before start of the FT test (i.e., after 14 days of moist curing at two different curing temperatures (23°C and 4°C). The values of the

dynamic modulus of elasticity (DME) were calculated following ASTM E1876 (ASTM, 2015a). Fundamental transverse frequency was measured in the lab with a typical setup of apparatus shown in Figure 5.1.

According to ASTM E1876-15, the dynamic modulus of elasticity can be calculated using Equation 5.5.

$$E = 0.9465 \times \left(\frac{mf_f^2}{b} \right) \left(\frac{L^3}{t^3} \right) T_1 \quad (\text{Eq. 5.5})$$

Where, E = dynamic modulus of elasticity, Pa; m = mass of the specimen, g; b = width of the specimen, mm; L = length of the specimen, mm; t = thickness of the specimen, mm; f_r = fundamental resonant frequency of the specimen in flexure, Hz; and T₁ = correction factor for fundamental flexural mode to account for finite thickness of specimen, Poisson's ratio (μ), and so forth (given by Equation 5.6). The value of the Poisson's ratio used in the calculations was assumed to be 0.15 (which is confirmed by performing the calculation prescribed in Section 10 of ASTM E1876-15 (2015a)).

$$T_1 = 1 + 6.585(1 + 0.0752\mu + 0.8109\mu^2) \left(\frac{t}{L} \right)^2 - 0.868 \left(\frac{t}{L} \right)^4 - \left[\frac{8.340(1 + 0.2023\mu + 2.173\mu^2) \left(\frac{t}{L} \right)^4}{1.000 + 6.338(1 + 0.1408\mu + 1.536\mu^2) \left(\frac{t}{L} \right)^2} \right] \quad (\text{Eq. 5.6})$$

5.2 Results and Discussions

5.2.1 Fresh Properties of Concretes

5.2.1.1 Slump. Figure 5.2 presents the slump test results for all types of concretes (with and without the addition of nano-TiO₂). The data show that addition of nano-TiO₂ reduces the slump of concretes for both plain mixtures and mixtures with SCMs (i.e., fly ash and slag mixtures). This can be explained by the increase in water demand of mixtures containing nanoparticles (due to their high specific surface area) (Li, Ding, et al., 2018).

5.2.1.2 Unit weight and air content of concretes. The influences of nano-TiO₂ on the unit weight and air content of fresh concretes are presented in Figure 5.3. The addition of nano-TiO₂ increases the unit weight (density) of concretes while it causes slight reduction in the air content.

5.2.2 Compressive Strength and Flexural Strength of Mortars

The values of the compressive strengths of the OPC and fly ash mortars with and without the addition of

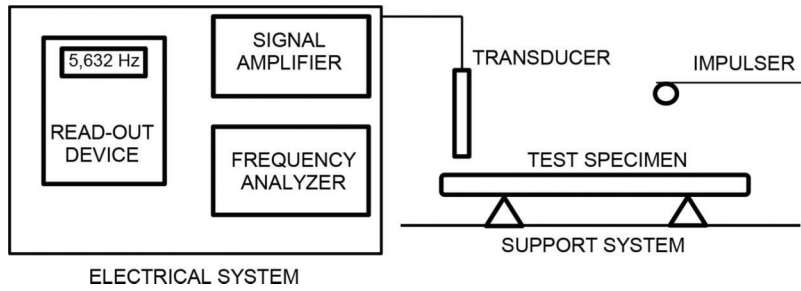


Figure 5.1 Schematic of typical test apparatus for fundamental transverse frequency (adapted from ASTM E1876 (ASTM, 2015a)).

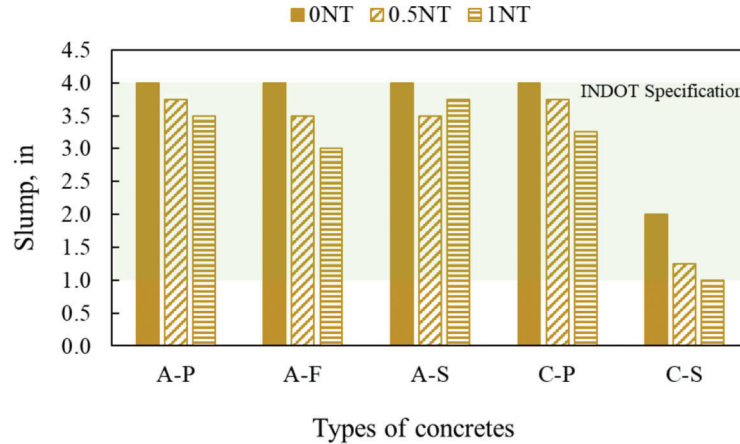


Figure 5.2 The slump of fresh concretes (Class A and C) with and without nano-TiO₂. The highlighted region represents the target range of slumps for Class A and C concretes given in the INDOT's Standard Specifications, Section 700 (INDOT, 2020a).

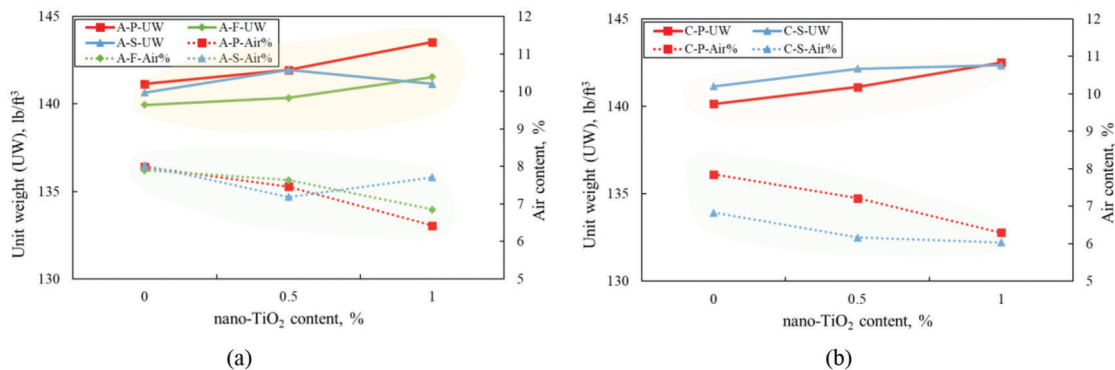


Figure 5.3 The unit weights and air contents of fresh concretes with and without nano-TiO₂: (a) Class A concretes, and (b) Class C concretes.

nano-TiO₂ as a function of age and the curing temperature are shown in Figure 5.4. For mortars cured at room temperature (Figure 5.4a), the addition of 0.5 wt.% of nano-TiO₂ improves the compressive strength of the OPC mortars when tested at 3, 7, and 28 days. Smaller improvements were also observed for room temperature cured fly ash mortars, especially at 3 and 7 days.

Similarly, the improvement of compressive strength was observed for the samples cured at low temperature (Figure 5.4b). As mentioned in Section 4.2.4, the addition

of nano-TiO₂ can lead to acceleration of the hydration process, and reduction of porosity within the paste matrix (reported by Li, Ding, et al., 2018). Therefore, the bulk strength of mortars can be enhanced. A significant increase in the 28-day compressive strength can be observed in the case of fly ash mortars cured at a low temperature (as indicated by the black arrow in Figure 5.4b). Again, this indicates that nano-TiO₂ is more effective when cured at low temperature.

The values of the flexural strengths of OPC and fly ash mortars with and without the addition of nano-

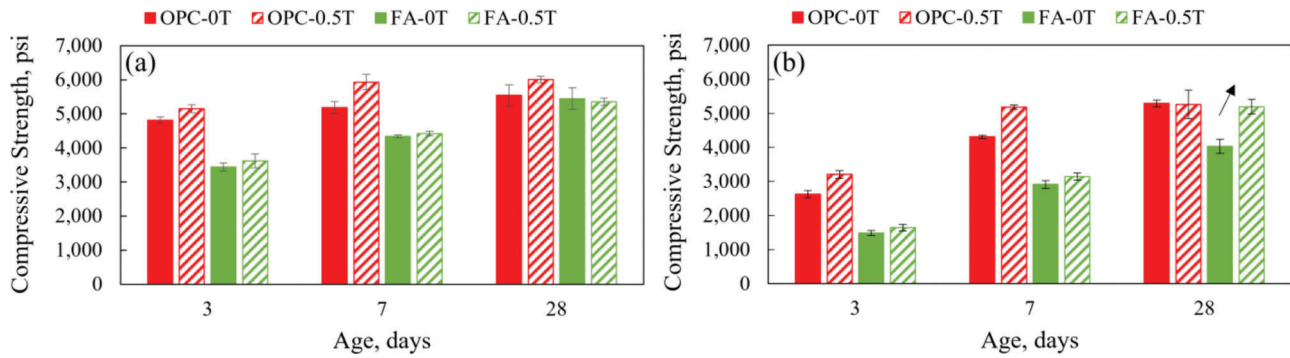


Figure 5.4 Values of the compressive strength of OPC and fly ash mortars at different ages for specimens cured at (a) room temperature (23°C), and (b) low temperature (4°C).

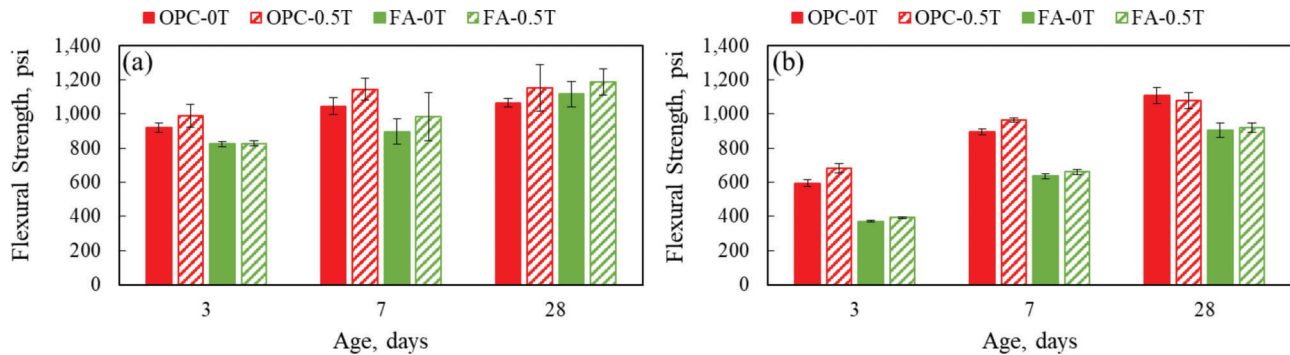


Figure 5.5 Values of the flexural strength of OPC and fly ash mortars at different ages for specimens cured at (a) room temperature (23°C), and (b) low temperature (4°C).

TiO₂ as a function of age and the curing temperature are presented in Figure 5.5. For specimens cured at room temperature (as shown in Figure 5.5a), the addition of 0.5 wt.% of nano-TiO₂ can increase the flexural strength of both OPC, and fly ash mortars cured for 3, 7, and 28 days. For both OPC and fly ash mortars, a slight improvement of flexural strength can be observed for specimens cured at low temperature (Figure 5.5b).

5.2.3 Compressive Strength of Concretes

The compressive strength of Class A concretes (series A-P, A-F, and A-S) with different levels of nano-TiO₂ and cured at both room and low temperatures for 7 and 28 days were shown in Figure 5.6. A-P reference concretes developed higher values of compressive strength compared to concretes with SCMs (series A-F and A-S). These findings agree with previously reported (see Section 4.2.4) TGA results as the total amount of hydration product was following the same trends. As presented in Figure 5.6a, the addition of nano-TiO₂ enhanced the compressive strength and resulted in an increased rate of strength gains for all types of Class A concretes, regardless of curing temperature. Specifically, there is a ~80% increase in strength of A-S concrete (compared to A-S reference concrete) due to addition of 0.5% of nano-TiO₂.

The enhancement of values of compressive strength upon addition of nano-TiO₂ can also be observed in specimens cured for 28 days. However, as shown in Figure 5.6b, and more quantitatively in Figure 5.8, this enhancing effect is less prominent when compared to results observed in specimens cured for 7 days. This is expected, as similar trends were observed in the TGA test. Specifically, in that test the effect of nano-TiO₂ on the later-age hydration process was somewhat limited when compared to its effect on the early-age hydration. While such observations are true for A-P and A-S concretes, it seems that the addition of nano-TiO₂ on compressive strength of A-F concretes was somewhat more pronounced (this is also shown more clearly in Figure 5.8). This can be expected as the addition of nano-TiO₂ can promote the pozzolanic reaction in concretes containing fly ash, which is a long-term effect.

The values of the compressive strength of Class C concretes (C-P and C-S series) with different levels of nano-TiO₂ cured at both room and low temperatures for 7 and 28 days are shown in Figure 5.7. The influence of nano-TiO₂ on the strength of Class C concrete is comparable to that observed in Class A concretes. Specifically, there is an enhancement in strength of Class C concretes due to the addition of nano-TiO₂, regardless of curing temperatures and ages. Similarly, addition of nano-TiO₂ resulted in greater strength increases in C-S concretes compared to the C-P concretes.

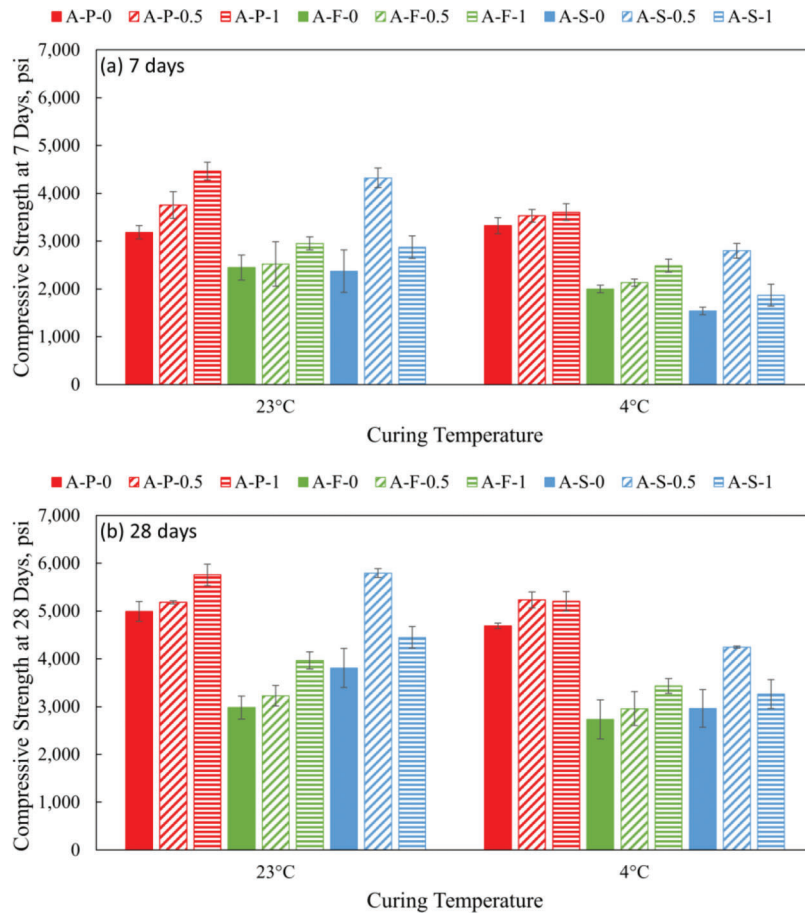


Figure 5.6 The values of the compressive strength of concretes (Class A) with different levels of nano-TiO₂ addition cured at both room and low temperatures for (a) 7 days, and (b) 28 days.

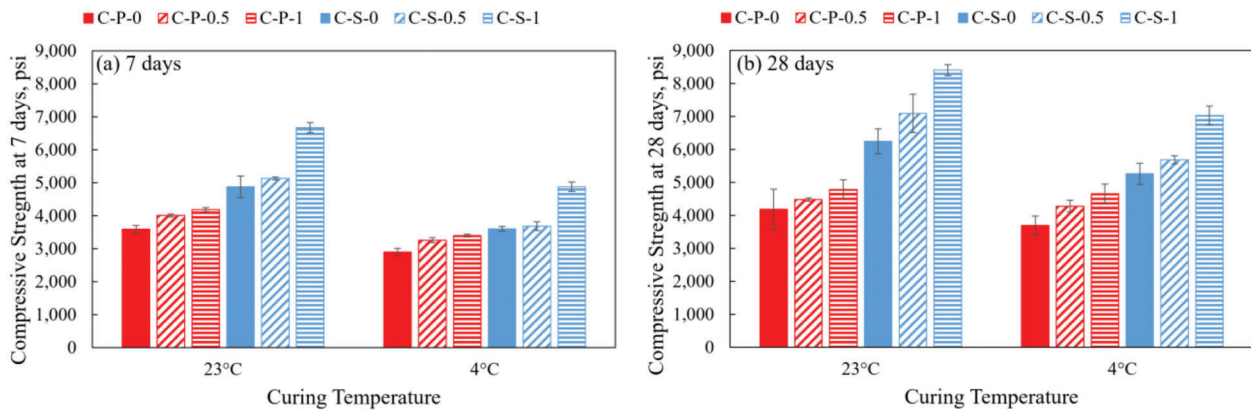


Figure 5.7 The values of the compressive strength of concretes (Class C) with different levels of nano-TiO₂ addition cured at both room and low temperatures for (a) 7 days and (b) 28 days.

Combining these results with the results obtained from Class A concretes, it seems that nano-TiO₂ can significantly improve the strength of concretes containing slag.

The relative increase in compressive strength values for both Class A and C concretes due to the addition of nano-TiO₂ at different ages cured at both room and low

temperatures are shown in Figure 5.8 and Figure 5.9, respectively. These graphs were prepared to better illustrate the effect of nano-TiO₂ on the strength in terms of different mixtures, curing ages, and temperatures.

Regardless of curing ages and temperatures, it seems that the influence of nano-TiO₂ is more pronounced in Class A concretes. It might be related to the different

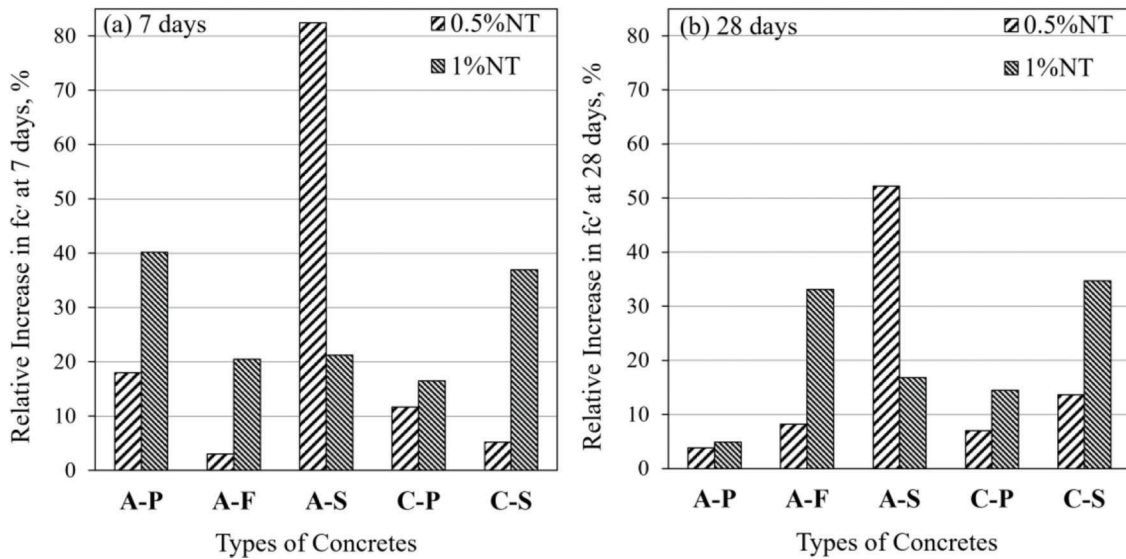


Figure 5.8 The effects of addition of nano-TiO₂ on the relative increase in compressive strength of Class A and C concretes cured at room (23°C) temperature for (a) 7 days and (b) 28 days.

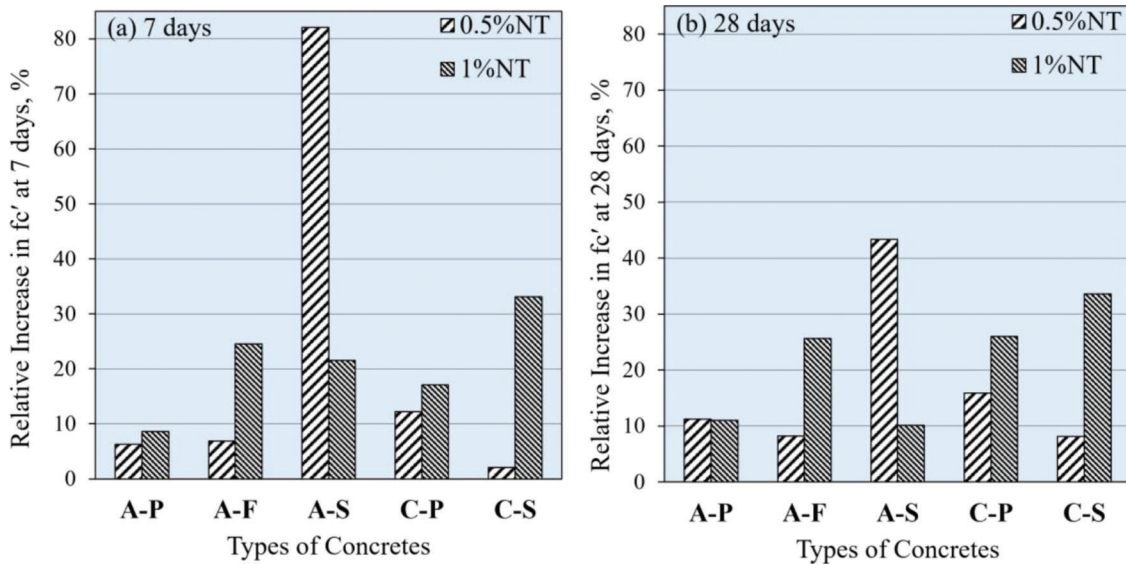


Figure 5.9 The effects of addition of nano-TiO₂ on the relative increase in compressive strength of Class A and C concretes cured at low (4°C) temperature for (a) 7 days and (b) 28 days.

w/cm used in different class of concretes. As shown in the mixture design of concrete, Class A concretes had higher w/cm ratio (0.44) compared to Class C concretes (0.42). It was previously reported (Moro et al., 2021), that with respect to enhancement of the extent of hydration and strength at earlier ages, mixtures with higher w/cm may benefit from higher dosages of nano-TiO₂. In case of mixtures containing the same amounts of nano-TiO₂, its influence on the strength might be more significant in concretes with higher w/cm (Class A concrete in this case). Concrete with higher w/cm will initially have higher number of capillary pores. As such, the addition of nano-TiO₂ to such mixtures could be more effective with regard to reducing their porosity and thus improving the strength significantly.

Furthermore, as previously discussed, the effects of addition of nano-TiO₂ on early-age strength are more significant than those observed for later-age strength, regardless of the curing temperature and the type of concrete. These trends are also observed in Figure 5.8 and Figure 5.9.

5.2.4 Flexural Strength of Concretes

Figure 5.10 presents the values of the 7-day and 28-day flexural strength of concretes (Class A with partial replacement of slag (A-S), and a modified Class A plain concrete with w/c = 0.45 (OPC) with and without the addition of nano-TiO₂ cured at both room and low temperatures. At early age (as shown in Figure 5.10a),

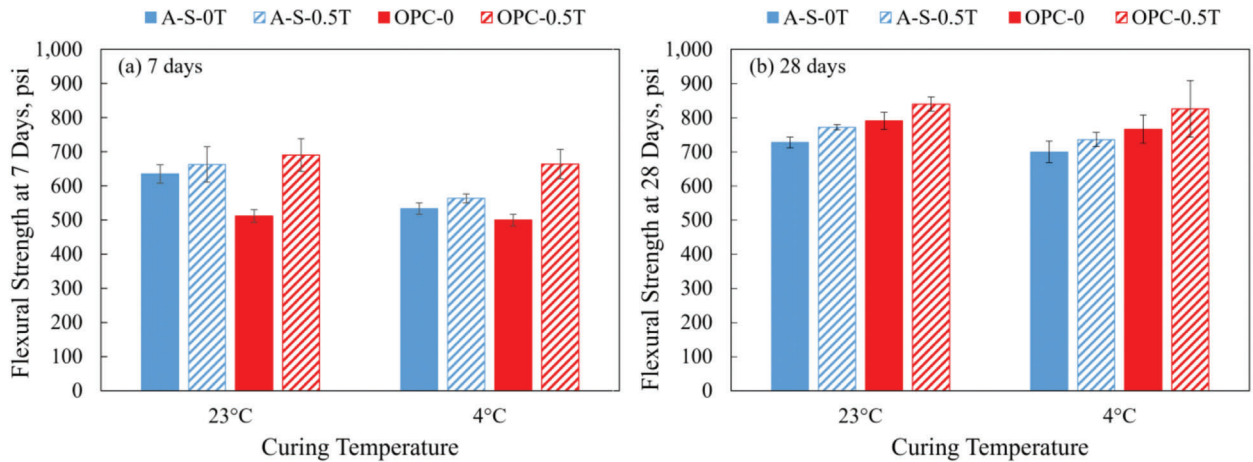


Figure 5.10 The values of the flexural strength of concretes without (0%) and with 0.5% of nano-TiO₂ cured at both room and low temperatures for (a) 7 days, and (b) 28 days.

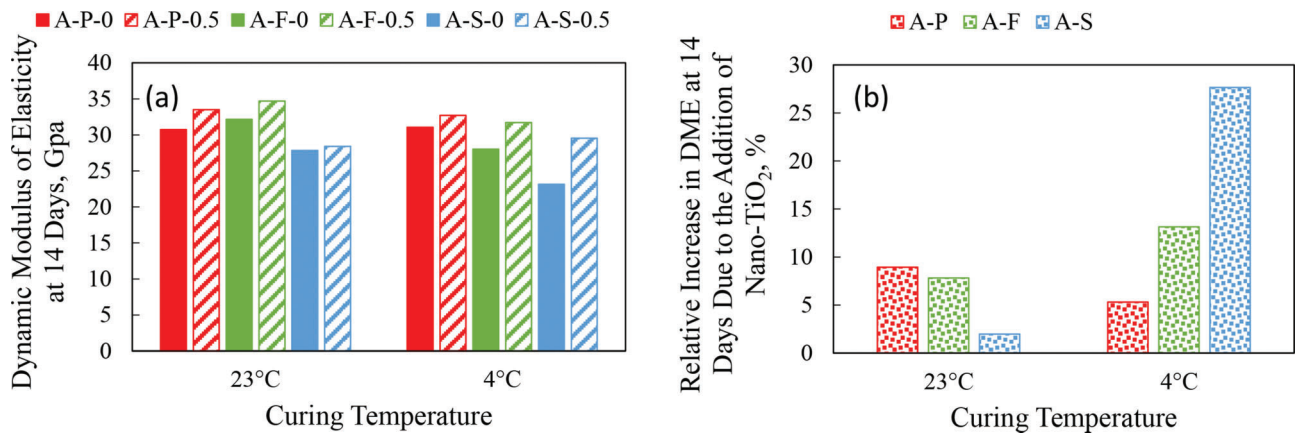


Figure 5.11 (a) The dynamic modulus of elasticity (DME) and (b) the relative increase in DME due to the addition of nano-TiO₂ for Class A concretes cured for 14 days at standard (23°C) and low (4°C) temperatures.

the addition of nano-TiO₂ to plain (i.e., OPC) concretes significantly enhanced their flexural strength, regardless of the curing temperature. The effect of nano-TiO₂ on the 7-day flexural strength of A-S concretes was minimal. After 28 days of curing, the influence of nano-TiO₂ on the flexural strength on both types of concretes seems to be limited, as shown in Figure 5.10b. This can be expected as the previous chapters also indicated the influence of nano-TiO₂ is more significant at earlier ages compared to later ages.

Furthermore, when comparing the reference slag and OPC concrete (as shown in Figure 5.10a), it seems that the early flexural strength of reference slag concrete is higher than OPC concrete without distinguishing the curing temperature. Besides the slightly lower w/c (0.01) of reference slag concrete, such higher early flexural strength (compared to OPC) suggests partially supplementing OPC with slag could be beneficial in improving the early flexural strength. However, such effect is not observed at 28 days of curing.

5.2.5 Static and Dynamic Moduli of Elasticity of Concretes

Figure 5.11 presents, respectively, the values of the dynamic modulus of elasticity (DME)—Figure 5.11a, and the relative increase in DME due to the addition of nano-TiO₂ for Class A concretes after 14 days of curing at both standard (23°C) and low (4°C) temperatures. As shown in Figure 5.11a, the low curing temperature seems to be negatively affecting the DME of reference concretes containing SCMs (A-F and A-S), while not affecting the DME values of the OPC reference concrete. Furthermore, it can be seen that addition of the nano-TiO₂ increased the values of the DME for all concretes, regardless of their composition and the curing temperature. The relative increases in DME due to the addition of nano-TiO₂ for all types of concretes at 14 days of curing are presented in Figure 5.11b. It seems that the effect of nano-TiO₂ is more significant when curing temperature is low, especially for A-S concrete.

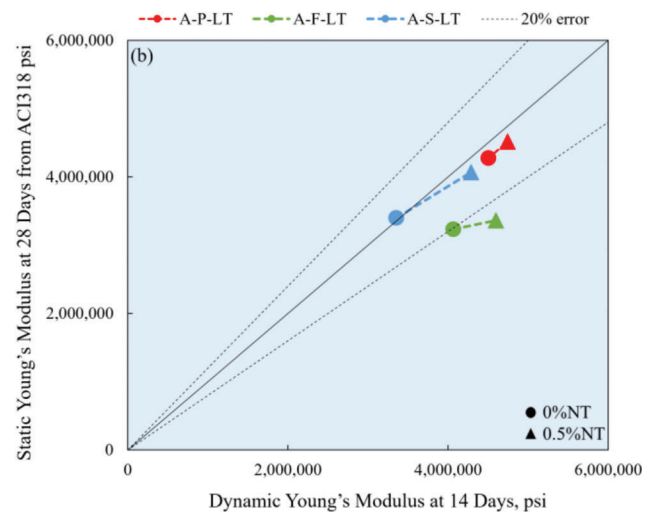
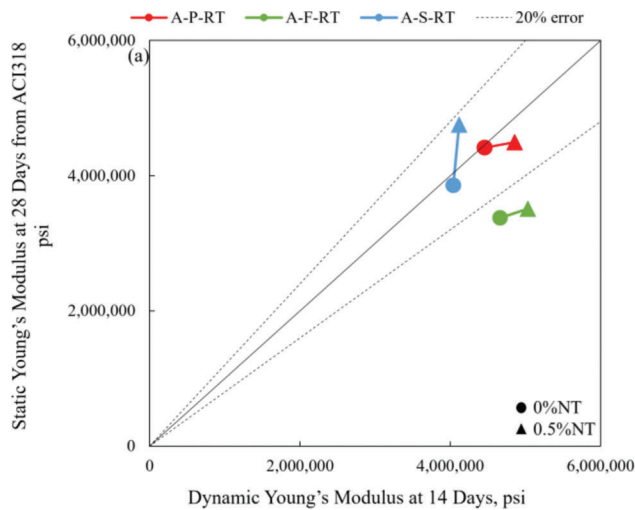


Figure 5.12 The effect of nano-TiO₂ on the relationship between the static and dynamic moduli of elasticity of concretes cured at (a) room temperature (23°C), and (b) low temperature (4°C).

Figure 5.12 presents the effect of nano-TiO₂ on the relationship between the values of the static and dynamic moduli of elasticity of concretes cured at different temperatures. For specimens cured at standard temperature, the influence of nano-TiO₂ on the static and dynamic moduli of elasticity of Class A concretes (A-P, A-F, and A-S) results in comparable trends, in a sense that both types do increase. However, the addition of nano-TiO₂ seems to enhance the static modulus of elasticity more significantly compared to dynamic modulus of elasticity of A-S concretes. As shown in Figure 5.12b, for specimens cured at low temperature nano-TiO₂ can promote the increase in both static and dynamic moduli of elasticity for all Class A concretes. Furthermore, there seems to be a more significant increase in the dynamic modulus of elasticity of concretes with SCMs. This indicates that when concrete with fly ash and slag is expected to be exposed to low curing temperatures at early ages, it may be beneficial to use nano-TiO₂ to improve its stiffness, and thus potential resistance to FT damage.

6. THE EFFECT OF NANO-TiO₂ AND CURING TEMPERATURES ON THE DURABILITY OF CONCRETES CONTAINING SCMs

6.1 Materials and Methods

All the details for materials have been introduced in Chapter 3. The mix designs and mixing procedures were the same as discussed in Chapter 5.

6.1.1 Determination of the Resistivity and the Formation Factor

The resistivity tests were performed on 28 days old 4 in. × 8 in. concrete cylinders following the procedure given in AASHTO TP 119-15 (AASHTO, 2019) on uniaxial resistance test. Prior to the test, the cylinders were stored in a saturated lime water at room

temperature (23°C). Right before measurement of resistivity the cylinders were removed from the water tank and their surfaces were wiped with a damp paper towel. The uniaxial resistivity measurement system used during the test consisted of the stainless-steel plate electrodes, electrical cables, resistivity meter and sponges which were saturated with lime and placed between the electrodes and end surfaces of the cylinders. The picture of the specimen in the assembled resistivity measurement unit is shown in Figure 6.1.

The resistance displayed by the resistivity meter during the test (R_{measured}) is actually the bulk resistance (i.e., the resistance of the system composed of the concrete cylinder plus two sponges). In order to obtain the actual value of the resistance of the cylinder (R_{cylinder}), the resistances of both the top and the bottom sponges ($R_{\text{top sponge}}$, $R_{\text{bottom sponge}}$, respectively) need to be determined separately and subtracted from the bulk resistance (R_{measured})—see Equation 6.1.

$$R_{\text{cylinders}} = R_{\text{measured}} - R_{\text{top sponge}} - R_{\text{bottom sponge}} \quad (\text{Eq. 6.1})$$



Figure 6.1 The setup of resistivity measurement.

The resistivity of cylinders can then be calculated as:

$$\rho = R_{\text{cylinders}} \times \frac{A}{L} \quad (\text{Eq. 6.2})$$

Where, ρ is the resistivity of cylinder, R_{cylinder} is the resistance of cylinder, A is the cross-sectional area of the cylinder, and L is the length of the cylinder.

The resistivity values determined following the AASHTO TP 119-15 (2019) procedure can then be used to calculate the values of the apparent formation factor as per AASHTO PP84-19:

$$F_{APP} = \frac{\rho(\Omega m)}{\rho_0(\Omega m)} \quad (\text{Eq. 6.3})$$

Where, F_{APP} is the formation factor that can be determined by dividing the resistivity ρ determined by AASHTO TP119-15 (2019) by a pore solution resistivity ρ_0 . According to AASHTO PP84 (AASHTO, 2020a), the resistivity of pore solution can be estimated using a combination of mixture proportions, chemistry of the cementitious materials, and a degree of hydration. These estimations were obtained using publicly available calculation software program (NIST, n.d.) This is the approach used in this study. Although the AASHTO PP84 prescribed the test age is 91 days, in this study, the resistivity of cylinders was tested at 28 days and most of the other properties were also determined at that age. Determination of bulk densities and the total pore volumes of concretes.

The total pore volumes and bulk densities of concretes used in the study were determined according to AASHTO TP135-20 (AASHTO, 2020b). As suggested by previous research (Bu et al., 2014), ASTM C642 does not result in filling all the voids in concrete, especially the air entrained voids, so it does not provide a measure of the pore volume at complete saturation. Therefore, this test does not provide a total volume void in concrete. On the other hand, AASHTO TP135 requires the use of vacuum saturation (at an absolute pressure of less than 20 Torr (2,666 Pa)) to ensure the saturation of all the voids in concrete.

This test involves preparing two duplicates of concrete discs (4-in. diameter and 2-in. thick). Three discs are oven-dried (at the temperature of $110 \pm 5^\circ\text{C}$) for no less than 24 hours. When the drying is completed, the specimens are removed from the oven and air cooled to room temperature ($23 \pm 2^\circ\text{C}$). Subsequently, there the mass (A) is determined to the nearest 0.01 g. Such procedure should be performed at least twice to have less than 0.1% difference between two successive measurements. Otherwise, additional measurements should be performed. The saturated mass (B) is then measured after 3 hours of vacuum saturation under water, followed by 18 hours of additional soaking. The apparent mass (C) should also be determined by weighing vacuum-saturated specimen placed in the wire basket suspended inside of the water tank.

The volume of permeable pore volume can be calculated as follows (Equation 6.4):

$$\text{Total volume of permeable pore,} \\ \% = \frac{B-A}{B-C} \times 100 \quad (\text{Eq. 6.4})$$

The bulk density of concrete specimen can be calculated by Equation 6.5.

$$\text{Bulk density} = \frac{A}{B-C} \times \rho \quad (\text{Eq. 6.5})$$

Where ρ is the density of water ($1 \text{ Mg/m}^3 = 1 \text{ g/cm}^3$).

6.1.2 Permeability and Absorption Test

The ASTM C1585-20 (2020) specifies the test procedure to determine the absorption and rate of absorption of water in unsaturated hydraulic cement concrete. This standard is based on the work reported by Hall (1989). The test is performed on two concrete discs (4-in. diameter and 2-in. thick), which need to be water saturated and then exposed to known moisture environment. Initially, the water-saturated specimens need to be kept in a $50^\circ\text{C}/80\%$ relative humidity (RH) oven for 3 days. After that, the specimens are subjected to 15 days long “equilibration period” during which they are placed in a sealed container which should be stored in an environmental chamber kept at the temperature of 23°C and 50% RH. Once the conditioning cycle is completed, the side surface of each specimen is sealed with suitable sealing material (in this case with electrical tape) and the end of the specimen that is not intended to be exposed to water is sealed with loosely attached plastic sheet (in this case cling plastic food wrap). The other end of the specimen is then exposed to room temperature water and the increases in mass of the specimen (m_t) are recorded at predetermined time intervals specified by the ASTM C1585 standard (ASTM, 2020). The schematic of the water absorption set-up procedure is illustrated in Figure 6.2.

The recorded changes in the mass of the specimen (m_t) are used to calculate the absorption values using the Equation 6.6 given below:

$$I = \frac{m_t}{(a \times d)} \quad (\text{Eq. 6.6})$$

Where I is the absorption, m_t is the change in concrete sample mass (in grams) at time t , a is the cross-section area of the sample exposed to the water (mm^2), and d is the density of the water (g/mm^3).

As described by ASTM C1585-20 (ASTM, 2020), the values of absorption (I) need to be plotted as a function of the square root of time. The initial rate of water absorption is defined as the slope of the line best fitting all points between 1 minute and 6 hours of testing. The secondary rate of water absorption is determined by the slope of the line best fitting the data points collected

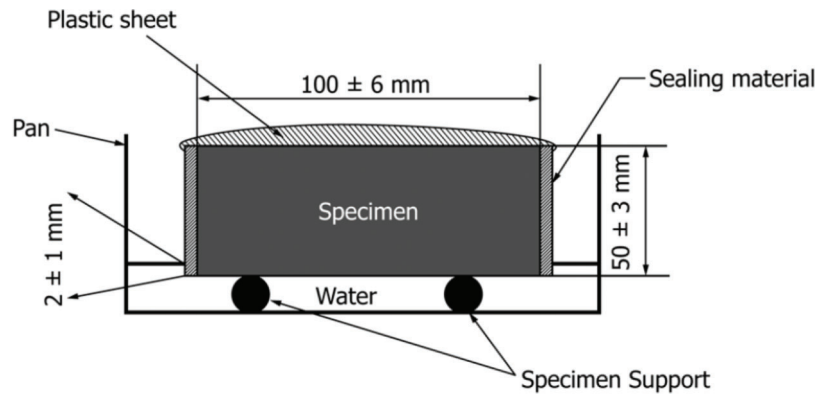


Figure 6.2 Schematic of the water absorption test (adapted from ASTM C1585-20 Standard (ASTM, 2020).

from 1 day to 7 days. Especially, the secondary rate of absorption is often used to correlate with the air void content of concrete. The results from water absorption can be used in evaluating the permeability and the connectivity of the pore network.

However, researchers pointed out that the water absorption strongly depends on the initial water content of the concrete sample (Hall, 1989; Nokken & Hooton, 2002; Zhutovsky & Hooton, 2019). Therefore, a modified absorption test was performed in this study to investigate the influence of initial water content on the result of water absorption.

The modified absorption test used different sample conditioning method than that provided in the ASTM C1585 standard (ASTM, 2020). Specifically, the conditioning process involved drying discs in an oven at the temperature of 60°C until constant mass (defined as the difference of two consecutive mass measurements being less than 0.2%). At the end of preconditioning procedure, samples were prepared for water absorption test according to ASTM C1585-20 (ASTM, 2020).

6.1.3 Scaling Resistance

The scaling resistance test was performed according to ASTM C672-03 (ASTM, 2012) using two 3 in. × 8 in. × 11 in. slabs prepared from each series of concrete. The surface areas of the test specimens (8 in. × 11 in. = 88 in.²) exceeded the ASTM C672-03 requirements for a minimum surface area (72 in.²). The specimens also met the minimum depth requirement of 3 in. The concrete was placed in the molds in one layer and consolidated by rodding (one stroke for each 2 in.² of surface area). The molds were tapped around the periphery with a rubber mallet (to close any visible voids) and the surface of the concrete was leveled using wood strike-off board. Once the bleeding stopped (usually around 2–4 hours), the surfaces of the specimens were finished with three sawing passes of the wood strike-off board and brushed with a medium-stiff brush. The specimens were then covered with the polyethylene sheet to prevent evaporation. The plastic sheet did not contact the surface of the specimens.

The slabs were demolded after 1 day of curing in the laboratory environment. Afterwards, all slabs were cured for 13 days in the saturated lime water at either standard (23°C) or low (4°C) temperatures. This was followed by a 2-week period of air drying (at the temperature of 23°C) before the first exposure to deicers. Prior to the initiation of the exposure to deicers, a small dike (about 1-in. wide and 0.75-in. tall) was installed around the perimeter of the top surface of the slabs. The purpose of the dike was to contain the deicing solution that the concrete specimens were exposed to during the entire scaling test. During the scaling resistance test, the depth of the deicing solution was maintained at 0.25 in. If necessary, water was added between each exposure cycle to maintain the required depth of the solution.

The scaling test was performed in the programmable environmental chamber which was capable of lowering the temperature of the specimens to $-18 \pm 3^\circ\text{C}$ within 1 hour and maintaining it with a full load of specimens for 16 hours. At the end of the freezing cycle, the chamber was programmed to start raising the temperature to $23 \pm 3^\circ\text{C}$ (within a period of about 1 hour) and maintaining it for 6 hours. The slabs were exposed to a standard (4%) deicing solution specified in the ASTM C672 (ASTM, 2012) (i.e., each 100 ml of solution contained 4 g of anhydrous calcium chloride (CaCl_2)). See Figure 6.3. The specimens were exposed to 50 freeze-thaw cycles, and the appearance of the surfaces was evaluated (after thorough flushing with water) at the end of each five cycles. At that time, the surfaces of the slabs were examined visually and photographed. In addition, any spalled flakes of concrete were collected and carefully weighed to determine the mass of concrete lost during the scaling test.

The severity of scaling was rated using the procedure provided in ASTM C672-03 (Figure 6.4 and Table 6.1). In addition to the rating of the surface, the recorded mass losses were used to quantify the scaling resistance according to the criterion established by the Ontario Ministry of Transportation (MTO) (Hooton & Vassilev, 2016). This criterion states that the cumulative mass loss after 50 freeze-thaw cycles should not be

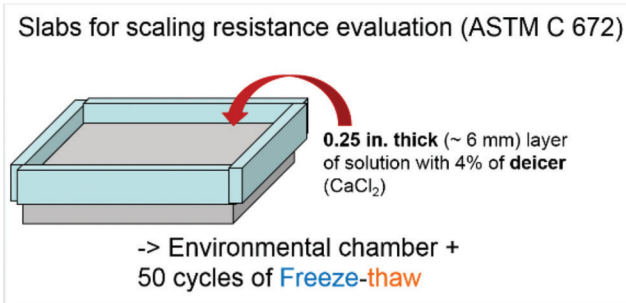


Figure 6.3 Schematic of the scaling test specimens.

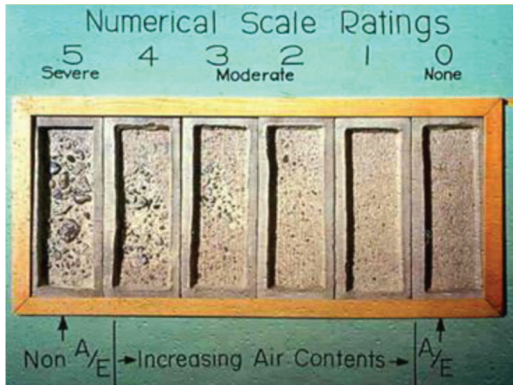


Figure 6.4 Illustration of the surface scaling rating scale for visual evaluation of scaling resistance (Kosmatka & Wilson, 2016).

TABLE 6.1
The rating for the surface scaling (adopted from ASTM C672/C672M-12 Standard (ASTM, 2012)).

Rating	Condition of Surface
0	No scaling
1	Very slight scaling (3 mm [1/8 in.] depth, max, no coarse aggregate visible)
2	Slight to moderate scaling
3	Moderate scaling (some coarse aggregate visible)
4	Moderate to severe scaling
5	Severe scaling (coarse aggregate visible over entire surface)

higher than 0.8 kg/m^2 for the concrete to be considered scaling resistant.

6.1.4 Freeze-Thaw Resistance

The freeze-thaw (FT) resistance test was performed according to ASTM C666-15 (ASTM, 2015b) procedure A (rapid freezing and thawing in water) using 3 in. \times 4 in. \times 16 in. concrete prisms. Three duplicates are required for each type of concrete. Once prepared, all concrete prisms were cured for 14 days in lime saturated water. The nominal freezing-and-thawing cycle consisted of 2 hours of freezing (from 40°F to 0°F) and 2 hours of thawing (from 0°F to 40°F). The measurements of the fundamental transverse frequencies were

conducted after every 30 cycles. The measured fundamental transverse frequencies were used to calculate the values of the relative dynamic modulus of elasticity (RDME) after specific numbers of cycles (n_c) using Equation 6.7.

$$RDME = \left(\frac{n_c^2}{n^2} \right) \times 100 \quad (\text{Eq. 6.7})$$

Where:

$RDME$ = the relative dynamic modulus of elasticity after c cycles of freezing and thawing, percent
 n = the fundamental transverse frequency at 0 cycles of freezing and thawing, and
 c = is the fundamental transverse frequency after c cycles of freezing and thawing.

6.2 Results and Discussions

6.2.1 Resistivity and Formation Factor of Concretes

The results of resistivity tests of Class A concretes, with and without nano-TiO₂, cured for 28 days at two different temperatures are shown in Figure 6.5. For all three types of concretes cured at standard temperature, (i.e., 23°C), the addition of 0.5 wt.% of nano-TiO₂ does not seem to affect their resistivity (see Figure 6.5a). This figure also shows that A-S concretes have higher resistivity compared to the resistivity of the reference concrete (i.e., A-P), and concert with fly ash (i.e., A-F). On the other hand, the resistivity of concretes cured at low temperature (i.e., 4°C), was significantly reduced, as shown in Figure 6.5b. In addition, the influence of low temperature curing on reduction of resistivity seems to be more prominent for concretes with SCMs (A-F and A-S). It can also be seen that the addition of nano-TiO₂ does not really affect resistivity of the A-P and A-S concretes. However, there was a small (about 8%) increase in the resistivity of the A-F concrete.

Figure 6.6 shows the values of the formation factor of Class A concretes with and without nano-TiO₂ cured at two different temperatures. As mentioned previously (Section 6.1.2), the formation factor of a concrete specimen was calculated by dividing the resistivity of the bulk concrete specimen by the resistivity of pore solution.

As shown in Figure 6.6a, the addition of nano-TiO₂ does not seem to have a significant effect on the values of the formation factor (i.e., connectivity of its pore system) for plain (i.e., A-P) and slag cement (A-S) concretes cured at room temperature. However, an increase in the formation factor resulting from the addition of nano-TiO₂ was observed in A-F concrete. In addition, the incorporation of fly ash significantly increased the value of the formation factor.

For concretes cured at low temperature (Figure 6.6b), the values of formation factors for all concretes were lower than those obtained for concretes cured at room temperature (Figure 6.6a). In particular, the values of the formation factors for A-F and A-S concretes were

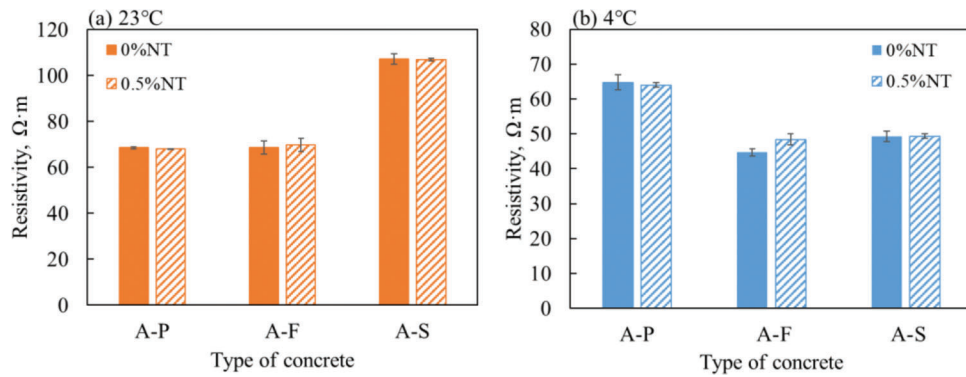


Figure 6.5 The 28 days resistivity of Class A concretes (with and without nano-TiO₂) cured at (a) room temperature, and (b) low temperature.

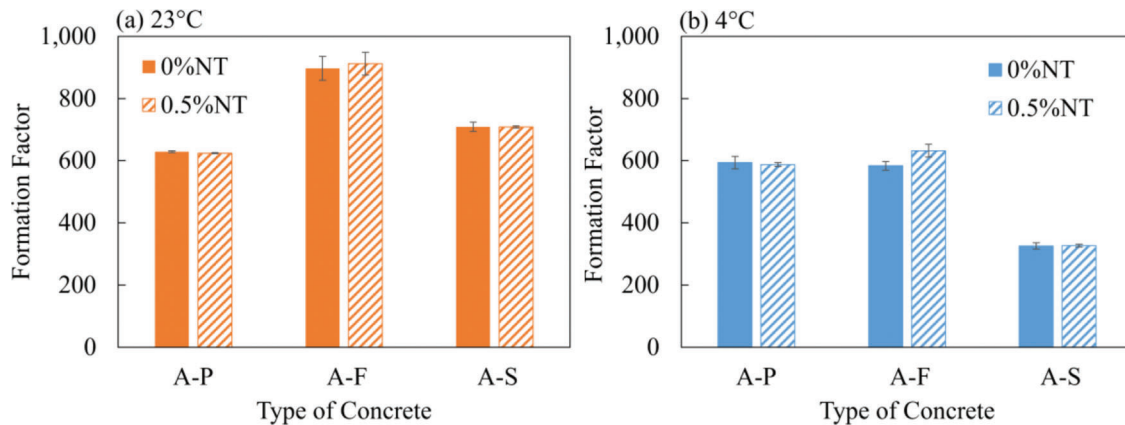


Figure 6.6 The 28-day formation factor of Class A concretes (with and without nano-TiO₂) cured at (a) room temperature, and (b) low temperature.

significantly reduced (especially for A-S concrete). Similar to what was observed in the case of room temperature curing, the addition of nano-TiO₂ improved the formation factor of A-F concrete.

The reason that nano-TiO₂ is not affecting the resistivity and formation factor of A-P and A-S concretes might be related to the fact that the influence of nano-TiO₂ is more significant at earlier ages. Since this test was performed at 28 days, there is a great chance that such test cannot capture the influence of nano-TiO₂ on the pore connectivity of concrete at earlier ages. However, for A-F concretes, nano-TiO₂ seems to be reducing the pore connectivity and potentially improve the durability of concretes. This might be because the hydration process of A-F concretes is delayed (especially at low curing temperature) compared to A-P and A-S concretes. As such, the effect of adding nano-TiO₂ might not be possible to capture even at 28 days.

6.2.2 Total Pore Volume

The total volume of pores in Class A concretes (with and without nano-TiO₂) and cured for 28 days at different temperatures is shown in Table 6.2. The porosities of reference (i.e., A-P) concretes with no addition of the nano-TiO₂ were lower than the porosities of the

same category (i.e., no nano-TiO₂ addition) A-F and A-S concretes, regardless of the curing temperature. The addition of nano-TiO₂ universally reduced the porosity of all types of concretes at both curing temperatures. The reduction in porosity due to the addition of nano-TiO₂ seems to be more significant in A-F concretes (presented in both Table 6.2 and Figure 6.7). This is observed at both standard and low curing temperatures.

6.2.3 Permeability and Water Absorption

Class A concrete samples were conditioned for water absorption tests, and the results are presented in Figure 6.8. The values of both the initial and the secondary rates of absorptions and the correlation coefficients R² for these concretes are shown in Table 6.3. Those parameters are required to report in a water absorption test, as described in ASTM C1585-20 (ASTM, 2020). The initial rate of absorption is mainly related to the amount of gel and capillary porosity of concrete, while the secondary rate of absorption is related to infilling of coarser (i.e., entrained and entrapped) air voids and can be correlated with both, the volume of air and the characteristics of the air void system (i.e., air void distribution) of concrete.

TABLE 6.2

The total volume of pores (in %) and bulk densities of Class A concretes (with and without nano-TiO₂) cured at different temperatures (28 days) with and without nano-TiO₂

Curing Temperature	Sample	Nano-TiO ₂ , wt. %	Total Pore Volume, %	Reduction in Porosity, %
23°C	A-P	0	12.81	7.27
		0.5	11.88	
	A-F	0	23.67	26.44
		0.5	17.41	
	A-S	0	22.86	11.18
		0.5	20.31	
4°C	A-P	0	13.44	5.79
		0.5	12.67	
	A-F	0	23.57	12.90
		0.5	20.53	
	A-S	0	22.88	10.40
		0.5	20.50	

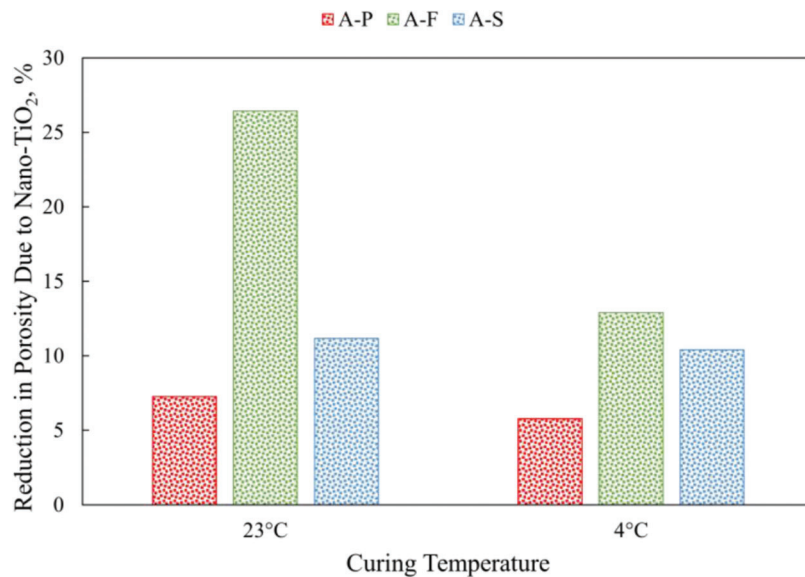


Figure 6.7 The reduction in porosity of Class A concretes due to the addition of nano-TiO₂.

Figure 6.8 a and b show the absorption test data for Class A concretes with and without nano-TiO₂ cured for 28 days at, respectively, room and low temperatures. The water absorption results for reference concretes (i.e., concretes without addition of nano-TiO₂) are represented by solid lines (red for A-P, green for A-F, and blue for A-S). It can be seen that both, the initial and secondary absorption values for concretes containing SCMs (i.e., A-F and A-S mixtures) are lower than the absorption values of the OPC concrete (A-P), regardless of the curing temperature. This clearly demonstrates that substituting part of the OPC with SCMs results in reduced permeability (similar findings have been reported by numerous other studies, e.g., Lothenbach et al., 2011). While, as mentioned earlier, the positive effects of addition of SCMs on water absorption were observed at both curing temperatures, comparing Figure 6.8 a and b shows that the reduction in absorption was even more pronounced when curing

temperature as indicated by greater separation of absorption curves (especially for initial absorption).

Figure 6.9 illustrates that the addition of nano-TiO₂ further reduced both the initial and secondary absorptions for all types of Class A concretes, regardless of the curing temperatures. As described earlier in the report, the addition of nano-TiO₂ reduces the total porosity and increases the bulk density of concretes. As a result, their permeabilities (and thus absorptions) are also reduced.

Furthermore, (as shown in Table 6.3), the initial and secondary rates of absorption of Class A concretes were also reduced due to the addition of nano-TiO₂. This is a proof that the amount of capillary porosity is reduced in concretes with nano-TiO₂ (as the initial rate of absorption is lower). In addition, the reduced secondary rate of absorption indicates that concretes with nano-TiO₂ had lower air content, in agreement with the results previously shown in Figure 5.3. The reductions

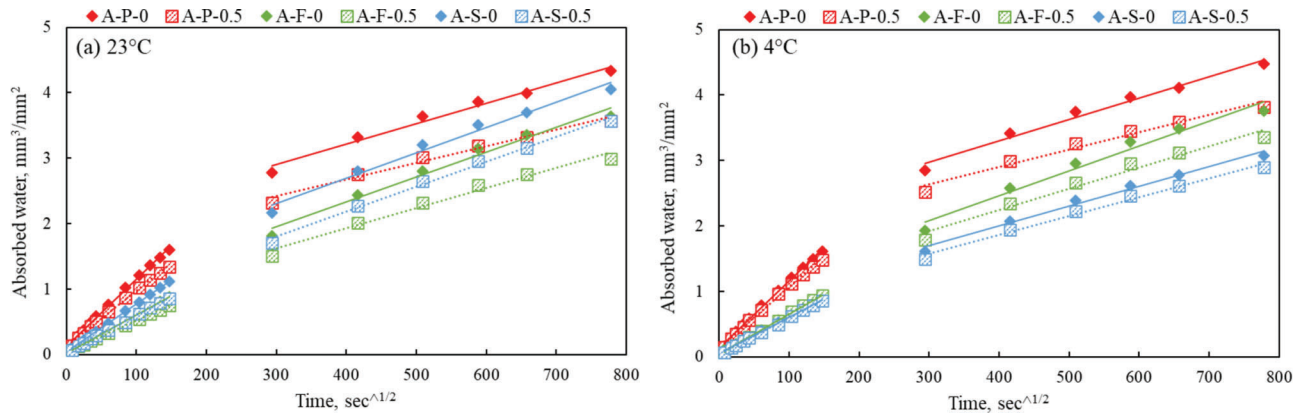


Figure 6.8 The results of water absorption test for Class A concretes with and without nano-TiO₂ after 28 days of curing at (a) room temperature, and (b) low temperature.

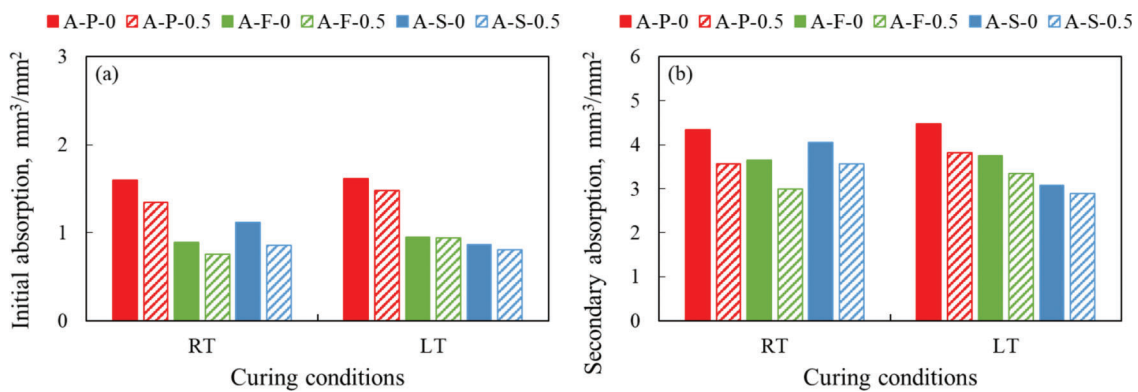


Figure 6.9 The results of (a) initial absorption, and (b) secondary absorption for Class A concretes with and without nano-TiO₂ cured at different temperatures.

TABLE 6.3
The initial and secondary rates of water absorption and the values of correlation coefficients R^2 for Class A concretes with and without nano-TiO₂ and cured at different temperatures

Curing Temperature	Sample	Initial Rate of Absorption,		Secondary Rate of Absorption,	
		$\times 10^{-4} \text{ mm}/\sqrt{s}$	R^2	$\times 10^{-4} \text{ mm}/\sqrt{s}$	R^2
23°C	A-P-0	102	0.9974	31	0.9801
	A-P-0.5	85	0.9970	25	0.9809
	A-F-0	58	0.9996	38	0.9797
	A-F-0.5	49	0.9999	31	0.9768
	A-S-0	73	0.9996	39	0.9806
	A-S-0.5	56	0.9990	38	0.9926
4°C	A-P-0	103	0.9974	33	0.9813
	A-P-0.5	94	0.9966	27	0.9763
	A-F-0	61	0.9994	38	0.9727
	A-F-0.5	63	0.9996	32	0.9728
	A-S-0	56	0.9985	30	0.9887
	A-S-0.5	51	0.9988	29	0.9896

in the initial and secondary rates of absorption were observed at both curing temperatures. In conclusion, nano-TiO₂ seems to be effective in reducing the permeability and porosity of concrete, regardless of mixture composition and curing temperature.

Another important observation is that the R^2 values for initial rate of absorption tend to be higher than those recorded for secondary rate of absorption. This might be because the initial degree of saturation of the samples is lowest during that initial period of testing,

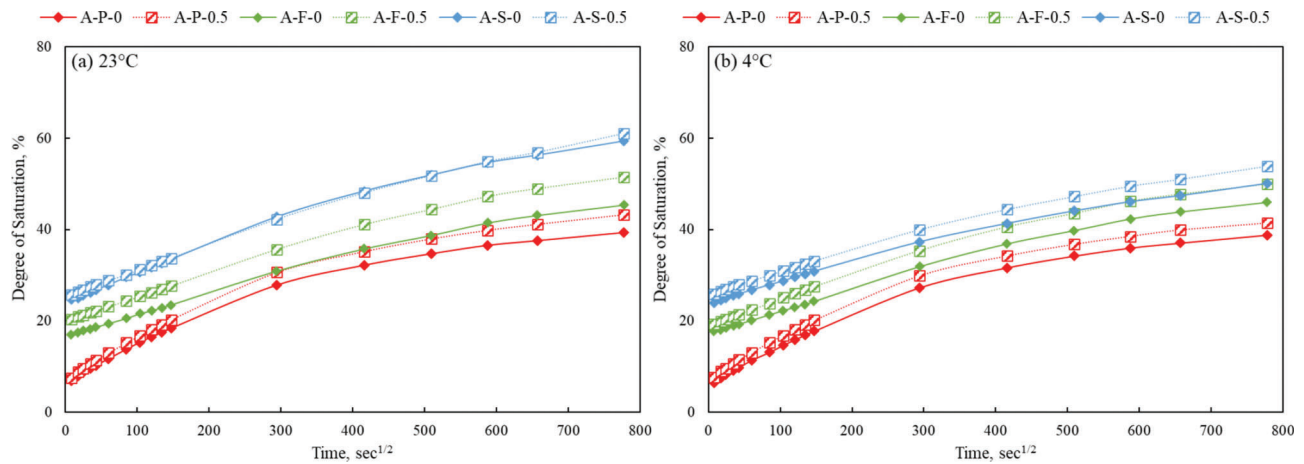


Figure 6.10 The evolution of the degree of saturation (DOS) of Class A concretes with and without nano-TiO₂ after 28 days of curing at (a) room temperature, and (b) low temperature during the water absorption test.

and thus the capillary suction force is the highest resulting in more “linear” correlation during the first stage of absorption compared to the second phase of this test.

While the mass of water absorbed can be directly presented in graphs, recent research has suggested that it may be very useful to convert these data to the degree of saturation (DOS), which is defined as the ratio of the instantaneously absorbed mass of water to the total mass of water that can be absorbed by a sample (Castro et al., 2011; Li et al., 2012). Therefore, data from water absorption test were converted to DOS in this study, with the results shown in Figure 6.10.

As suggested by both Figure 6.10 a and b, A-P reference concrete tends to have a lower DOS throughout the entire duration of water absorption test compared to A-F and A-S reference concretes, which is an indication that OPC concrete has a higher amount of air void content (entrained and/or entrapped air) (Fagerlund, 1977, 2004). Furthermore, as indicated by the dotted lines in Figure 6.10 a and b, the addition of nano-TiO₂ can slightly increase the DOS of all types of concretes during the testing period, regardless of curing temperatures. This confirms the observation presented previously that the addition of nano-TiO₂ can reduce the amount of air voids, regardless of mixture composition and curing temperature.

6.2.4 Scaling Resistance

Table 6.4 presents the visual appearance of surfaces of scaling specimens after 50 freeze-thaw cycles for Class A (A-P, A-F, and A-S) concretes with and without nano-TiO₂ addition. Figure 6.11 shows the cumulative mass loss after 50 freeze-thaw cycles for all Class A concretes with and without nano-TiO₂. In general, all concretes exhibited good scaling resistance as they have an air content of $6.5 \pm 1.5\%$. Therefore, for most slabs, only a minor scaling was observed. However, the addition of nano-TiO₂ still played an important role in modifying the scaling resistance of these concretes, especially those containing fly ash.






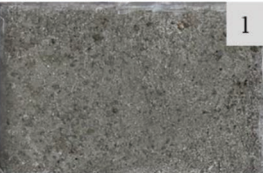


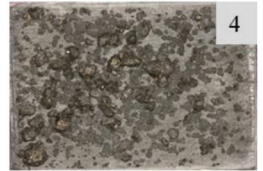


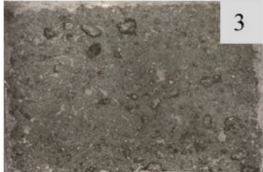






In general, all A-P concretes are scaling resistant as the cumulative mass loss is much less than 0.8 kg/m^2 even after 50 FT cycles, as shown in Figure 6.11 a and b. For plain Class A concretes cured at standard (23°C) temperature (designated as A-P-RT), lowest amount of scaling was observed in concretes with 0.5% and 1% of nano-TiO₂ addition compared to the reference concretes (without nano-TiO₂ addition), as shown in Table 6.4 and Figure 6.11. For plain Class A concretes cured at low (4°C) temperature (designated as A-P-LT), 1% of nano-TiO₂ addition reduced the cumulative mass loss compared the reference samples (without nano-TiO₂ addition). This improvement of scaling resistance can be explained by the fact that the microstructure of concrete was refined by the addition of nano-TiO₂, and the permeability of concrete was reduced before the exposure of FT cycles.

In general, Class A concretes with 24% replacement of fly ash (labeled as A-F-RT and A-F-LT), had highest degree of scaling when compared to A-P concrete, as shown in Table 6.4 and Figure 6.11. The lower degree of scaling was observed in concretes with 0.5% of nano-TiO₂ addition compared to the reference concretes (without nano-TiO₂ addition). However, an even more severe scaling was observed in samples with 1% of nano-TiO₂ addition compared to reference samples (without any nano-TiO₂ addition). This might be related to the fact that addition of 1% of nano-TiO₂ causes greatest reduction in the amount of air voids, which are critical with respect to providing good scaling resistance. Similar observation was made for Class A concretes with fly ash replacement cured at low (4°C) temperature (designated as A-F-LT).

For Class A concretes with 30% replacement of slag cured at both standard (23°C) and low (4°C) temperatures (labeled as A-S-RT and A-S-LT, respectively), no significant changes in the appearance of the surface were observed in samples with nano-TiO₂ addition (both 0.5% and 1%) compared to the reference samples (without nano-TiO₂ addition). As presented earlier, since the compressive strength was significantly

TABLE 6.4

The visual appearance of Class A concretes (A-P, A-F, and A-S) with and without nano-TiO₂ cured at different temperatures at the end of scaling test (after 50 freezing and thawing cycles)

Sample	Nano-TiO ₂ Addition, %		
	0%	0.5%	1%
A-P-RT			
A-P-LT			
A-F-RT			
A-F-LT			
A-S-RT			
A-S-LT			

improved by the addition of nano-TiO₂ for A-S concrete, one would expect the scaling resistance of these concretes will also increase. However, one needs to keep in mind that in addition to strength, the scaling resistance is also strongly related to the air void system of the concrete. The addition of nano-TiO₂ might have reduced the porosity to such a level that less air voids were available to release the hydraulic pressure upon freezing. Therefore, no significant effect can be observed by the addition of nano-TiO₂ on the scaling resistance of A-S concrete. All A-S concretes have a good scaling

resistance as the cumulative mass loss due to scaling is less than 0.8 kg/m², indicated in Figure 6.11 e and f.

Table 6.5 presents the appearance of surface of specimens after 50 freeze-thaw cycles for Class C (C-P and C-S) concretes with and without nano-TiO₂ addition. Figure 6.12 shows the cumulative mass loss after 50 freeze-thaw cycles for all Class C concretes with and without nano-TiO₂. Similar to the overall observations reported for Class A concretes, all the Class C concretes have good scaling resistance as they have an air content of 6.5 ± 1.5%. Therefore, for most C-P

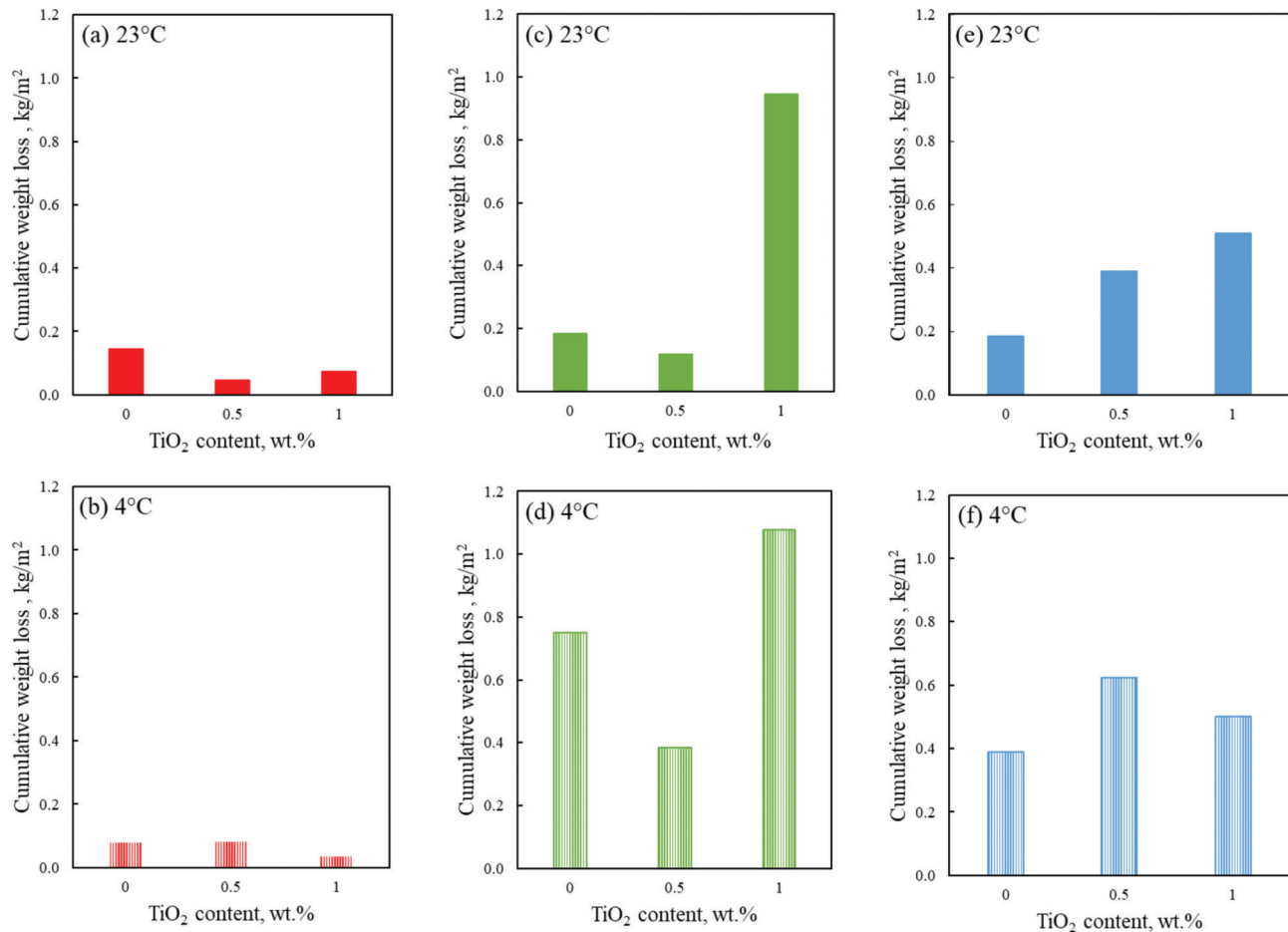


Figure 6.11 The cumulative mass loss due to scaling for Class A concretes with and without nano-TiO₂ cured at different temperatures: (a) A-P-RT; (b) A-P-LT; (c) A-F-RT; (d) A-F-LT; (e) A-S-RT; and (f) A-S-LT.

and C-S slabs, only a minor scaling was observed. However, the addition of nano-TiO₂ still played an important role in modifying the scaling resistance for those slabs.

The scaling resistance of plain Class C concretes cured at standard (23°C) temperature (labeled as C-P-RT) with 0.5% of nano-TiO₂ addition is comparable to the scaling resistance of reference concretes (without nano-TiO₂ addition) as shown in Table 6.5. However, samples with 1% of nano-TiO₂ addition did show a reduced scaling resistance compared to reference samples (without any nano-TiO₂ addition). For plain Class C concretes cured at low (4°C) temperature (designated as C-P-LT), slabs with nano-TiO₂ addition (both 0.5% and 1%) achieved a higher scaling resistance compared to the reference samples (without nano-TiO₂ addition). In general, all C-P concretes showed high scaling resistance as the cumulative mass loss due to scaling was less than 0.8 kg/m², as shown in Figure 6.12 a and b.

For Class C concretes with 30% replacement of slag cured at both standard (23°C) and low (4°C) temperature (named as C-S-RT and C-S-LT, respectively), no significant changes in surface scaling were observed in samples with nano-TiO₂ addition (both 0.5% and 1%)

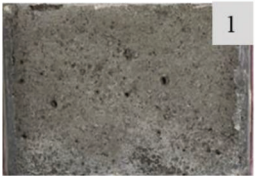






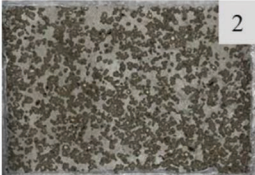

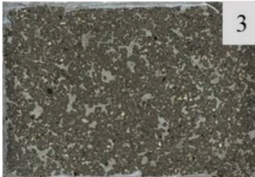

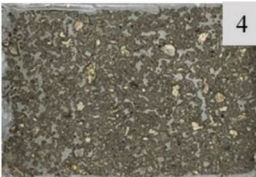
compared the reference samples (without nano-TiO₂ addition), as shown in Table 6.5. The same was observed for A-S concretes.

6.2.5 Freeze-Thaw Resistance

The changes in values of the relative dynamic modulus of elasticity (RDME) and actual dynamic Young's modulus (DME) of A-P concretes with and without the addition of nano-TiO₂ cured at different temperatures are presented in Figure 6.13 a and b. Regardless of curing temperature, the initial (i.e., before the start of the FT testing) dynamic modulus of all specimens with nano-TiO₂ was higher than that of the reference specimens (compare the crosshatched bars to the solid bars). This might be related to the fact that nano-TiO₂ can densify the paste matrix due to the acceleration of hydration process. Furthermore, porosity and permeability of concrete are reduced by the addition of nano-TiO₂. Therefore, the initial DME can be increased when nano-TiO₂ is used in concretes. When comparing the initial DME of reference A-P concrete cured at standard and low temperatures, it seems that low temperature is not affecting the DME of A-P concrete to any significant extend.

TABLE 6.5

The visual appearance of Class C concretes (C-P and C-S) with and without nano-TiO₂ cured at different temperatures at the end of scaling test (after 50 freezing and thawing cycles)

Sample	Nano-TiO ₂ Addition, %		
	0%	0.5%	1%
C-P-RT	 1	 1	 2
C-P-LT	 2	 1	 1
C-S-RT	 2	 2	 3
C-S-LT	 3	 3	 4

There was a major reduction of RDME of A-P concretes after the first 30 FT cycles, as shown in Figure 6.13 a and b. The reduction during the subsequent cycles was more gradual. When analyzed during the period of the 300 freeze-thaw cycles, the rate of reduction of RDME of A-P concretes with nano-TiO₂ addition was comparable to that of the reference concrete, regardless of the curing temperature.

The relative dynamic modulus of elasticity (RDME) and actual dynamic modulus (DME) of A-F concretes with and without nano-TiO₂ cured at different temperatures and subjected to around 800 FT cycles are presented in Figure 6.14 a and b. Similar to what was discussed in the previous paragraph, the addition of nano-TiO₂ improved the values of the initial DME (at #0 FT cycle) of A-F concretes, regardless of curing temperature. Furthermore, such enhancement due to the addition of nano-TiO₂ is more significant compared the that of on A-P concrete. Besides the reasons discussed above, for A-F concrete the use of nano-TiO₂ can also accelerate pozzolanic reaction. Therefore, the addition of nano-TiO₂ can lead to an even denser and less permeable concrete. When comparing

Figure 6.14b to 6.14a, it can be seen that A-F reference concretes cured at low temperature had comparatively lower DME than concretes cured at room temperature. This is not unexpected as low temperature can delay the hydration process of A-F concretes.

As shown in Figure 6.14a, the RDME of A-F concretes with 0.5% of nano-TiO₂ cured at standard temperature is reducing at a slower rate than the RDME of reference concretes, which indicates a higher freeze-thaw resistance can be achieved in fly ash concrete when nano-TiO₂ is added. The addition of nano-TiO₂ might be helpful with respect to mitigation of the microcracking due to the FT damage. However, such difference is not significant until more than FT 300 cycles, and even with about 800 FT cycles, and the RDME of both A-F concretes (with and without nano-TiO₂) is still around 95%. This is indicating that, originally, A-F concretes fabricated for this research have a good freeze-thaw resistance.

On the other hand, as shown in Figure 6.14b, the DME and RDME for both reference concrete and concrete with nano-TiO₂ cured at low temperature were found to be increasing, even throughout the first 400

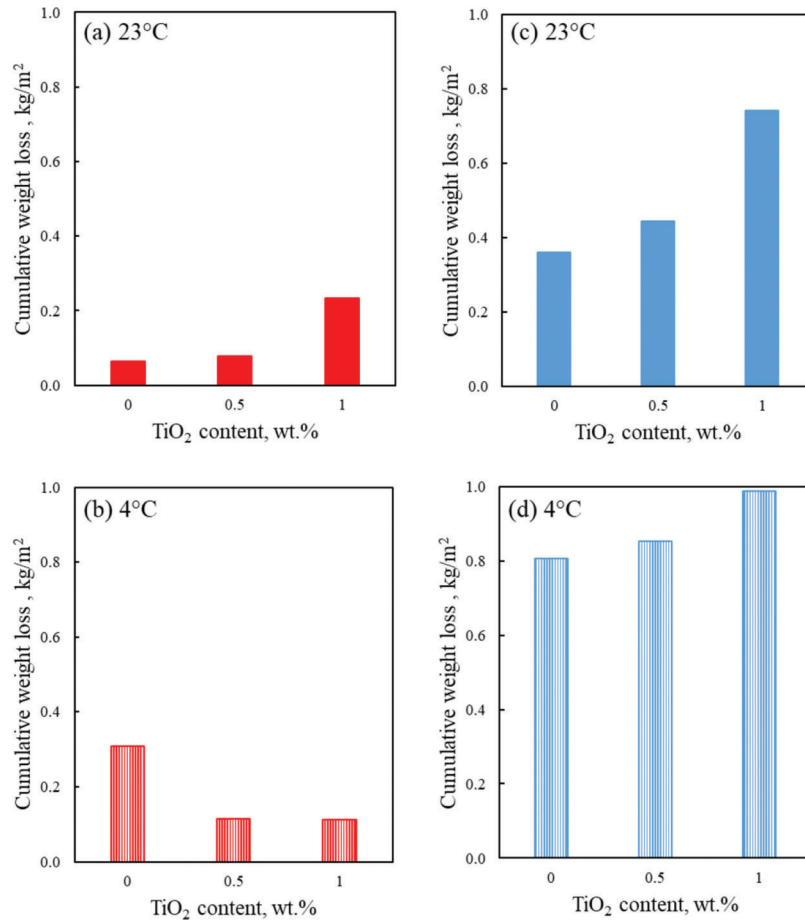


Figure 6.12 The cumulative mass loss due to scaling of Class C concretes with and without nano-TiO₂ cured at different temperatures: (a) C-P-RT; (b) C-P-LT; (c) C-S-RT; and (d) C-S-LT.

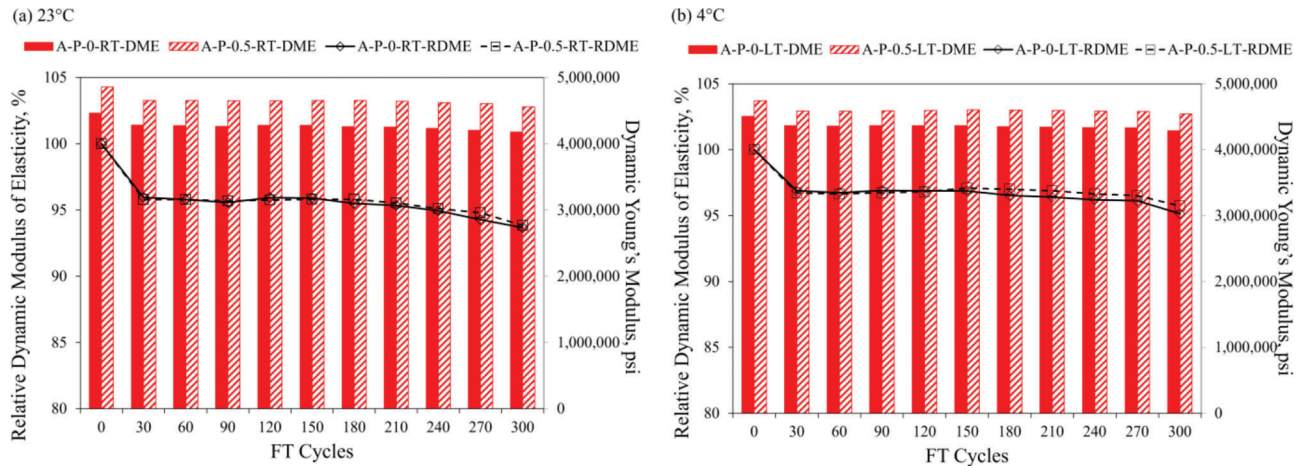


Figure 6.13 The relative dynamic modulus of elasticity (RDME) and actual dynamic modulus (DME) of A-P concretes with and without nano-TiO₂ cured at (a) room temperature, and (b) low temperature and exposed to 300 FT cycles.

FT cycles. This might be because the hydrating process in A-F concretes was much delayed during the 14-day curing low temperatures before FT tests. Therefore, even after the start of the FT test, the hydration is still ongoing, which leads to increased values of DME and RDME in A-F concretes. Comparing the RDME

values of reference concrete and concrete with 0.5% of nano-TiO₂ (solid line and dashed line), it seems that reference concrete holds a higher potential to develop more DME after 14 days of low temperature curing compared to the concrete with nano-TiO₂. This might be related to the fact that the hydration of concrete with

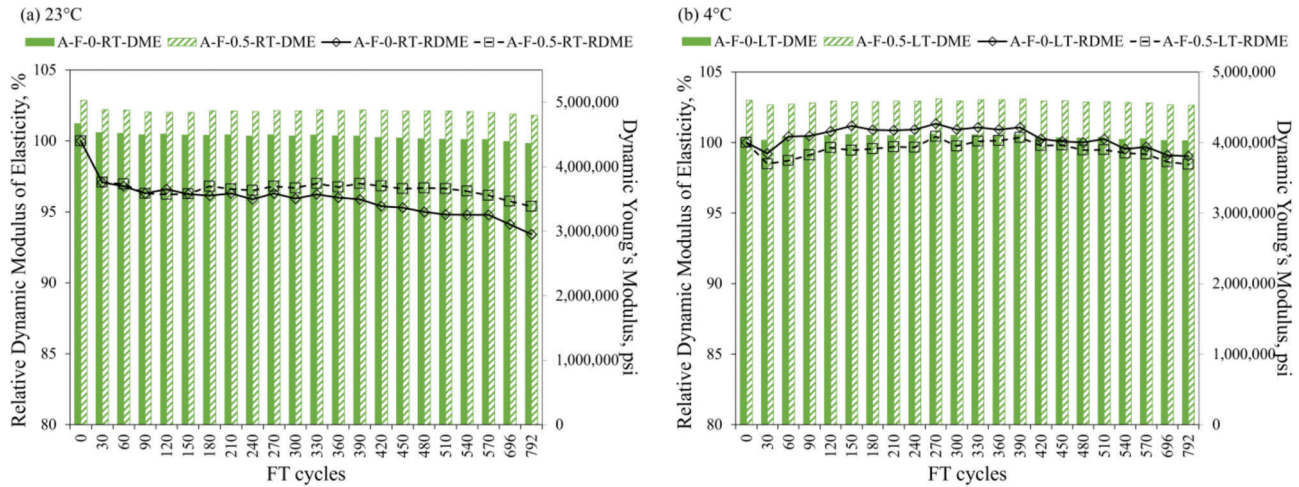


Figure 6.14 The relative dynamic modulus of elasticity (RDME) and actual dynamic modulus (DME) of A-F concretes with and without nano-TiO₂ cured at (a) room temperature, and (b) low temperature and exposed to ~ 800 FT cycles.

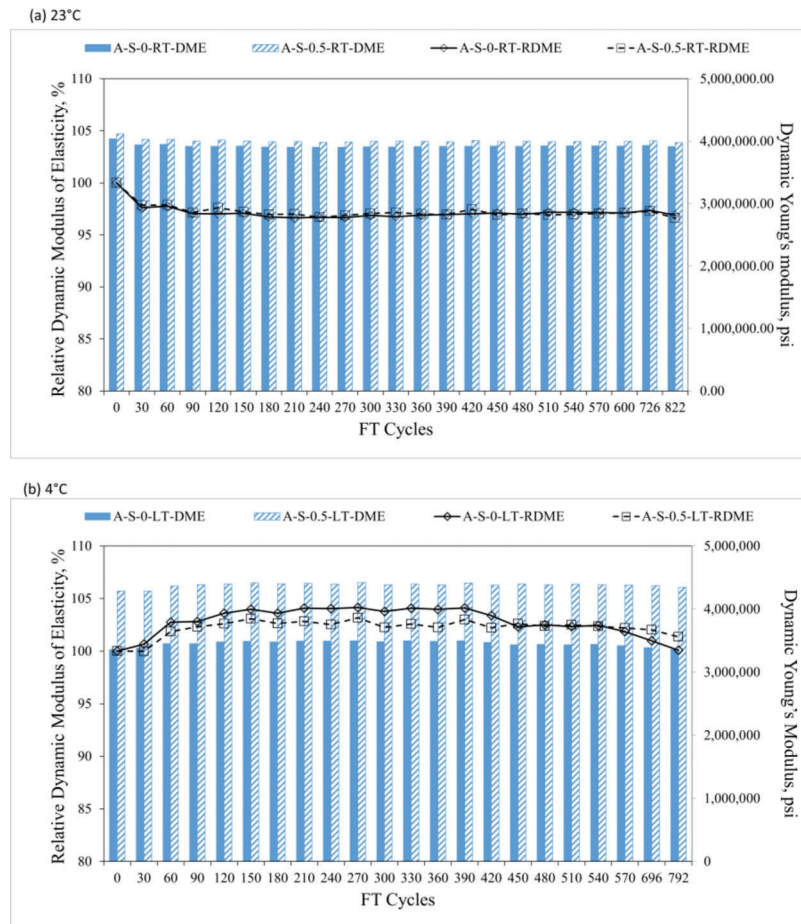


Figure 6.15 The relative dynamic modulus of elasticity (RDME) and actual dynamic modulus (DME) of A-S concretes with and without nano-TiO₂ cured at (a) room temperature and (b) low temperature and exposed to ~ 800 FT cycles.

nano-TiO₂ is accelerated (DME is improved) compared to the reference concrete, which results in lower potential for additional hydration.

The relative dynamic modulus of elasticity (RDME) and actual dynamic modulus (DME) of A-S concretes

with and without nano-TiO₂ cured at both standard and low temperatures are shown in Figure 6.15. Similarly, to what was reported earlier, the addition of nano-TiO₂ can enhance the initial values of the DME of A-S concretes, regardless of curing temperature.

Furthermore, when curing temperature is low, such effect is much more pronounced. This implies that the addition of nano-TiO₂ can be more beneficial to the microstructural modification when the curing temperature is comparatively low. Also, the influence of low curing temperature on the reduction of initial DME is observed in A-S reference concretes.

As seen in Figure 6.15a, the reduction rates of RDME of A-S concretes with and without the addition of nano-TiO₂ cured at room temperature are very comparable. It should be noted, however, that the overall decrease in the values of the RDME was very small, and all specimens retained 95% of the original levels even after ~800 FT cycles. This indicates that both concretes had excellent freeze-thaw resistance.

The DME and RDME values of A-S concretes cured at low temperature seem to be during the first ~400 FT cycles. This, again, indicates that concretes with SCMs were not mature enough after a 14-day low temperature curing. Hydration process continued even after initiation of the FT test. Furthermore, reference A-S concrete seems to have more unreacted hydrating phases as its DME curve (solid line) is higher than that of concrete with nano-TiO₂ (dashed line). Slag is a latent hydraulic SCM, and as discussed previously, the addition of nano-TiO₂ accelerates the hydration process. Therefore, after 14-days of low temperature curing, concrete with nano-TiO₂ might have less unhydrated cementitious materials, thus its DME is developing slower than that of the reference concrete (without nano-TiO₂). It was not until ~600 cycles of FT that the both reference concrete and concrete with nano-TiO₂ showed a decrease in RDME. A lower reducing rate of RDME in concrete with nano-TiO₂ compared to that of reference A-S concrete is observed after ~600 FT cycles.

7. THE EFFECT OF NANOSILICA AND CURING TEMPERATURES ON THE DURABILITY OF CONCRETE CONTAINING SCMs

7.1 Materials and Methods

7.1.1 Sample Preparation

Nanosilica-modified concretes were fabricated in laboratory to investigate its impact of these nanoadditives on the strength, porosity, and durability of concretes cured at different temperatures, following the mix design shown in Table 7.1. In total, four different types of concrete were prepared and then cured at two

different temperatures (standard: 23°C and low: 4°C). According to the recommendations from the manufacturer, E5-LFA (E5-liquid fly ash) was added at a rate of 8 oz/cwt (i.e., per hundred pounds of cementitious materials) while E5-IC (E5-Internal Cure) was added at the rate of 4 oz/cwt. One of the mixtures (E5-LFA_IC) use both, LFA and IC version of nanosilica admixtures.

All the materials needed for mixing were conditioned at room temperature and weighted before mixing. Moreover, the moisture contents of both fine and coarse aggregates were calculated, and the batching water was adjusted accordingly. Mixing process started by first placing 50% to 70% of the weight of batch water in the mixer. Then fine and coarse aggregates were added, and the mixing process was initiated. After about 2 minutes of mixing the cement, AEA, and superplasticizer were added in sequence and all the ingredients were then mixed for a period of 3 minutes. The nanosilica was combined with the remaining batch water in a separate bucket and added into the mixer using a syringe. The application of syringe replicates tail water addition from a dispenser. This process took about 4 minutes and help to evenly distribute the product over the entire surface of the mix. Once the addition of nanosilica was completed, the mixing continued for another 5 minutes. In total, the entire mixing cycle took about 15 minutes.

The resulting concretes were molded after the mixing and demolded the following day. Curing was carried out at two different temperatures (standard: 23°C and low 4°C) for prescribed number of days.

7.1.2 Methods

All details of all relevant testing methods (i.e., slump, air content (unit weight), resistivity, formation factor, total pore volume, water absorption, and scaling resistance) have been discussed in Chapters 5 and 6.

7.2 Results and Discussions

7.2.1 Fresh Properties of Concrete

The test results of fresh properties of concretes (slump, unit weight, and air content) are presented in Figure 7.1. As shown in Figure 7.1a, the addition of nanosilica (with other components kept at the same levels) resulted in reduction of the slump of concretes. The slump of concrete with combined types of

TABLE 7.1
The mix design for nanosilica-modified concretes

Mix No.	Content (lb/ft ³)				Nano-Additives and Admixtures (oz/cwt)		
	Water	Cement	Fine Aggregate	Coarse Aggregate	Nano-Silica	SP	AEA
Ref.	253.8	564	1,345	1,700	0	5.3	1.5
E5-LFA_IC	253.8	564	1,345	1,700	12	5.3	1.5
E5-LFA	253.8	564	1,345	1,700	8	5.3	1.5
E5-IC	253.8	564	1,345	1,700	4	5.3	1.5

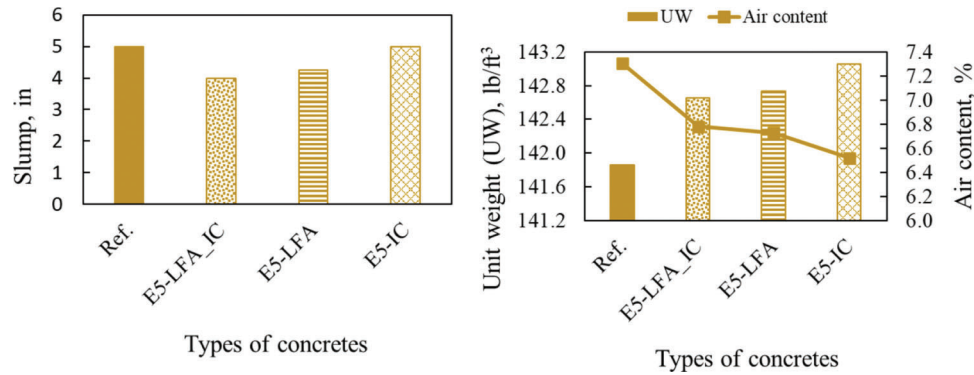


Figure 7.1 The fresh properties of concrete (slump, unit weight, and air content) with and without nanosilica.

nanosilica was the lowest among four types of concretes studied. Many researchers reported that the addition of nanosilica results in so-called “filler effect,” where small particles of the additive fill-up the voids between cement grains and enhance the packing density of the matrix making it less flowable (Du et al., 2014; Singh et al., 2013). This can explain the reduced slump of concrete with the addition of nanosilica observed in this study.

The densification of the fresh matrix, at the expense of the total air content upon addition of nanosilica is confirmed by the data shown in Figure 7.1b which shows inverse relationship between the unit weight and the air content.

7.2.2 Compressive and Flexural Strength

The 28-day compressive strengths of concretes with and without nanosilica cured at room and low temperatures are shown in Figure 7.2. It is clear from this data that the addition of nanosilica increased the strength of concrete, regardless of the curing temperature. Specifically, an increase of 14.5%, 7.2%, and 4.7% in the strength (with respect to the reference concrete) was observed for, respectively, concretes with combined (LFA + IC), LFA-only, and IC-only types of nanosilica. The mechanism of such strength enhancement is mainly related to the previously mentioned nano-filler effect and the accelerated pozzolanic reaction. Nano-sized silica can partially fill the large voids and capillary pores to refine the pore structure of cement paste (Du et al., 2014). On the other hand, the pozzolanic reaction due to the addition of nanosilica consumes calcium hydroxide (CH) and produces additional C-S-H-phase. Other potential contributing factors include reduction in the size of the CH crystal which leads to more homogenous C-S-H phase (Du et al., 2014). Potentially, the above-mentioned mechanisms can improve the bonding between aggregates and cement paste. As a result, a denser and stronger ITZ can be formed with the addition of nanosilica.

For concretes cured at low temperature the enhancement of strength of concrete due to the addition of nanosilica appears to be more significant, as higher increases relative to the reference concretes were observed compared to that of room temperature curing

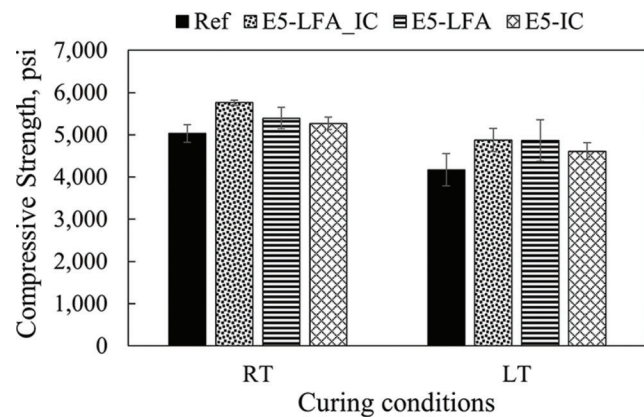


Figure 7.2 The 28-days compressive strength values of concretes with and without nanosilica cured at different temperatures.

(16.9% vs. 14.5%, 16.7% vs. 7.2%, and 10.6% vs. 4.7%, for combined types, LFA-only, and IC-only, respectively). This suggests that the addition of nano-silica might be more effective in improving the compressive strength of concretes when curing temperature is low. Furthermore, concretes cured at low temperature yield a lower strength and higher standard deviation of strength data compared to that of room curing temperature condition.

Figure 7.3 presents the influence of nanosilica (with both types combined) on the flexural strength of plain concretes cured at different temperatures. At early age (as shown in Figure 7.3a), a significant increase in flexural strength in plain concrete was observed due to the addition of nanosilica, while such effect is minimal after 28 days of curing, as presented in Figure 7.3b. This observation seems to be similar to that of nano-TiO₂ on the flexural strength as presented previously (enhancement in flexural strength is more significant at earlier ages).

7.2.3 Pore Connectivity

The results of resistivity and formation factor for concretes with and without nanosilica cured at both room and low temperatures are shown in Figure 7.4.

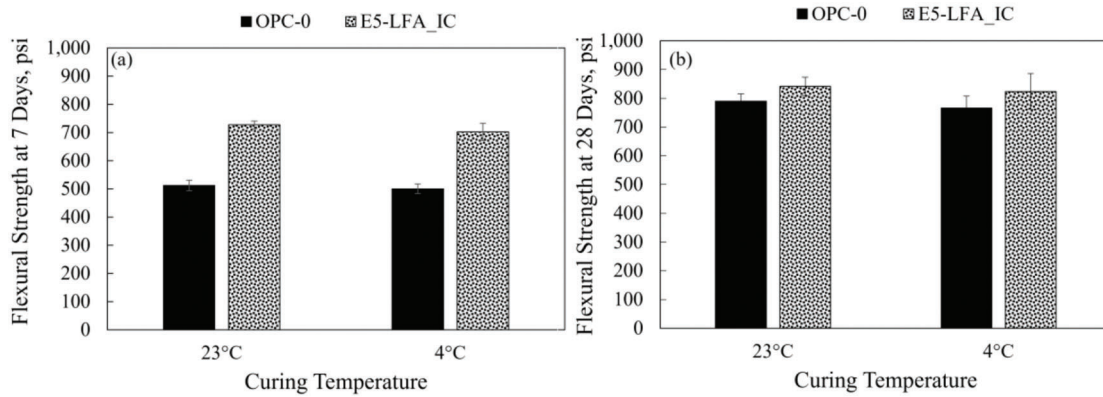


Figure 7.3 The flexural strength of concretes with and without nanosilica at different curing temperatures for (a) 7 days, and (b) 28 days.

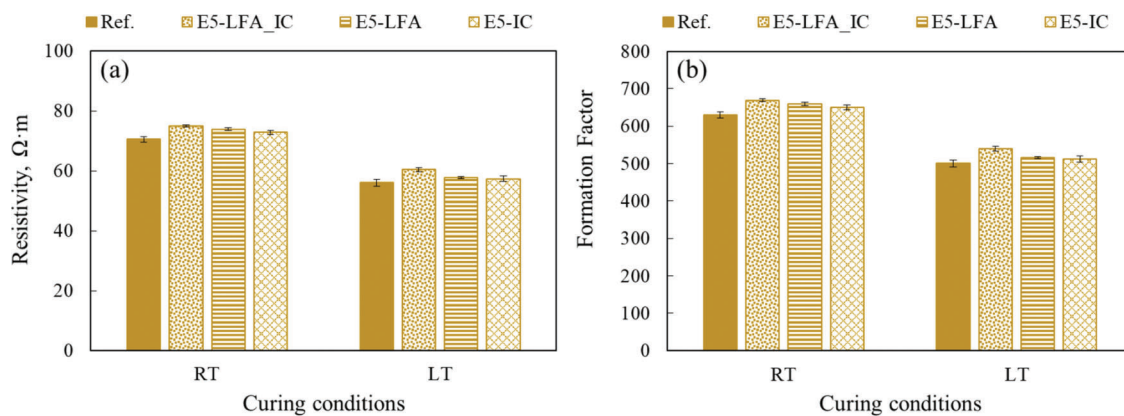


Figure 7.4 The 28 days values of (a) resistivity and (b) formation factor of concretes with and without nanosilica and cured at different temperatures.

As mentioned before, the formation factor was calculated based on AASHTO TP84-19.

As shown in Figure 7.4, concretes (all types) cured at low temperature tend to have a lower formation factor. This is because lower temperature slowed down the hydration process, resulting in more open and connected pore system. The addition of nanosilica (regardless of the type) increased the formation factor of concretes, regardless of the curing temperature. This observation corroborates previously reported observations that nanosilica can improve the particle packing and reduce porosity in concrete. The trends in the formation factor further suggest that nanosilica can reduce the connectivity of pores in concretes.

7.2.4 Total Pore Volume

Figure 7.5 shows the results for the total volume of the pores in concretes with and without nanosilica cured at both room and low temperatures. It appears that addition of nanosilica reduces the total permeable porosity of concrete, regardless of curing temperature and type of nanosilica used.

The correlation between the total pore volume and formation factor of concretes with and without

nanosilica cured at different temperatures can be found in Figure 7.6. When cured at low temperature, all concretes (regardless of the composition) had higher number of permeable pores and lower value of formation factor (indicating more connected porosity). The addition of nanosilica can not only reduce the number of pores but also reduce the connectivity of pores. This suggests that the addition of nanosilica can be beneficial with respect to improving the durability of concretes. Furthermore, such effect of nanosilica was more significant at lower temperatures.

7.2.5 Water Absorption

After 28-day curing, concretes with and without nanosilica were prepared for water absorption test, and the results are presented in Figure 7.7. The initial rate of water absorption can be related to the amount of gel and capillary porosity of concretes, while the secondary rate of absorption is indicative of the amount and the quality of the air-void system present in concrete.

When cured at low temperature, reference concrete (without the addition of nanosilica) seems to have higher absorption levels (both initial and secondary), which is expected as concretes cured at low temperature

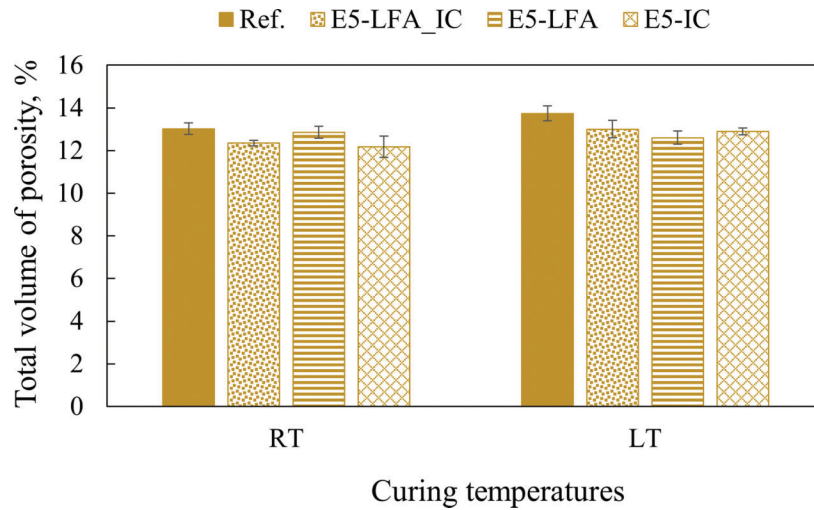


Figure 7.5 The total pore volume of concretes with and without nanosilica cured at different temperatures.

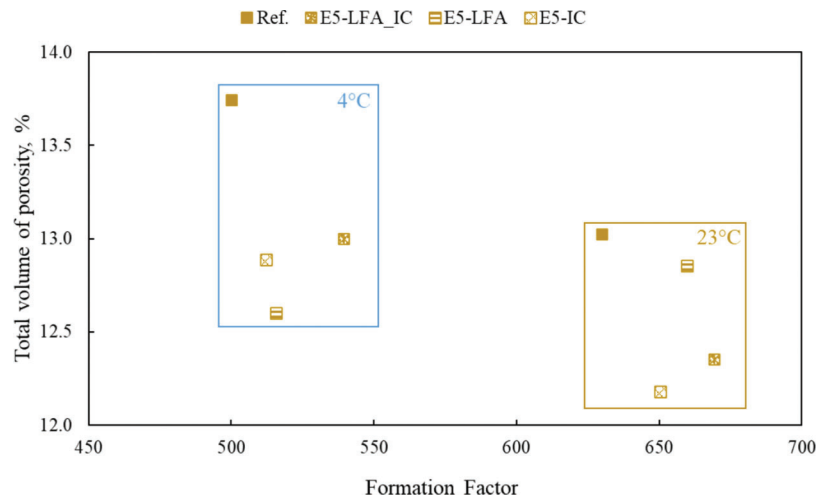


Figure 7.6 The correlation between the total pore volume and the value of the formation factor for concretes with and without nanosilica cured at both room and low temperatures.

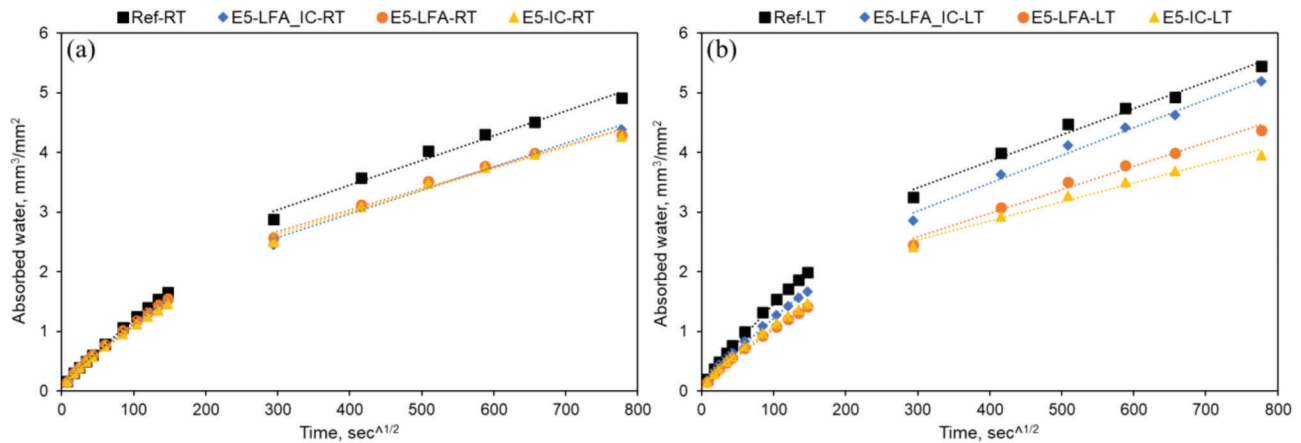


Figure 7.7 The results of water absorption for concretes with and without nanosilica after 28-day curing at (a) room temperature, and (b) low temperature.

can have higher amount of porosity. The addition of nanosilica can reduce both the initial and secondary absorption, regardless of the types of nanosilica and curing temperatures used, as shown in Figure 7.7.

Another observation can be made when comparing the water absorption results of concretes with and without nanosilica at different curing temperatures. It seems that a more significant impact of various types of nanosilica on the results of water absorption can be found when curing temperature is low as curves shown in Figure 7.7b are more separated. This suggests that the addition of different types of nanosilica might have a more profound influence on the permeability of concretes when curing at low temperature. Specifically, IC-type of nanosilica is more beneficial in reducing the water absorption of concretes compared to the other two scenarios (combined types of nanosilica and LFA-only).

Previous results suggest that nanosilica can reduce the total permeable pores. Therefore, the permeability of concrete can be reduced due to the addition of nanosilica. Furthermore, the rates of both initial and secondary absorption of concretes can be reduced due to nanosilica, as shown in Table 7.2. Table 7.2 presents the data of the rate of initial and secondary absorption and R^2 of water absorption results of concretes with and without nanosilica cured at different temperatures. This finding suggests that the gel and capillary porosity

can be reduced, and the air void content can be lowered when nanosilica is added to concretes. This observation is true for concretes cured at both room and low temperatures. Therefore, nanosilica seems to be effective to reduce the permeability and porosity of concrete regardless of the type and curing temperatures used.

Similarly, as discussed in previous chapter, the R^2 for initial rate of absorption seems to be higher than R^2 value for the secondary absorption (as shown in Table 7.2), regardless of the type of concretes and curing temperatures. This might be related to the fact that during the stage of initial absorption, the degree of saturation of concretes is lower compared to the degree of saturation experienced during later stages of absorption. Therefore, the suction force due to the porosity at initial state is higher, and this can lead to a higher linearity of absorption results.

The results of both initial and secondary water absorption test are presented in Figure 7.8 to better illustrate the influence of curing temperatures on the effect of nanosilica on reducing the absorption of concretes. As shown in Figure 7.8a, the addition of nanosilica (regardless of the type) can reduce the initial absorption of concretes, and such effect is more significant when curing temperature is low. Similarly, nanosilica seems to be more beneficial in reducing the secondary absorption of concrete at low curing temperature, as shown in Figure 7.8b. When cured at low

TABLE 7.2
Initial and secondary rates of water absorption results for concretes with and without nanosilica cured at different temperatures

Curing Temperature	Sample	Rate of Initial Absorption, $\times 10^{-4}$	R^2	Rate of Secondary Absorption, $\times 10^{-4}$	R^2
23°C	Ref.	106	0.9976	41	0.9802
	E5-LFA_IC	93	0.9905	39	0.9882
	E5-LFA	98	0.9941	36	0.9839
	E5-IC	90	0.9944	36	0.9811
4°C	Ref.	128	0.9948	44	0.9818
	E5-LFA_IC	105	0.0058	47	0.9861
	E5-LFA	88	0.9946	39	0.9844
	E5-IC	92	0.9934	32	0.9828

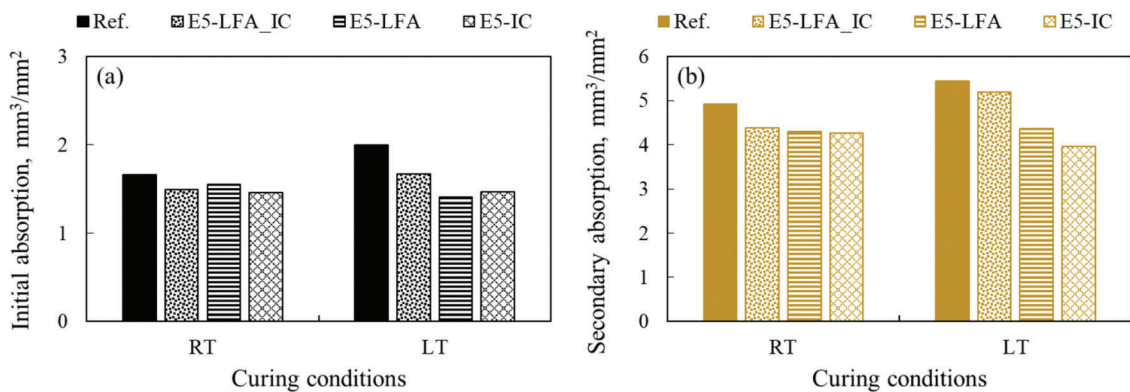










Figure 7.8 The results of (a) initial absorption and (b) secondary absorption of concrete with and without nanosilica at different curing temperatures.

TABLE 7.3

The visual appearance of concretes with and without nano-silica after 50 FT cycles of scaling test with and without nanosilica cured at different temperatures

Sample	Nano-Silica Addition			
	Ref.	E5-LFA_IC	E5-LFA	E5-IC
RT				
LT				

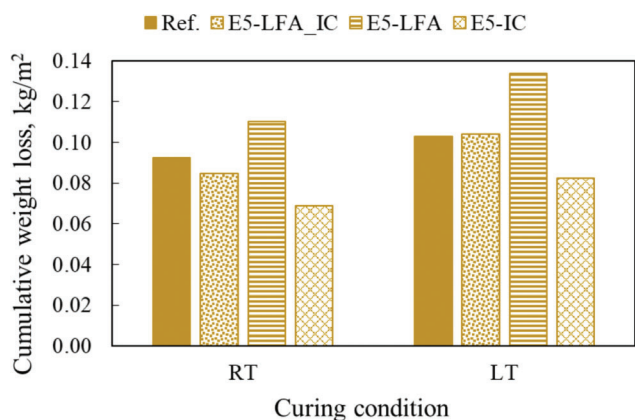


Figure 7.9 The cumulative mass due to scaling of concretes with and without nanosilica cured at different temperatures.

temperature, the hydration process of concrete is negatively affected, and thus the paste may have more open porosity than the paste cured at standard temperature.

7.2.6 Scaling Resistance

Table 7.3 presents the appearance of surfaces of concretes with and without nanosilica after 50 scaling (i.e., freeze-thaw) cycles. Figure 7.9 shows the cumulative mass loss for the same concretes. In general, all concretes tested in this study have a good scaling resistance. This is somewhat expected as all of them were designed to have the air content of about $6.5 \pm 1.5\%$. Therefore, only a minor scaling was observed for all types of concretes tested. However, the data suggests that addition of nanosilica, especially IC-type, can still lead to improvement of scaling resistance.

8. THE INFLUENCE OF NANO-TiO₂ AND NANOSILICA ON THE MICROSTRUCTURE OF CONCRETES CONTAINING SCMs

8.1 Sample Preparation and Methods

8.1.1 Sample Preparation

Nanoparticles-modified concretes were fabricated in laboratory to investigate the impact of these admixtures on the microstructure and air void system of concretes cured at different temperatures, following the mix design shown in Table 8.1 a and b.

8.1.2 Methods

8.1.2.1 Scanning Electron Microscopy (SEM). Approximately 1" cube was cut from the bulk concrete specimens. After cutting, samples were dried in the oven at the temperature of $35 \pm 5^\circ\text{C}$ for 3 days to remove free water. Subsequently, the specimens were impregnated with a low viscosity epoxy. When the epoxy hardened, the top layer of the specimen was cut off, ground (45 micron, 30 micron, and 15 micron) and polished (9 μm , 6 μm , 3 μm , 1 μm , 0.25 μm) in successive steps. Samples were then coated with palladium (Pd) to provide a conductive layer. The SEM analysis was performed using the ASPEX Personal SEM equipped with the energy dispersive x-ray (EDX) analyzer and operated in the backscattered electron mode. The accelerating voltage used in the examination was 15 keV.

8.1.2.2 RapidAir. The RapidAir, shown in Figure 8.1, is an automated system for analyzing the air void content of hardened concrete. Prior the test, surfaces of concrete samples were polished following the procedure described in ASTM C457. The polished surfaces were

TABLE 8.1
The mix design for concretes with the addition of (a) nanosilica and (b) nano-TiO₂

(a) Mix No.	Content (lb/ft ³)				Nano-Additive (oz/cwt) and Admixtures (oz/cwt)		
	Water	Cement	Fine Aggregate	Coarse Aggregate	Nano-Silica	SP	AEA
Ref.	253.8	564	1,345	1,700	0	5.3	1.5
E5-LFA	253.8	564	1,345	1,700	8	5.3	1.5

(b) Mix No.	Content (lb/ft ³)				Nano-Additive (wt. %) and Admixtures (oz/cwt)		
	Water	Cement	Fine Aggregate	Coarse Aggregate	Nano-TiO ₂	SP	AEA
F-0	260.5	592	1,315	1,670	0	5.3	1.5
F-0.5	260.5	592	1,315	1,670	0.5 wt. %	5.3	1.5
S-0	248.2	564	1,350	1,700	0	5.3	1.5
S-0.5	248.2	564	1,350	1,700	0.5 wt. %	5.3	1.5



Figure 8.1 The RapidAir system for automatic analysis of the air void system in hardened concrete (Jakobsen et al., 2006).

then painted black while the voids were filled with contrast enhancing white powder (BaSO₄) as described in the next paragraph.

Concrete samples, with dimensions of approximately 100 × 100 × 20 mm was from the cylinders using a concrete saw having a smooth, continuous blade with a small diamond cutting edge. The resulting saw cutting was smooth without major damage of the concrete surface. Afterwards, concrete samples were polished on a cast iron plate using a slurry consisting of silicon carbide and water. Five different grit sizes were used, starting with grit 80, then 120, 240, 400, and finished with grit 800. During the lapping process, water was constantly provided to provide lubrication between the concrete samples and the grit. The sample preparation, including cutting, and polishing is crucial for obtaining good results in the air void analysis.

After finalizing the polishing, concrete samples were colored black by gently dragging a broad tipped marker pen over the surface in slightly overlapping lines. After a few seconds, (to allow for the drying of the ink),

samples were turned 90°, and the coloring process was repeated. Such process was done to make sure that aggregate was covered while the voids were not filled with black ink. Following that, a dry white powder (BaSO₄) was sprinkled over the surface. The BaSO₄ powder was packed into the air voids by tamping a hard rubber stopper over the surface of the sample. When all voids appeared to be filled, the excess powder was removed by using a low-pressure air hose. The surface was then cleaned by moving the palm of a hand in circular motion over the surface until it appeared shiny and not covered with a white dust. Finally, a fine tipped marker was used to paint the holes and pores present in aggregate black.

After completion of the above-mentioned procedure, concrete samples were analyzed using a RapidAir 457 Air Void Analyzer (purchased from Concrete Experts International ApS, located in Denmark). To distinguish between black and white pixels, a threshold value needs to be preset by the operator. The actual threshold value depends on several factors, such as the light/contrast

setting of the system, the general brightness of the room, and the type of the black ink used for the coloring of the concrete surface. During this research, a threshold value was set to be the same for all specimens to allow for direct comparison. The paste contents of the samples were determined by the ASTM 457-point count method while ASTM 457 liner traverse method was used for air void analysis.

8.2 Results and Discussions

8.2.1 The Effect of Nano-TiO₂ and Nanosilica on the Microstructure of Concretes

The microstructure of concrete specimens was evaluated by the application of scanning electron microscope (SEM). Such technique enables the analysis of the general microstructural characteristics of a concrete sample (e.g., the arrangement of aggregates, condition of the paste and any defects). Moreover, the possibility to apply energy dispersive x-ray (EDX) analyzer provides a powerful tool to perform local chemical microanalyses.

In this study, the characteristics of the interfacial transition zone (ITZ), which is the boundary region between aggregates and cement paste, was one of the focuses of this analysis. This area can contain higher porosity and lower number of cement particles compared to other regions (Scrivener, 2004). Microcracks often initiate and propagate preferentially in ITZ. In addition, the collected images were analyzed using the ImageJ software to determine the average size of unhydrated cement particles in concrete specimens.

Table 8.2 presents the representative SEM images based on the observation of ITZ for fly ash concrete samples. As shown in the first row of Table 8.2, extensive cracks were observed in ITZ in the SEM images of F-0-RT (reference fly ash concrete cured at room temperature) specimen. As highlighted by red arrows, those cracks are either originating from ITZ or propagating through ITZ, both scenarios suggesting possibly weak ITZ for such specimen. On the other hand, such crack patterns were not observed in specimen with nano-TiO₂ addition, as shown in the 2nd row of Table 8.2. In this case, the ITZ seems to be denser, with less cracks and defects. Similarly, when comparing the images in the 3rd and 4th rows in Table 8.2 (obtained from low curing temperature samples), more cracks were found in the reference specimen compared to the specimen with nano-TiO₂. It seems that the addition of nano-TiO₂ improves packing of the particles and thus enhances the quality of ITZ.

However, for slag concrete with and without nano-TiO₂ (as shown in Table 8.3), such enhancement in the microstructure due to addition of nano-TiO₂ was not as significant as in fly ash concrete as the quality of the ITZs observed in S-0 and S-0.5 concrete specimens were very comparable. The greater enhancement of the microstructure due to nano-TiO₂ addition observed in

concretes with fly ash than in concretes with slag agree with the trends regarding the effects of nano-TiO₂ on scaling resistance concretes with fly ash versus concretes with slag.

Table 8.4 presents a comparison between the microstructure of reference OPC concrete and OPC concrete with the addition of nanosilica (LFA). The cracks in the reference OPC concrete seems to be more frequent compared to the samples with nanosilica. Furthermore, the average size of air void of reference OPC concretes tends to be larger.

Table 8.5, Table 8.6, and Table 8.7 present a similar arrangement of SEM images from all concrete specimens studied but obtained at higher magnification (200×). The addition of nano-TiO₂ seems to be more significant with respect to reducing the cracks around ITZ in fly ash concrete compared to slag concrete. OPC concrete with the addition of nanosilica has less cracks and smaller air void sizes compared to the reference concrete (i.e., concrete without the addition of nanosilica), as shown in Table 8.7.

The average particle size of unhydrated cement in concrete samples with and without nanoadditives. Figure 8.2 presents the results of the analysis of the average size of unhydrated cement particles in the corresponding concrete samples (obtained using ImageJ software). Three different areas/images were analyzed and the particle size of unhydrated cement particles were calculated. Compared to the reference concrete samples (i.e., samples without the addition of nanoadditives), the average size of unhydrated cement particles in samples with nanoadditives (nano-TiO₂ or nanosilica) is reduced. This indicates the addition of nanoadditives tends to accelerate the degree of hydration of cement particles, which agrees with the conclusions from Chapter 4.

8.2.2 The Effect of Nano-TiO₂ and Nanosilica on the Air-Void System in Hardened Concretes

8.2.2.1 Effects of nano-TiO₂. Table 8.8 presents the effects of nano-TiO₂ on the characteristics of the air void systems in concretes containing fly ash and slag. The results are based on the air voids ranging in size from 30 to 4,000 μm. Air voids that are smaller than 30 μm were excluded as they cannot be observed by the operator if manual air void counting method is used (Kevern et al., 2009). To ensure comparable parameters between the manual and automatic air void counting, such small sizes of air voids were not calculated. In both types of concretes (i.e., fly ash concrete or slag concrete), the addition of nano-TiO₂ slightly reduced the air content. However, the specific surface area of air voids was observed to increase, and the spacing factor was observed to decrease. It appears that the addition of nano-TiO₂ to concretes containing SCMs resulted in a finer and more closely spaced air-void system compared to the same types of concretes but without nano-TiO₂ addition.

TABLE 8.2
 The characteristics of ITZ of fly ash concrete samples with and without nano-TiO₂ (mag 100 ×)

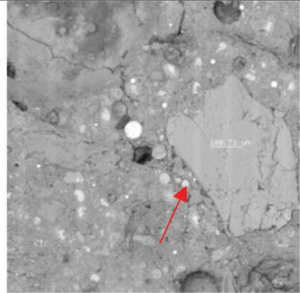
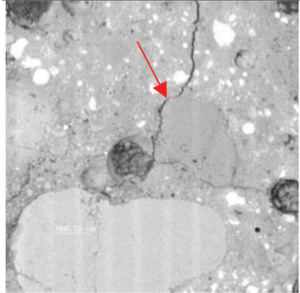
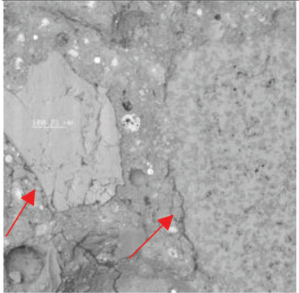
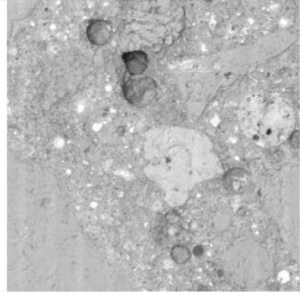
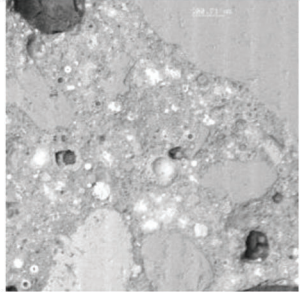
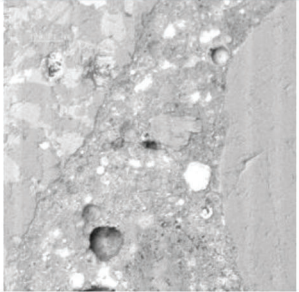
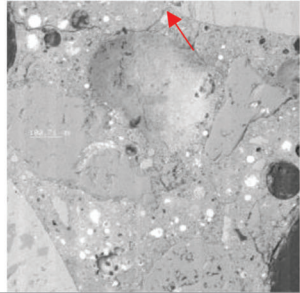
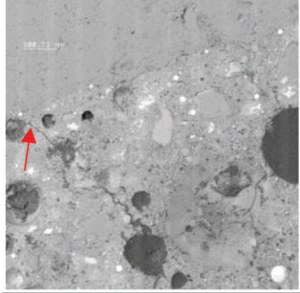
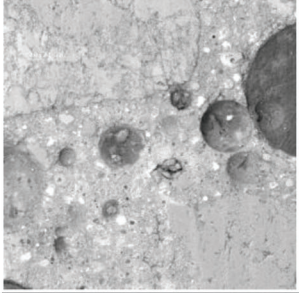
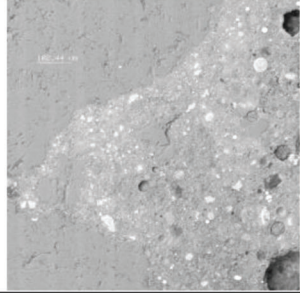
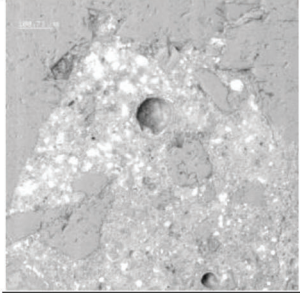
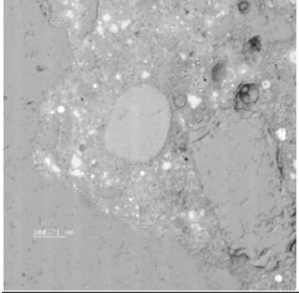
Sample	Microstructure of ITZ (100 ×)		
F-0-RT			
F-0.5-RT 100 μm			
F-0-LT			
F-0.5-LT 100 μm			

TABLE 8.3
 The characteristics of ITZ of slag concrete samples with and without nano-TiO₂ (mag 100 ×)

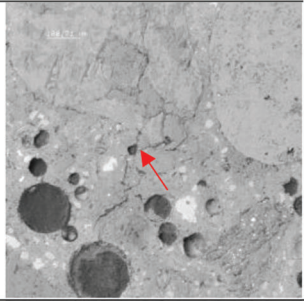
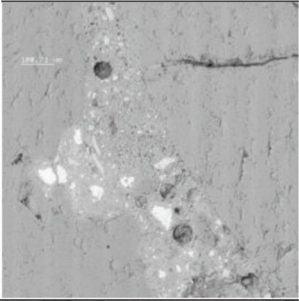
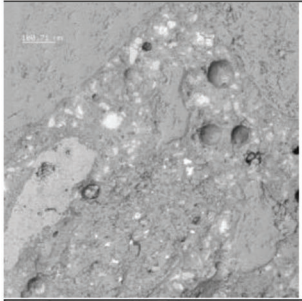
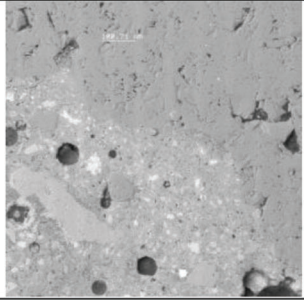
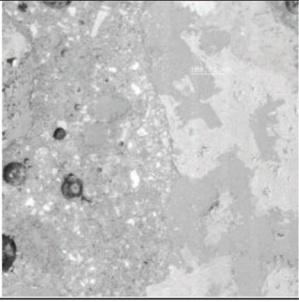
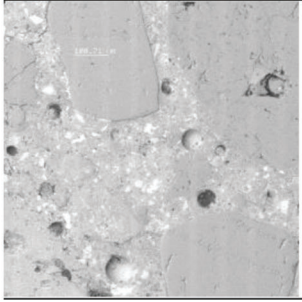
Sample	Microstructure of ITZ (100 ×)		
S-0-RT 100 μm			
S-0.5-RT 100 μm			

TABLE 8.4
 The characteristics of ITZ of OPC concrete samples with and without nanosilica (mag 100 ×)

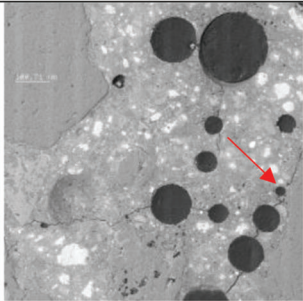
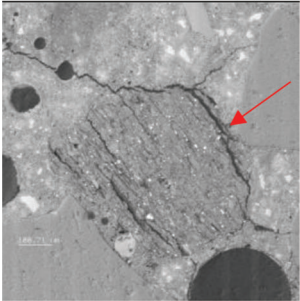
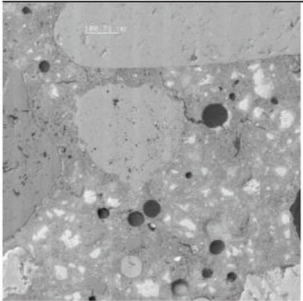
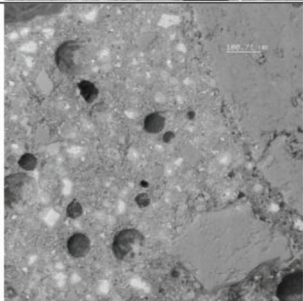
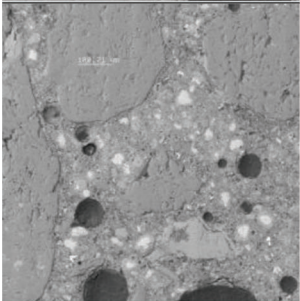
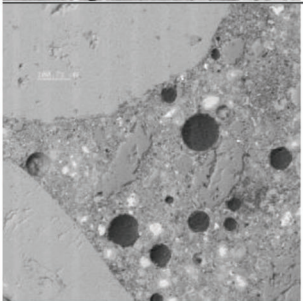
Sample	Microstructure of ITZ (100 ×)		
OPC-0-RT 100 μm			
OPC-LFA-RT 100 μm			

TABLE 8.5
 The characteristics of ITZ of fly ash concrete samples with and without nano-TiO₂ (mag 200 ×)

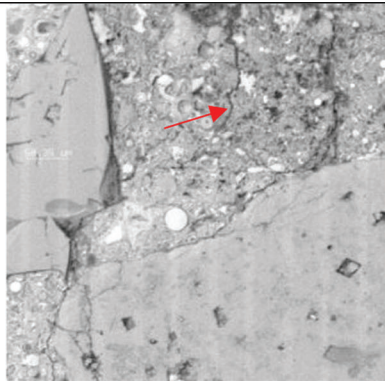
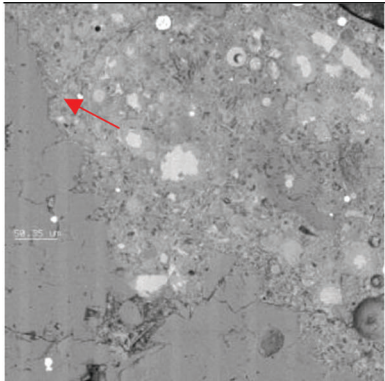
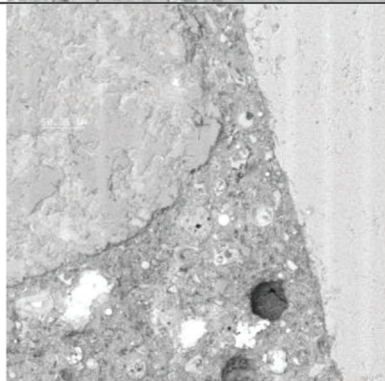
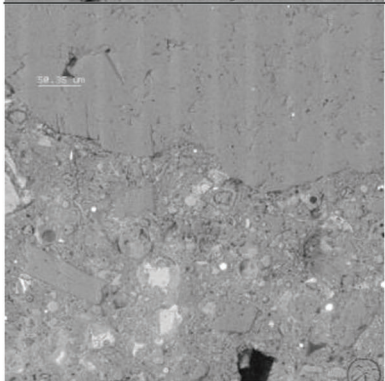
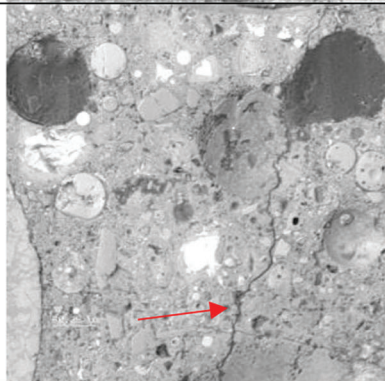
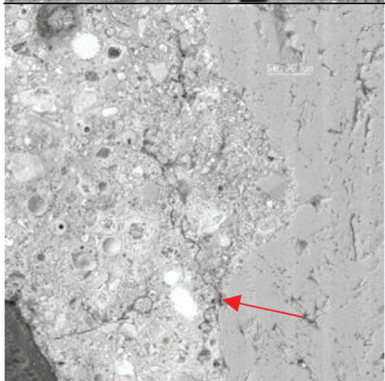
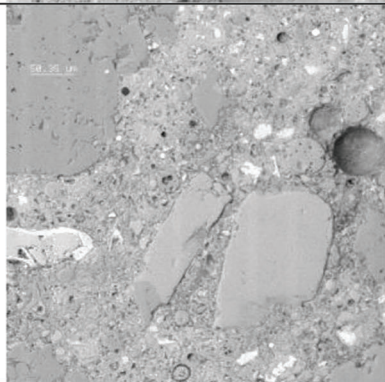
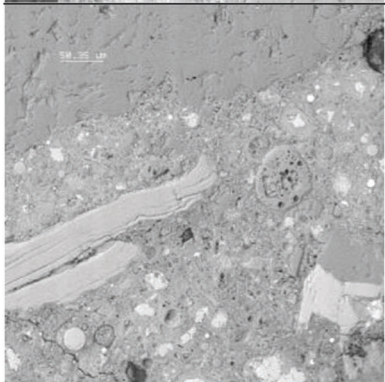
Sample	Microstructure of ITZ (200 ×)	
F-0-RT 50 μm		
F-0.5-RT 50 μm		
F-0-LT 50 μm		
F-0.5-LT 50 μm		

TABLE 8.6
 The characteristics of ITZ of slag concrete samples with and without nano-TiO₂ (mag 200 ×)

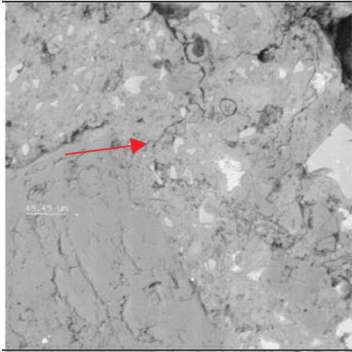
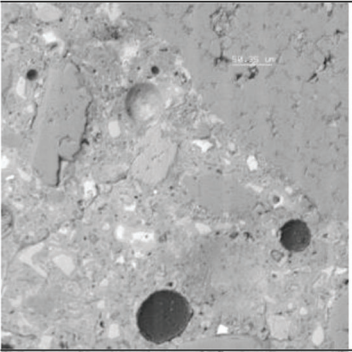
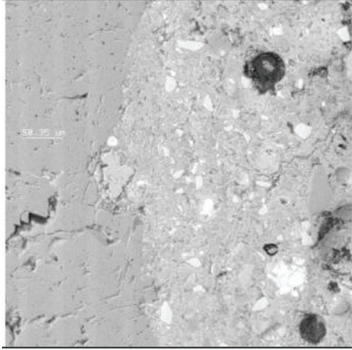
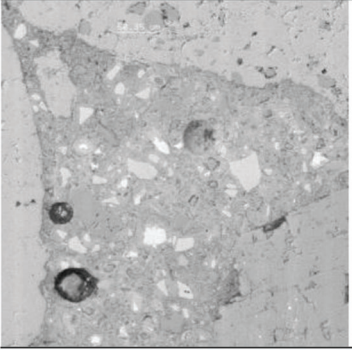
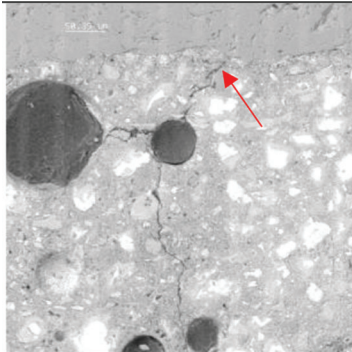
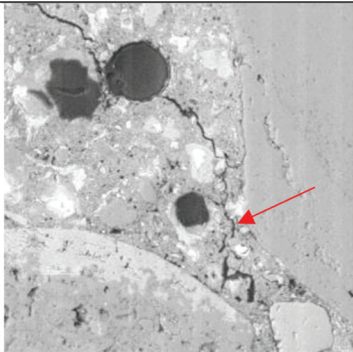
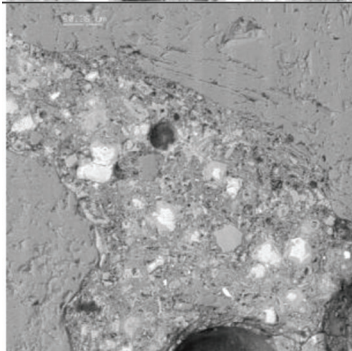
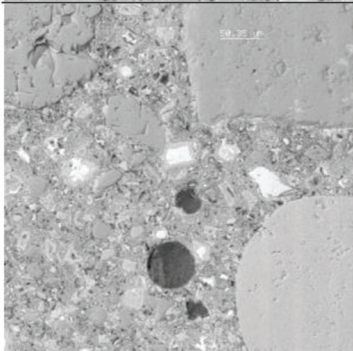
Sample	Microstructure of ITZ (200 ×)	
S-0-RT 50 μm		
S-0.5-RT 50 μm		

TABLE 8.7
 The characteristics of ITZ of OPC concrete samples with and without nanosilica. (mag 200 ×)

Sample	Microstructure of ITZ (200 ×)	
OPC-0-RT 50 μm		
OPC-LFA-RT 50 μm		

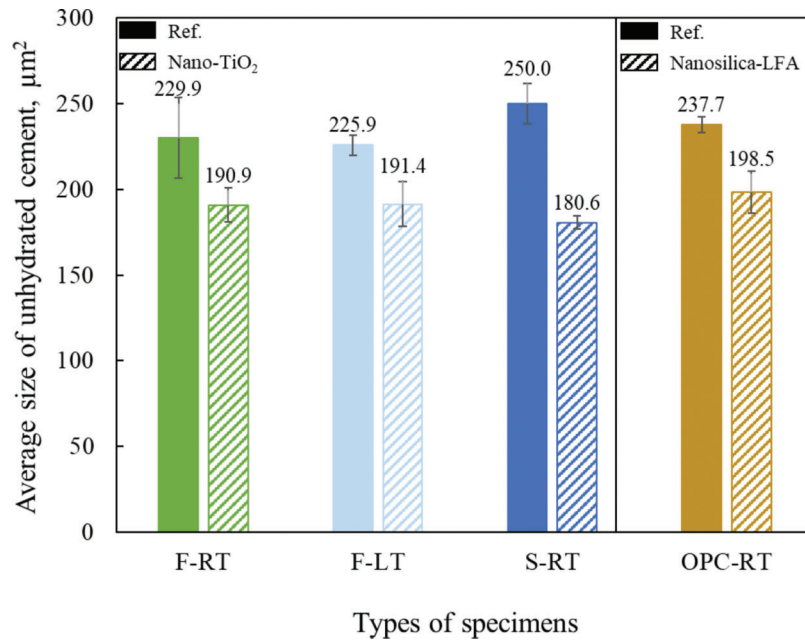


Figure 8.2 The average particle size of unhydrated cement in concrete samples with and without nanoadditives.

TABLE 8.8
The air content, specific surface area (SSA), and spacing factor (SF) values for concretes with and without nano-TiO₂

Sample	Air Void Content, %	Specific Surface Area (SSA), mm ⁻¹	Spacing Factor (SF), mm
F-0-RT	8.78	18.81	0.151
F-0.5-RT	7.68	23.54	0.138
F-0-LT	8.30	31.76	0.095
F-0.5-LT	7.85	32.58	0.098
S-0-RT	7.62	20.45	0.16
S-0.5-RT	6.85	24.24	0.151

TABLE 8.9
Results of the air content, specific surface area (SSA), and spacing factor (SF) of concrete with and without nanosilica

Sample	Air Void Content, %	Specific Surface Area (SSA), mm ⁻¹	Spacing Factor (SF), mm
Ref.	6.63	24.93	0.183
E5-LFA	6.70	27.33	0.153

8.2.2.2 Nanosilica. The results of the RapidAir analysis for concretes with and without nanosilica are presented in Table 8.9. The addition of nanosilica did not seem to affect the air void content of concrete significantly. On the other hand, the specific surface area (SSA) and spacing factor (SF) were modified by nanosilica. Specifically, when E5-LFA was added to concrete, its air void system seems to have a higher SSA and smaller SF. This indicates the air-void system contains finer and more closely spaced voids.

9. CONCLUSIONS

9.1 Findings

9.1.1 The Effect of Nano-TiO₂ on the Hydration Kinetics of Pastes

- As indicated by the IC data, the addition of nano-TiO₂ accelerated the hydration process of OPC, fly ash, and slag pastes. The acceleration effect intensified with the increase in the addition level of the nano-TiO₂, especially

for pastes cured at the low temperature. Specifically, the IC data suggest that the addition of nano-TiO₂ accelerates the appearance of the main hydration peaks in pastes, especially in fly ash pastes. For low curing temperature such acceleration can be 3–7 times (in terms of the length of the time shift) higher than that observed for room curing temperature, except for slag pastes.

2. Thermal indicators of setting time, inferred from the IC results, show that the addition of nano-TiO₂ shortened the setting of OPC, fly ash, and slag mixtures, especially those cured at low temperature. This observation agrees with the results of Vicat setting time test.
3. For OPC and fly ash pastes, the effect of the addition of nano-TiO₂ on the quantitative increases in the amount of hydration products (QI_{ahp}) was higher at early ages (3 and 7 days) than at later ages (28 days), regardless of curing temperatures. At later ages (28 days), the addition of nano-TiO₂ seems to be more effective in accelerating hydration of specimens cured at low temperature. However, such effect of nano-TiO₂ is not significant in slag pastes.

9.1.2 The Effect of Nano-TiO₂ on the Mechanical Properties of Mortars and Concretes

1. The addition of nano-TiO₂ can enhance the compressive and flexural strengths for both OPC and fly ash mortars. Such effect is more significant in systems cured at low temperature and containing fly ash.
2. The 7-day and 28-day compressive strengths of concretes can be improved by the addition of nano-TiO₂, regardless of the mix composition (i.e., with or without SCMs) and curing temperature. This effect was more significant in concretes containing slag and having higher values of w/cm.
3. The addition of nano-TiO₂ to concretes with and without slag increased their 7- and 28-days
4. Flexural strength for both room and low temperature curing regimes.
5. Results from fundamental resonant frequency test suggest that nano-TiO₂ addition improves the dynamic modulus of elasticity after 14 days of curing, especially at low curing temperature.

9.1.3 The Effect of Nano-TiO₂ on the Durability of Concretes

1. The addition of nano-TiO₂ tends to reduce the slump of the fresh concrete. At the same time, the unit weight of fresh concrete was increased while the fresh air content was reduced.
2. The addition of nano-TiO₂ seems to be especially beneficial with respect to increasing electrical resistivity and formation factor of fly ash concretes cured at low temperature. However, the addition of nano-TiO₂ was not found to affect the resistivity of A-P and A-S concretes. This finding suggests that nano-TiO₂ seems to be effective in modifying (reducing) pore connectivity of concretes containing fly ash.
3. The results from measurements of the total pore volume and bulk density suggest that the addition of nano-TiO₂

can reduce the porosity and densify the microstructure of concretes containing SCMs (i.e., fly ash and slag), especially those cured at low temperature. This finding correlates with previous findings regarding acceleration of hydration by addition of nano-TiO₂ hydration as this process leads to reduction in porosity.

4. Water absorption tests revealed that the addition of nano-TiO₂ reduces both the initial and secondary absorption, which is an indication of reduced permeability of concrete. Furthermore, adding nano-TiO₂ to concretes also decreases the rate of both initial and secondary absorption, which indicates that nano-TiO₂ can modify the porosity system of concretes (reduce gel and capillary porosity, and reduce the entrained and/ or entrapped air content). This trend has been observed for every concrete mixture studied in this project at both standard and low curing temperatures.
5. The results of the scaling resistance test on the concretes with and without SCMs cured at different temperatures suggest the following.
 - The overall scaling resistance of plain reference concretes (A-P and C-P) was generally good and the addition of nano-TiO₂ lead only to small improvements.
 - The scaling resistance of A-F concrete at both standard and low curing temperatures can be significantly enhanced by addition of about 0.5% of nano-TiO₂. However, the addition of 1% of nano-TiO₂ resulted in lower scaling resistance. The addition of nano-TiO₂ seems to be more effective in fly ash concrete (A-F) as compared to the plain concrete (A-P).
 - The overall scaling resistance of slag concrete was good, regardless of whether it did or did not contain nano-TiO₂ addition. The scaling resistance of A-S and C-S concretes was not affected by the addition of nano-TiO₂ at neither of the two curing temperatures used in the study.
6. The results of freeze-thaw resistance test suggested that the addition of nano-TiO₂ can improve the initial (before FT cycle starts) DME in all types of concrete (A-P, A-F, and A-S) for both standard and low curing temperatures. Such effect was more pronounced in concretes with SCMs cured at low temperature. This is expected because, as previously discussed, addition of nano-TiO₂ modifies (reduces) the porosity. Moreover, the addition of nano-TiO₂ slowed the rate of decrease of the RDME of A-F concrete exposed to FT cycles. This indicates that nano-TiO₂ can improve the freeze-thaw resistance of A-F concretes. However, such behavior was not observed in A-P and A-S concretes.

9.1.4 The Effect of Nanosilica on the Durability of OPC Concretes

The addition of nanosilica to OPC concretes was found to have similar effects on the strengths, porosity, permeability, and scaling resistance of concretes as the addition of nano-TiO₂. Specifically, nanosilica enhanced both the compressive and flexural strengths, reduces the total porosity and permeability, and slightly increased the scaling resistance of concretes.

9.1.5 The Effect of Nano-TiO₂ and Nanosilica on the Microstructure of Concretes

The addition of nano-TiO₂ reduces the occurrence of cracks and defects near the ITZ in concretes with fly ash. However, such effect was not significant in slag concretes. The addition of nanosilica seems to reduce the defects around the ITZ and decrease the size of air voids in OPC concrete. Furthermore, the addition of nanoparticles (i.e., nano-TiO₂ or nanosilica) reduces the average size of unhydrated cement particles.

9.2 Recommendations and Future Work

Results showed that nanoadditives could improve the scaling resistance of concretes containing supplementary cementitious materials. Results also show that this improvement is even more substantial when concretes are cured at low temperatures. Thus, the use of nanoadditives in low temperature environments can be even more beneficial.

However, the results also showed with respect to improvement of scaling resistance of concrete that there is an optimum percentage of nanoparticles that can be added, and that optimum percentage is different for each system. Furthermore, use of the amounts higher than the optimum percentage may actually reduce the scaling resistance. Thus, it is critical to establish an optimum percentage of nanoadditives to obtain the maximum benefit from their usage and to avoid undesirable side effects. Water-to-cement ratio and presence of supplementary cementitious materials are expected to be the two main factors that affect the optimum percentage of nanoadditives. If the porosity of a concrete without nanoparticles is already very low, adding excessive amounts of nanoparticles to the mixture might negatively affect the air void systems and jeopardize the freeze-thaw resistance.

Based on the results of this study, it appears that full-scale implementation of nanoadditives may benefit from addressing the following issues.

1. The mechanisms behind the observation that addition of 1% or higher amounts of nano-TiO₂ could negatively affect the scaling resistance of fly ash concrete should be explored.
2. More studies should be conducted to understand the effect of nano-TiO₂ on the slag concretes. Even though many properties (e.g., strength, porosity, and permeability) of slag concretes were modified by the addition of nano-TiO₂, it seems that the effect of this admixture on scaling resistance was minimal.
3. More experimental test for long-term durability of concretes with and without the addition of nanoadditives are needed to provide a more comprehensive understanding of the influence of these materials on the durability of concrete (i.e., sulfate attack, alkali-aggregate reaction).
4. The effect of nanoadditives used in the field should be compared to their effect observed in the lab. It is very important to understand how different conditions of

placement and consolidations may affect the final air void system and durability in general.

REFERENCES

- AASHTO. (2019). *Electrical resistivity of a concrete cylinder tested in a uniaxial resistance test* (AASHTO TP 119-15). American Association of State Highway and Transportation Officials. <https://www.techincalengineering.com/product/AASHTO-TP-119-15-2019/>
- AASHTO. (2020a). *Determine the total pore volume in hardened concrete using vacuum saturation* (AASHTO TP 135-20). American Association of State Highway and Transportation Officials. https://www.techstreet.com/standards/aashto-tp-135-20?product_id=2110501
- AASHTO. (2020b). *Developing performance engineering concrete pavement mixtures* (AASHTO PP 84-20). American Association of State Highway and Transportation Officials. https://www.techstreet.com/standards/aashto-pp-84-20-2021?product_id=2110484
- ASTM. (2012). *Standard test method for scaling resistance of concrete surfaces exposed to deicing chemicals* (ASTM C672/C672M-12). ASTM International.
- ASTM. (2015a). *Standard test method for Dynamic Young's Modulus, Shear Modulus, and Poisson's Ratio by impulse excitation of vibration* (ASTM E1876-15), 1–15. ASTM International. <https://doi.org/10.1520/E1876-15>
- ASTM. (2015b). *Standard test method for resistance of concrete to rapid freezing and thawing* ASTM C666/C666M. ASTM International.
- ASTM. (2019). *ACI CODE-318-19: Building code requirements for structural concrete and commentary*. Retrieved June 16, 2022, from https://www.concrete.org/store/productdetail.aspx?ItemID=318U19&Language=English&Units=US_Units
- ASTM. (2020). *Standard test method for measurement of rate of absorption of water by hydraulic-cement concretes* (ASTM C1585-20). ASTM International. <https://www.astm.org/c1585-20.html>
- Berry, E. E., & Malhotra, V. M. (1980). Fly ash for use in concrete - A critical review. *ACI Journal Proceedings*, 77(2), 59–73. <https://doi.org/10.14359/6991>
- Bilodeau, A., Carrette, G. G., Malhotra, V. M., & Langley, W. S. (1991, August). Influence of curing and drying on salt scaling resistance of fly ash concrete. *Special Publication*, 126(11), 201–228. American Concrete Institute. <https://doi.org/10.14359/2126>
- Bouzoubaâ, N., Bilodeau, A., Fournier, B., Hooton, R. D., Gagné, R., & Jolin, M. (2008). Deicing salt scaling resistance of concrete incorporating supplementary cementing materials: Laboratory and field test data. *Canadian Journal of Civil Engineering*, 35(11), 1261–1275. <https://doi.org/10.1139/L08-067>
- Bu, Y., Spragg, R., & Weiss, W. J. (2014). Comparison of the pore volume in concrete as determined using ASTM C642 and vacuum saturation. *Advances in Civil Engineering Materials*, 3(1), 308–315. <https://doi.org/10.1520/acem20130090>
- Castro, J., Bentz, D., & Weiss, J. (2011, September). Effect of sample conditioning on the water absorption of concrete. *Cement and Concrete Composites*, 33(8), 805–813. <https://doi.org/10.1016/j.cemconcomp.2011.05.007>
- Chen, J., Kou, S., & Poon, C. (2012, May). Hydration and properties of nano-TiO₂ blended cement composites.

- Cement and Concrete Composites*, 34(5), 642–649. <https://doi.org/10.1016/J.CEMCONCOMP.2012.02.009>
- Du, H., Du, S., & Liu, X. (2014, December). Durability performances of concrete with nano-silica. *Construction and Building Materials*, 73, 705–712. <https://doi.org/10.1016/j.conbuildmat.2014.10.014>
- ENR. (2021, January 18/25). *ENR: Engineering news-record* (p. 27). Retrieved July 22, 2022, from <https://digital.bnmedia.com/publication/?m=39147&i=690851&p=124&ver=html5>
- Fagerlund, G. (1977). The international cooperative test of the critical degree of saturation method of assessing the freeze/thaw resistance of concrete. *Matériaux et Constructions*, 10(4), 231–253. <https://doi.org/10.1007/BF02478694>
- Fagerlund, G. (2004). *A service life model for internal frost damage in concrete* (Report TVBM, Vol. 3119). Division of Building Materials, LTH, Lund University.
- Gaitero, J. J., Campillo, I., & Guerrero, A. (2008, August). Reduction of the calcium leaching rate of cement paste by addition of silica nanoparticles. *Cement and Concrete Research*, 38(8–9), 1112–1118. <https://doi.org/10.1016/J.CEMCONRES.2008.03.021>
- Gebler, S. H., & Klieger, P. (1986). Effect of fly ash on the durability of air-entrained concrete. *Special Publication*, 91, 483–520. <https://doi.org/10.14359/10085>
- Hager, I. (2013). Behaviour of cement concrete at high temperature. *Bulletin of the Polish Academy of Sciences: Technical Sciences*, 61(1), 145–154. <https://doi.org/10.2478/bpasts-2013-0013>
- Hall, C. (1989, June). Water sorptivity of mortars and concretes: A review. *Magazine of Concrete Research*, 41(147), 51–61. <https://doi.org/10.1680/mac.1989.41.147.51>
- Harnik, A. B., Meier, U., & Rösli, A. (1980). Combined influence of freezing and deicing salt on concrete—Physical aspects. In *Durability of Building Materials and Components* (pp. 474–484). ASTM International. <https://doi.org/10.1520/STP36082S>
- Hooton, R. D., & Vassilev, D. G. (2016). Evaluation of modifications to the ASTM C672 deicer salt scaling test for concrete containing slag cement. *Advances in Civil Engineering Materials*, 5(2), 51–79. <https://doi.org/10.1520/ACEM20160034>
- Hou, P., Kawashima, S., Kong, D., Corr, D. J., Qian, J., & Shah, S. P. (2013, February). Modification effects of colloidal nanoSiO₂ on cement hydration and its gel property. *Composites Part B: Engineering*, 45(1), 440–448. <https://doi.org/10.1016/j.compositesb.2012.05.056>
- INDOT. (2020a). *Indiana Department of Transportation standard specifications, Section 700*. <https://www.in.gov/dot/div/contracts/standards/book/sep19/700-2020.pdf>
- INDOT. (2020b). *Indiana Department of Transportation Standard Specifications, Section 900*. <https://www.in.gov/dot/div/contracts/standards/book/sep19/900-2020.pdf>
- Jakobsen, U. H., Pade, C., Thaulow, N., Brown, D., Sahu, S., Magnusson, O., De Buck, S., & De Schutter, G. (2006). Automated air void analysis of hardened concrete - a Round Robin study. *Cement and Concrete Research*, 36(8), 1444–1452. <https://doi.org/10.1016/J.CEMCONRES.2006.03.005>
- Jalal, M., Fathi, M., & Farzad, M. (2013, July). Effects of fly ash and TiO₂ nanoparticles on rheological, mechanical, microstructural and thermal properties of high strength self compacting concrete. *Mechanics of Materials*, 61, 11–27. <https://doi.org/10.1016/J.MECHMAT.2013.01.010>
- Jeong, H., Velay-Lizancos, M., Olek, J., Pannell, D. K., & Geiger, R. (2018, June 19–21). *Influence of type of deicers on scaling resistance of plain and fly ash concretes*. World Salt Symposium, Park City, Utah.
- Ji, T. (2005, October). Preliminary study on the water permeability and microstructure of concrete incorporating nano-SiO₂. *Cement and Concrete Research*, 35(10), 1943–1947. <https://doi.org/10.1016/J.CEMCONRES.2005.07.004>
- Jo, B. W., Kim, C. H., & Lim, J. H. (2007a). Characteristics of cement mortar with nano-SiO₂ particles. *ACI Materials Journal*, 104(4), 404–407. <https://doi.org/10.14359/18830>
- Jo, B. W., Kim, C. H., & Lim, J. H. (2007b). Investigations on the development of powder concrete with nano-SiO₂ particles. In *KSCCE Journal of Civil Engineering*, 11(1), 37–42. <https://doi.org/10.1007/BF02823370>
- Johnston, C. D. (1987). Effects of microsilica and class C fly ash on resistance of concrete to rapid freezing and thawing and scaling in the presence of deicing agents. *Special Publication*, 100, 1183–1204. <https://doi.org/10.14359/2082>
- Kevern, J. T., Wang, K., & Schaefer, V. R. (2009). Test methods for characterizing air void systems in Portland cement pervious concrete. *Journal of ASTM International*, 6(9). <https://doi.org/10.1520/JAI102451>
- Kim, T., & Olek, J. (2012). Effects of sample preparation and interpretation of thermogravimetric curves on calcium hydroxide in hydrated pastes and mortars. *Transportation Research Record: Journal of the Transportation Research Board*, 2290(1), 10–18. <https://doi.org/10.3141/2290-02>
- Kosmatka, S. H., & Wilson, M. L. (2016). *Design and control of concrete mixtures* (16th ed.). Portland Cement Association.
- Li, W., Pour-Ghaz, M., Castro, J., & Weiss, J. (2012, March). Water absorption and critical degree of saturation relating to freeze-thaw damage in concrete pavement joints. *Journal of Materials in Civil Engineering*, 24(3), 299–307. [https://doi.org/10.1061/\(asce\)mt.1943-5533.0000383](https://doi.org/10.1061/(asce)mt.1943-5533.0000383)
- Li, Z., Ding, S., Yu, X., Han, B., & Ou, J. (2018). Multifunctional cementitious composites modified with nano titanium dioxide: A review. *Composites Part A: Applied Science and Manufacturing*, 111, 115–137. <https://doi.org/10.1016/J.COMPOSITESA.2018.05.019>
- Li, Z., Han, B., Yu, X., Dong, S., Zhang, L., Dong, X., & Ou, J. (2017). Effect of nano-titanium dioxide on mechanical and electrical properties and microstructure of reactive powder concrete. *Materials Research Express*, 4(9), 095008. <https://doi.org/10.1088/2053-1591/aa87db>
- Li, Z., Wang, J., Li, Y., Yu, X., & Han, B. (2018). Investigating size effect of anatase phase nano TiO₂ on the property of cement-based composites. *Materials Research Express*, 5(8), 85034. <https://doi.org/10.1088/2053-1591/aad4e3>
- Lothenbach, B., Scrivener, K., & Hooton, R. D. (2011, December). Supplementary cementitious materials. *Cement and Concrete Research*, 41(12), 1244–1256. <https://doi.org/10.1016/j.cemconres.2010.12.001>
- Ma, B., Li, H., Li, X., Mei, J., & Lv, Y. (2016). Influence of nano-TiO₂ on physical and hydration characteristics of fly ash-cement systems. *Construction and Building Materials*, 122, 242–253. <https://doi.org/10.1016/J.CONBUILDMAT.2016.02.087>
- Madani, H., Bagheri, A., & Parhizkar, T. (2012). The pozzolanic reactivity of monodispersed nanosilica hydrosols and their influence on the hydration characteristics of Portland cement. *Cement and Concrete Research*, 42(12), 1563–1570. <https://doi.org/10.1016/J.CEMCONRES.2012.09.004>

- Mehta, P. K., & Monteiro, P. J. M. (2006). *Concrete: Microstructure, properties, and materials* (3rd ed). <https://doi.org/10.1036/0071462899>
- Mohseni, E., Miyandehi, B. M., Yang, J., & Yazdi, M. A. (2015). Single and combined effects of nano-SiO₂, nano-Al₂O₃ and nano-TiO₂ on the mechanical, rheological and durability properties of self-compacting mortar containing fly ash. *Construction and Building Materials*, *84*, 331–340. <https://doi.org/10.1016/J.CONBUILDMAT.2015.03.006>
- Mondal, P., Shah, S. P., Marks, L. D., & Gaitero, J. J. (2010). *Comparative study of the effects of microsilica and nanosilica in concrete*, *2141*(1). <https://doi.org/10.3141/2141-02>
- Moro, C., El Fil, H., Francioso, V., & Velay-Lizancos, M. (2020). Influence of water-to-binder ratio on the optimum percentage of nano-TiO₂ addition in terms of compressive strength of mortars: A laboratory and virtual experimental study based on ANN model. *Construction and Building Materials*, *267*, 120960. <https://doi.org/10.1016/j.conbuildmat.2020.120960>
- Moro, C., El Fil, H., Francioso, V., & Velay-Lizancos, M. (2021). Influence of water-to-binder ratio on the optimum percentage of nano-TiO₂ addition in terms of compressive strength of mortars: A laboratory and virtual experimental study based on ANN model. *Construction and Building Materials*, *267*, 120960. <https://doi.org/10.1016/J.CONBUILDMAT.2020.120960>
- Nazari, A., & Riahi, S. (2010). The effect of TiO₂ nanoparticles on water permeability and thermal and mechanical properties of high strength self-compacting concrete. *Materials Science and Engineering: A*, *528*(2), 756–763. <https://doi.org/10.1016/j.msea.2010.09.074>
- Nazari, A., & Riahi, S. (2011). TiO₂ nanoparticles' effects on properties of concrete using ground granulated blast furnace slag as binder. *Science China Technological Sciences*, *54*(11), 3109–3118. <https://doi.org/10.1007/s11431-011-4421-1>
- NIST. (n.d.). *Estimation of pore solution conductivity*. Retrieved June 27, 2022, from <https://www.nist.gov/el/materials-and-structural-systems-division-73100/inorganic-materials-group-73103/estimation-pore>
- Nokken, M. R., & Hooton, R. D. (2002). Dependence of rate of absorption on degree of saturation of concrete. *Cement, Concrete and Aggregates*, *24*(1), 20–24. <https://doi.org/10.1520/cca10487j>
- Pigeon, M., Marchand, J., & Pleau, R. (1996, June). Frost resistant concrete. *Construction and Building Materials*, *10*(5), 339–348. [https://doi.org/10.1016/0950-0618\(95\)00067-4](https://doi.org/10.1016/0950-0618(95)00067-4)
- Powers, T. C. (1945). A working hypothesis for further studies of frost resistance of concrete. *ACI Journal Proceedings*, *41*(1), 245–272. <https://doi.org/10.14359/8684>
- Powers, T. C. (1975). Freezing effects in concrete. *Durability of Concrete*, *47*, 1–12. <https://doi.org/10.14359/17603>
- Ren, J., Lai, Y., & Gao, J. (2018). Exploring the influence of SiO₂ and TiO₂ nanoparticles on the mechanical properties of concrete. *Construction and Building Materials*, *175*, 277–285. <https://doi.org/10.1016/j.conbuildmat.2018.04.181>
- Riahi, S., & Nazari, A. (2011). Compressive strength and abrasion resistance of concrete containing SiO₂ and CuO nanoparticles in different curing media. *Science China Technological Sciences*, *54*, 2349–2357. <https://doi.org/10.1007/s11431-011-4463-4>
- Said, A. M., Zeidan, M. S., Bassuoni, M. T., & Tian, Y. (2012). Properties of concrete incorporating nano-silica. *Construction and Building Materials*, *36*, 838–844. <https://doi.org/10.1016/j.conbuildmat.2012.06.044>
- Salemi, N., & Behfarnia, K. (2013, November). Effect of nano-particles on durability of fiber-reinforced concrete pavement. *Construction and Building Materials*, *48*, 934–941. <https://doi.org/10.1016/j.conbuildmat.2013.07.037>
- Salemi, N., Behfarnia, K., & Zaree, S. A. (2014). Effect of nanoparticles on frost durability of concrete. *Asian Journal of Civil Engineering (BHRC)*, *15*(3), 411–420. <https://www.sid.ir/FileServer/JE/103820140307.pdf>
- Scrivener, K. L. (2004, November). Backscattered electron imaging of cementitious microstructures: Understanding and quantification. *Cement and Concrete Composites*, *26*(8), 935–945. <https://doi.org/10.1016/j.cemconcomp.2004.02.029>
- Scrivener, K., Ouzia, A., Juilland, P., & Mohamed, A. K. (2019). Advances in understanding cement hydration mechanisms. *Cement and Concrete Research*, *124*, 105823. <https://doi.org/10.1016/j.cemconres.2019.105823>
- Scrivener, K., Snellings, R., & Lothenbach, B. (Eds.). (2016). *A practical guide to microstructural analysis of cementitious materials*. CRC Press.
- Senff, L., Labrincha, J. A., Ferreira, V. M., Hotza, D., & Repette, W. L. (2009, July). Effect of nano-silica on rheology and fresh properties of cement pastes and mortars. *Construction and Building Materials*, *23*(7), 2487–2491. <https://doi.org/10.1016/j.conbuildmat.2009.02.005>
- Singh, L. P., Bhattacharyya, S. K., Mishra, G., & Ahalawat, S. (2012). Reduction of calcium leaching in cement hydration process using nanomaterials. *Materials Technology*, *27*(3), 233–238. <https://doi.org/10.1179/175355712Y.0000000005>
- Singh, L. P., Karade, S. R., Bhattacharyya, S. K., Yousuf, M. M., & Ahalawat, S. (2013). Beneficial role of nanosilica in cement based materials – A review. *Construction and Building Materials*, *47*, 1069–1077. <https://doi.org/10.1016/j.conbuildmat.2013.05.052>
- Sukharsh, J., & Nicholas, H. (2007). Effect of fly ash content and aggregate gradation on the durability of concrete pavements. *Journal of Materials in Civil Engineering*, *19*(5), 367–375. [https://doi.org/10.1061/\(ASCE\)0899-1561\(2007\)19:5\(367\)](https://doi.org/10.1061/(ASCE)0899-1561(2007)19:5(367))
- Thomas, M. (2007). *Optimizing the use of fly ash in concrete*. Portland Cement Association.
- US Research Nanomaterials. (n.d.). *Titanium oxide nanopowder / nanoparticles (TiO₂, anatase, 99.9%, 18nm)* [Webpage]. Retrieved March 30, 2023, from <https://www.us-nano.com/inc/sdetail/269>
- Valenza II, J. J., & Scherer, G. W. (2007a). A review of salt scaling: I. Phenomenology. *Cement and Concrete Research*, *37*(7), 1007–1021. <https://doi.org/10.1016/j.cemconres.2007.03.005>
- Valenza II, J. J., & Scherer, G. W. (2007b). A review of salt scaling: II. Mechanisms. *Cement and Concrete Research*, *37*(7), 1022–1034. <https://doi.org/10.1016/j.cemconres.2007.03.003>
- Verian, K. P., & Behnood, A. (2018). Effects of deicers on the performance of concrete pavements containing air-cooled blast furnace slag and supplementary cementitious materials. *Cement and Concrete Composites*, *90*, 27–41. <https://doi.org/10.1016/j.cemconcomp.2018.03.009>
- Xu, G., & Shi, X. (2018, September). Characteristics and applications of fly ash as a sustainable construction material: A state-of-the-art review. *Resources, Conservation and Recycling*, *136*, 95–109. <https://doi.org/10.1016/j.resconrec.2018.04.010>
- Ying, J., Zhou, B., & Xiao, J. (2017). Pore structure and chloride diffusivity of recycled aggregate concrete with nano-SiO₂ and nano-TiO₂. *Construction and Building*

- Materials*, 150, 49–55. <https://doi.org/10.1016/J.CONBUILDMAT.2017.05.168>
- Yu, J., Li, G., & Leung, C. K. Y. (2018, February). Hydration and physical characteristics of ultrahigh-volume fly ash-cement systems with low water/binder ratio. *Construction and Building Materials*, 161, 509–518. <https://doi.org/10.1016/j.conbuildmat.2017.11.104>
- Yuan, J., Lu, H., Yang, Q., & Ling, J. (2015). Mechanisms on the salt–frost scaling of concrete. *Journal of Materials in Civil Engineering*, 29(3), D4015002-1–D4015002-5. [https://doi.org/10.1061/\(ASCE\)MT.1943-5533.0001448](https://doi.org/10.1061/(ASCE)MT.1943-5533.0001448)
- Zhang, M., & Li, H. (2011). Pore structure and chloride permeability of concrete containing nano-particles for pavement. *Construction and Building Materials*, 25(2), 608–616. <https://doi.org/10.1016/J.CONBUILDMAT.2010.07.032>
- Zhutovsky, S., & Hooton, R. D. (2019). Role of sample conditioning in water absorption tests. *Construction and Building Materials*, 215, 918–924. <https://doi.org/10.1016/j.conbuildmat.2019.04.249>

APPENDIX

Appendix A. The Effects of Curing Temperature on the Hydration Kinetics of Plain and Fly Ash Pastes and Compressive Strength of Corresponding Mortars With and Without Nano-TiO₂ Addition

APPENDIX A. THE EFFECTS OF CURING TEMPERATURE ON THE HYDRATION KINETICS OF PLAIN AND FLY ASH PASTES AND COMPRESSIVE STRENGTH OF CORRESPONDING MORTARS WITH AND WITHOUT NANO-TiO₂ ADDITION

Huang, D., Velay-Lizancos, M., & Olek, J. (2022). *The effects of curing temperature on the hydration kinetics of plain and fly ash pastes and compressive strength of corresponding mortars with and without nano-TiO₂ addition.*

<https://docs.lib.purdue.edu/cgi/viewcontent.cgi?article=1651&context=icdcs>

Publication abstract: Incorporation of fly ash in cementitious systems containing ordinary Portland cement (OPC) increases their long-term strength and durability. However, replacement of cement by fly ash also reduces the heat of hydration of such systems and reduces early-age strength development. The reduced rate of strength development can increase the risk of durability problems, e.g., scaling, in cases when young concrete is exposed to low temperatures and deicing chemicals. This study investigated the potential of nano-titanium dioxide (nanoTiO₂) particles to modify the hydration kinetics of fly ash pastes and compressive strength development of corresponding mortars cured under low (4°C) and standard (23°C) temperatures. The kinetics of the hydration study was performed on paste specimens using the thermogravimetric analysis (TGA) and isothermal calorimetry (IC) methods. The mortar specimens used for compressive strength testing were prepared using the same w/cm values and the same types of binders as those used to prepare the paste specimens. It was found that although the addition of nano-TiO₂ accelerated the hydration rate of all pastes, that treatment was, however, more effective in the fly ash pastes than in the ordinary Portland cement (OPC) pastes, especially for the cases of low temperature curing. These findings were confirmed by the results of strength testing as the specimens experiencing accelerated rates of hydration were also found to be stronger.

About the Joint Transportation Research Program (JTRP)

On March 11, 1937, the Indiana Legislature passed an act which authorized the Indiana State Highway Commission to cooperate with and assist Purdue University in developing the best methods of improving and maintaining the highways of the state and the respective counties thereof. That collaborative effort was called the Joint Highway Research Project (JHRP). In 1997 the collaborative venture was renamed as the Joint Transportation Research Program (JTRP) to reflect the state and national efforts to integrate the management and operation of various transportation modes.

The first studies of JHRP were concerned with Test Road No. 1 — evaluation of the weathering characteristics of stabilized materials. After World War II, the JHRP program grew substantially and was regularly producing technical reports. Over 1,600 technical reports are now available, published as part of the JHRP and subsequently JTRP collaborative venture between Purdue University and what is now the Indiana Department of Transportation.

Free online access to all reports is provided through a unique collaboration between JTRP and Purdue Libraries. These are available at <http://docs.lib.purdue.edu/jtrp>.

Further information about JTRP and its current research program is available at <http://www.purdue.edu/jtrp>.

About This Report

An open access version of this publication is available online. See the URL in the citation below.

Huang, D., Velay-Lizancos, M., & Olek, J. (2022). *Improving scaling resistance of pavement concrete using titanium dioxide (TiO_2) and nanosilica* (Joint Transportation Research Program Publication No. FHWA/IN/JTRP-2022/32). West Lafayette, IN: Purdue University. <https://doi.org/10.5703/1288284317583>